Fluorescence Resonance Energy Transfer Assays in Prion Biology

DISSERTATION

Zur

Erlangung der naturwissenschaftlichen Doktorwürde

(Dr. sc. nat.)

vorgelegt der

Mathematisch-naturwissenschaftlichen Fakultät

der

Universität Zürich

von

Boris Alexander Ballmer

aus

Lausen, Basel-Landschaft

Promotionskommitee

Prof. Dr. Adriano Aguzzi

Prof. Dr. Lucas Pelkmans

Dr. Simone Hornemann

Zürich, 2014

TABLE OF CONTENT

SUMMARY 4

ZUSAMMENFASSUNG 6

PRION GLOSSARY 8

ABBREVIATIONS 9

INTRODUCTION 11

History of Prion Diseases (PDs) and Research 11
Prion Diseases 13
Prion Diseases in Animals 14
Prion Diseases in Humans 15
The Cellular Prion Protein (PrP^{C}) 16
PrP^{C} Internalization 17
The Scrapie Prion Protein (PrP^{Sc}) 18
Prion Conversion Reaction 19
Prion Pathogenesis 21
Prion Diagnosis 22
Prion Drug Treatment 23
Prion Bioassays 23
Förster/Fluorescence Resonance Energy Transfer (FRET) 24
Principles and Requirements of FRET 24
Terminology and FRET Assays in Prion Biology 25

AIMS OF THE THESIS 27

PART I RESULTS 29

PrP^{C} and PrP^{Sc} Enzyme-Linked Immunosorbent Assay (ELISA) 29
Principle of the Sandwich ELISA 29
Prion Infectivity Protocol for Murine Cell Lines 30
Cell Lysis Conditions 31
Proteinase K (PK) Digestion and its Inactivation 32
Denaturation of PrP^{Sc} with Guanidinium Thiocyanate (GdnSCN) 34
Antibody Titration 35
Limit of Detection (LOD) for recPrP and PrP^{Sc} Detection 36
Validation of the PrP ELISA 37
Detection of PrP^{Sc} with the same Coating and Primary POM Antibody by ELISA 38
Detection of N-GPI-PrP^{C} 39
PTAA Drug Treatment of Prion-Infected Tissue Cultures 40
The Prion Organotypic Slice Culture Assay (POSCA) 40

DISCUSSION 47

PrP^{C}/PrP^{Sc} Sandwich ELISA 47
PTAA Drug Treatment of Prion-Infected Slices 48

OUTLOOK 50

PART II RESULTS 51

PrP Time-Resolved Fluorescence Resonance Energy Transfer Assays 51
Overview of FRET-Based PrP Assays 51
FRET Calculation and Parameters 52
Dynamic Range of the Wallac EnVision Multilabel Reader for Europium Measurements 52
Measurement Time of the Wallac EnVision Multilabel Reader and Signal Stability 53
Preparation and Characterization of FRET Antibody Tandem Pairs 54
Development of a Homogeneous recPrP TR-FRET Assay 56
Development of a Homogeneous PrP^{C} TR-FRET Assay 58
Development of a Homogeneous PrP^{Sc} TR-FRET Assay 61
Development of a Heterogeneous PrP^{C} Cell Surface TR-FRET Assay 63
Interfering PrP^{C} Cell Surface FRET Signals with Prions 69
Development of a Heterogeneous PrP^{C} endocytosis TR-FRET Assay 71
PrP^{C} Cell Surface Detection of Human Cells with TR-FRET 72
AlamarBlue Cell Viability Assay 72
PrP^{C} Cell Surface Detection of Intact Human Cells with TR-FRET 74
PrP^{C} Endocytosis Assay in Human Cells with solid-phase TR-FRET 82
Pharmacological Inhibition of PrP^{C} Endocytosis 84
Inhibition of PrP^{C} Endocytosis by Gene Silencing 88
Induction of PrP^{C} Endocytosis 90

DISCUSSION 93

Prion Protein Time-Resolved FRET Assay 93
Recombinant PrP Time-Resolved FRET assay 93
PrP^{C} Time-Resolved FRET Assay 93
PrP^{Sc} Time-Resolved FRET Assay 94
PrP^{C} Cell Surface Time-Resolved FRET Assay 94
PrP^{C} Endocytosis Time-Resolved FRET Assay 95

OUTLOOK 97

MATERIAL AND METHODS 98

Mice 98
Cell Culture 98
Preparation of CD1 and RML6 Crude Brain Homogenate 98
Scrapie Cell End-Point Assay of COCSBH 98
Proteolysis of COCSBH and Western Blot Analysis 99
ELISA 99
FRET Antibody Labelling 100
FRET Experiments 101
Preparation of Recombinant Mouse mPrP (23-231) 102
siRNA Treatment 102
Quantitative PCR 102
Cell Viability Assay 103

REFERENCES 104

ACKNOWLEDGEMENT 127

CURRICULUM VITAE 128

SUMMARY

Prions are unprecedented infectious pathogens responsible for a group of neurodegenerative disorders termed prion diseases (PDs) or transmissible spongiform encephalopathies (TSEs). Among the most notable PDs belong the Creutzfeldt-Jakob disease (CJD) in humans, the bovine spongiform encephalopathie (BSE) in cattle and scrapie in sheep. PDs appear either as genetic, infectious or sporadic disorders. Prions destroy the brain while the body remains mainly unaffected. The basic principle of all PDs is the conversion of the normal prion protein (PrP^{C}) into a misfolded aggregated form, termed scrapie form of PrP (PrP^{Sc}). According to the prion protein hypothesis it is believed that PrP^{Sc}, either in a monomeric or in an oligomeric or aggregated state, promotes the conversion of PrP^{C} into PrP^{Sc} by a self-propagating mechanism. The molecular composition of PrP^{Sc} and how the conversion of PrP^{C} into PrP^{Sc} leads to pathology is not clear. Moreover, all familiar prion diseases have mutations within the *Prnp* locus and ablation of *Prnp* in mice confers resistance to prions.

The goal of my thesis was to establish a Fluorescence Resonance Energy Transfer (FRET)-based high-throughput assay which enables the detection of PrP^{C} and PrP^{Sc}. To achieve this aim, I first established an enzyme-linked sandwich immuno assay (ELISA) with our in-house anti-PrP POM antibody library. By using enzymatic digestion and denaturation steps, I was able to discriminate between PrP^{C} and PrP^{Sc}. Results from *in vitro* experiments revealed an excellent performance criteria for high-throughput applications by calculating the Z' factor. A detection limit of 40 ng/ml recombinant PrP spiked in PrP knock out brain homogenate was determined. The ELISA was used to detect PrP^{Sc} in prion-infected organotypic slice cultures. Three weeks post-inoculution, accumulated PrP^{Sc} could be detected in organotypic slice culture homogenates which corresponds to a limit of detection of 1 ng PrP^{Sc}/µg total protein. Next, we were interested whether one of the luminescent conjugated polymers (LCPs) is able to inhibit the accumulation of PrP^{Sc} in the prion-infected slices. We found that the accumulation of PrP^{Sc} was inhibited by the use of the LCP, Poly(thiophene-3-acetic acid) [PTAA], which also decreased the amount of PK-resistant material detected by ELISA. The obtained ELISA results were compared with two other prion assays, the scrapie cell assay (SCA) which measures prion infectivity and the misfolding protein assay (MPA), which measures the amount of PrP^{Sc} aggregates. I found a good correlation between these results which shows that the ELISA is suitable to detect PK-resistant PrP^{Sc} in organotypic tissue cultures.

In the second and main part of my thesis, I established various FRET-based immunoassays, either in a homogeneous or in a solid phase, which enabled the detection of PrP^{C} and PrP^{Sc} from different biological samples. I tested several POM antibodies, coupled either to the donor fluorophore Europium (Eu) or to the acceptor fluorophore APC, as FRET tandem pairs. The antibody pair POM1Eu and POM2APC were identified as the best pair. With ths combination a limit of detection lower than 125 pg/ml was obtained for recombinant PrP in the homogeneous phase. In addition, depending on the use of the POM antibodies, wild type and mutant recombinant PrP, as well as monomeric and aggregated recombinant PrP, could be distinguished by the newly established FRET assay. The recombinant PrP FRET assay revealed excellent performance criteria for high-throughput applications.

Next, I detected PrP^{C} and PrP^{Sc} in either cell lysates or mouse brain homogenates. The detection limit of PrP^{C} in murine neuroblastoma cell lysates spiked with PrP knock out cell lysate was 16 µg/ml of total protein concentration. Including a proteolysis and denaturation step, PrP^{Sc} was detected in prion-infected 22L brain homogenate with a sensitivity of 5.5 log $TCID_{50}$ units/g, which is less sensitive compared to the scrapie cell assay (up to 8 log $TCID_{50}$ units/g).

The FRET assay also allows the detection of PrP^{C} on the surface of intact murine and human cells. Pharmacological, genetic and enzymatic manipulation of the PrP^{C} cell surface expression without affecting cell viability was monitored with 500 cells/well in a 384-plate format. The assay performance was excellent for high-throughput applications as determined by calculating the Z' factor.

In the last part of my thesis I established a novel FRET assay for the endocytosis of the PrP. I determined a half-life time of about 30 min for PrP^{C} at the surface of human cells. After 45 min a steady state was reached of endocytosed and recycled PrP^{C}. The various different endocytosis pathways of PrP^{C} can be blocked pharmacologically without affecting cell viability and monitored by FRET. Using siRNA treatment, genes involved in PrP^{C} endocytosis were investigated. Two genes, AP2M1 and Rab5a blocked the internalisation, whereas EHD1 induced the uptake of PrP^{C}.

Overall, I have established various FRET-based immunoassays which are extremely valuable in the characterisation of both PrP isoforms and are intensively utilized for different applications in prion biology.

ZUSAMMENFASSUNG

Prionen sind einzigartige infektiöse Pathogene, die für eine Reihe von neurodegenerativen Erkrankungen, zusammengefasst als Prionerkrankungen (PD) oder transmissible spongiforme Encephalopathien (TSE), verantwortlich sind. Dazu gehören die Creutzfeldt-Jakob Erkrankung (CJD) im Menschen, die bovine spongiform Encephalopathien (BSE) im Rind und Scrapie im Schaf. PD haben entweder einen genetischen, infektiösen oder sporadischen Ursprung. In allen drei Fällen wird das Gehirn von den Prionen zerstört, wobei der übrige Körper nicht in Mitleidenschaft gezogen wird. Das grundlegende Prinzip in allen PD ist die Umwandlung des normalen Prion Proteins (PrP^{C}) in eine Erkrankungs-assoziierte Form (PrP^{Sc}), die „Prion“ bezeichnet wird. Gemäss der Prion Protein Hypothese wird angenommen, dass PrP^{Sc}, entweder in einer monomeren oder aggregierten Form, die Umwandlung von PrP^{C} zu PrP^{Sc} fördert und dadurch selbstreplizierend und infektiös wird.

Das Ziel meiner Doktorarbeit war die Etablierung einer FRET-basierten Hochdurchsatz-Methode, die die Detektion von PrP^{C} und PrP^{Sc} ermöglicht. Als Voraussetung hierfür musste zuerst ein Enzym-gekoppelter Sandwich Immunoassay (ELISA) mit unseren eigenen anti-PrP POM Antikörpern etabliert werden. Durch eine enzymatische Verdauung und einen Denaturationsschritt war ich in der Lage, PrP^{C} und PrP^{Sc} voneinander zu unterscheiden. Resultate von *in vitro* Experimenten zeigten eine exzellente Leistung für Hochdurchsatz-Anwendungen durch die Berechnung des Z’ Faktors. Für rekombinantes PrP wurde eine Detektionslimite von 40 ng/ml bestimmt. PrP^{Sc} konnte in organotypischen zerebellären Gewebskulturen 19 Tage nach Inokulation bestimmt werden. Zusätzlich habe ich den PrP^{Sc} ELISA mit zwei anderen Prion Methoden verglichen und fand eine gute Korrelation zwischen den Resultaten.

Im zweiten und Hauptteil meiner Doktorarbeit habe ich zahlreiche FRET-basierte Immunoassays entweder in der homogenen oder in der soliden Phase etabliert, die die Detektion von PrP^{C} und PrP^{Sc} aus verschiedenen biologischen Proben ermöglichen. Dazu verwendete ich POM Antikörper, die entweder an das Donorfluorophor Europium oder an das Akzeptorfluorophor APC gekoppelt sind, als FRET Tandempaare. Eine Detektions-limite tiefer als 125 pg/ml wurde für rekombinantes PrP bestimmt. Kein FRET Signal wurde in PrP defizienten Zelllysaten detektiert. Zusätzlich, abhängig von der POM Anti-körper Kombination, konnten sowohl Wildtyp und Mutanten als auch monomeres und aggregiertes rekombinantes PrP unterschieden werden. Der neu etablierte FRET assay

ermöglicht ausserdem Bindungsstudien als auch enzymatische Manipulation von rekombinantem PrP. Der rekombinante PrP FRET Assay glänzt mit exzellenter Leistung für Hochdurchsatz Anwendungen.

Im weiteren Verlauf habe ich PrP^{C} und PrP^{Sc} entweder in Zelllysaten oder murinen Hirnhomogenaten detektiert. Die Detektionslimite für PrP^{C} in N2a Zelllysaten ergab 16 µg/ml. Durch einen enzymatischen Verdau und einen Denaturierungsschritt konnte ich PrP^{Sc} in Prion-infizierten 22L Hirnhomogenat bei einer Verdünnung von 10^{-5} nachweisen, was weniger sensitiv ist verglichen mit dem Scrapie Cell Assay (bis zu 10^{-9}).

Der FRET Assay erlaubt ausserdem die Detektion von PrP^{C} auf intakten murinen und humanen Zellen. Pharmakologische, genetische und enzymatische Manipulation der PrP^{C} Zelloberflächenexpression, die die Zellviabilität nicht beieinflussen, wurden mit 500 Zellen/ml im 384-Plattenformat durchgeführt. Die FRET Assay Leistung war hervorragend und ermöglicht Hochdurchsatz-Anwendungen.

Im letzten Teil meiner Doktorarbeit habe ich einen neuen und sehr cleveren FRET assay etabliert, der die Endocytose von PrP misst. Dabei habe ich eine Halbwertszeit der PrP^{C} Zelloberflächen-Expression von 30 min bestimmt. Nach 45 min hat sich ein Gleichgewicht eingestellt von endozytierten und recyclenden PrP^{C}. Die verschiedenen Endozytose Wege von PrP^{C} wurden pharmakologisch blockiert, ohne die Zellviabilität zu beeinträchtigen. Mittels siRNA Behandlung wurden Gene identifiziert, die an der Endozytose von PrP^{C} beteiligt sind. Zwei Gene, AP2M1 und Rab5a blockieren die Endocytose, während EHD1 die Internalisierung von PrP^{C} induziert.

PRION GLOSSARY

Prion: Agent of transmissible spongiform encephalopathy (TSE), with unconventional properties. The term does not have structural implications other than that a protein is an essential component.

'Protein-only' hypothesis: Maintains, that the prion is devoid of informational nucleic acid, and that the essential pathogenic component is protein (or glycoprotein). Gentic evidence indicates that the protein is an abnormal form of PrP (perhaps identical with PrP^{Sc}). The association with other 'non-informational' molecules (such as glycosaminoglycans, or maybe even short nucleic acids) is not excluded.

PrP^{C}: the naturally occurring form of the mature *Prnp* gene product. Its presence in a given cell type is necessary, but not sufficient, for replication of the prion.

PrP^{Sc}: An 'abnormal' form of the mature Prnp gene product found in tissue of TSE sufferers, defined as being partly resistant to digestion by proteinase K (PK) under standardized conditions. It is believed to differ from PrP^{C} only (or mainly) conformationally, and is often considered to be the transmissible agent or prion.

Adapted from Aguzzi and Weissmann (Aguzzi and Weissmann, 1997)

ABBREVIATIONS

2Eu	POM2 antibody coupled to Europium (Eu)
2APC	POM2 antibody coupled to Allophycocyanin (APC)
2Eu/APC	POM2 Europium/APC FRET antibody pair
%CV	Coefficient of variation
APC	Allophycocyanin
BFA	Brefeldin A
BH	Brain homogenate
BSE	Bovine spongiform encephalopathy
CJD	Creutzfeldt-Jakob disease
CNS	Central nervous system
COCSBH	Cultured organotypic cerebellar slice brain homogenate
CPZ	Chlorpromazine
CWD	Chronic wasting disease
DPI	Days post-inoculation
DIV	Days *in vitro*
Eu	Europium
FFI	Fatal familial insomnia
FRET	Förster/Fluorescence resonance energy transfer
GdnSCN	Guanidinium thiocyanate
GPI	Glycosylphosphatidylinositol
GSS	Gerstmann-Sträussler-Scheinker disease
HTRF	Homogeneous time-resolved fluorescence
KO	Knockout
LOD	Limit of detection
MβCD	Methyl-β-cyclodextrine
OHSCs	Organotypic hippocampal slice cultures
PD	Prion diseases
PI-PLC	Phosphoinositide phosholipase C
PK	Proteinase K
PMSF	Phenylmethylsulfonyl fluoride
POSCA	Prion organotypic slice culture assay
PRNP	Prion protein gene
PrP^{C}	Cellular prion protein

PrP^{Sc}	Scrapie-associated prion protein
PTAA	Poly(thiophene-3-acetic acid)
RecPrP	Recombinant prion protein
RML	Rocky Mountain laboratory strain
SCA	Scrapie cell assay
SCEPA	Scrapie cell assay in end point format
TR	Time-resolved
TSE	Transmissible spongiform encephalopathy
vCJD	Variant Creutzfeldt-Jakob disease

INTRODUCTION

History of Prion Diseases (PDs) and Research

The existence of prions is known in one or the other form for more than three centuries. The earliest written record describing ataxic illnesses was reported in the mid 18th century [Brown and Bradley 1998]. This PD killed entire flocks of sheep and was named scrapie. At that time, scrapie was already prevalent in central Europe and it was well known that this disease is transmissible. By isolating animals with scrapie from healthy stock, the spread was kept in check and the damage limited [Leopoldt, 1759]. Experimentally, 200 years later Stewart Stockman described that the incubation time for scrapie transmission takes two to three years [Aguzzi and Calella, 2009]. In the late nineteen thirties, accidental and experimental transmission of scrapie in sheep was reported [Cuille and Chelle 1939; Wilson et al. 1950]. The hypothesis that scrapie is caused by a filterable virus became widely held [Cuille and Chelle 1939; Wilson et al. 1950].

In the 1920s and 1930s, a high incidence of a rapidly progressive dementia was described in humans [Creutzfeldt, 1920; Jakob, 1921]. It was Creutzfeldt and Jacob nosological classification that lead to the eponym of this disease (Creutzfeldt-Jacob disease (CJD)) which has been maintained until nowadays. In the 1950s among the Fore people of New Guinea, an outbreak of Kuru occurred [Gajdusek and Zigas, 1957]. William Hadlow, an American veternarian pathologist recognised similar lesions in Kuru and scrapie and he hypothesised a link between both diseases [Hadlow, 1959]. A crucial turning point in the field of prions were the mid 1960s, when Carleton Gajdusek and collegues found the transmissible nature of a small-sized infectious agent by experimental transmission of Kuru and CJD to chimpanzees [Gajdusek et al., 1966; Gibbs et al., 1968]. Unfortunately, transmission of infectivity was also proven in humans many years later. Dozens of people had died from CJD after having been infected by prion-infected surgical instruments or after having received contaminated growth hormone injections [Duffy et al., 1974]. Like Hadlow, Igor Klatzo made a similar intellectual leap between kuru and CJD [Klatzo et al., 1959]. At that time, speculations to the nature of the scrapie agent ranged from DNA viruses to membrane fragments to polysaccharides to proteins.

In 1966/7, the findings of Tikvah Alper that the scrapie agent resists to DNA elimination by ultraviolet and ionising irradiation, and therefore disproved the involvement of a virus in the pathological process [Alper et al., 1966; Alper et al., 1967]. The protein-only hypothesis was

proposed by the mathematician J.S. Griffith [Griffith 1967]. It states that under certain circumstances proteins might be able to self-replicate and misfold. Patricia Merz discovered scrapie-associated fibrils in all TSEs by EM images [Merz et al., 1983].

The absence of a conventional microorganism responsible for this group of rare neurodegenerative conditions of unknown etiology remained curious throughout the first description. However, PDs remained ill-defined. This may explain the large number of names given to this neurological disorder. CJD, kuru and scrapie are now referred to as prion diseases.

The arduous scientific odyssey in understanding PDs ended up in 1982 as Stanley B. Prusiner coined the term "prion", a PROteinaceous INfectious particle that lack nucleic acids longer than 50 bases. This hypothesis known as the "protein-only hypothesis" defines the prion problem as one of protein structure. The prion concept readily explains how a disease can be manifested as a heritable as well as an infectious illness [Prusiner SB, 1982].

This theory led to a better understanding of the unknown mechanism of prion diseases, including CJD, scrapie and BSE. In 1985, the gene encoding the PrP was identified [Oesch et al., 1985]. Scientists discovered that uninfected people produce a normal form of the PrP protein [Basler et al., 1986]. Shortly afterwards, the first mutation in PRNP was linked to familial PDs [Hsiao et al., 1989] and PrP transgenic mice with the same mutation developed neurodegeneration. Mice lacking PrP (PrP-/-) are resistant to prion infection [Büeler et al., 1993; Sailer et al., 1994]. Essential findings in prion research for the last 20 years are summarized in **Table 1**.

1994	Cell-free conversion of PrP^C to protease-resistant PrP [Kocisko et al., 1994]
1996	First NMR structure of murine PrP^C [Riek et al., 1996]
	New variant of CJD (nvCJD) identified [Will et al., 1996]
	BSE prion strain carries a distinct glycotype signature [Collinge et al., 1996]
1997	Evidence that nvCJD is caused by the BSE agent [Bruce et al., 1997; Hill et al., 1997]
	B-lymphocytes are necessary for peripheral prion pathogenesis [Klein et al., 1997]
1998	Genes controlling incubation period are congruent with *Prnp* [Moore et al., 1998]
1999	Discovery of Doppel, the PrP^C homolog [Moore et al., 1999]
2000	Temporary depletion of lymphoid FDCs impairs prion replication [Montrasio et al., 2000]
2001	Complement involved in prion pathogenesis [Klein et al., 2001; Mabbott et al., 2001]
2003	Transgenic expression of soluble PrP inhibits prion replication [Meier et al., 2003]
2004	Intracerebral inoculation of fibrils consisting of recMoPrP(89-230) produced a transmissible neurologic disease with protease-resistant PrP [Legname et al., 2004]
2005	In vitro generation of infectious scrapie prions [Castilla et al., 2005]
2006	Production of cattle lacking prion protein [Richt et al., 2006]
2007	Formation of native prions from minimal components in vitro [Deleault et al., 2007]

2008	A versatile prion replication assay in organotypic brain slices [Falsig et al., 2008]
2009	PrP^C mediates impairment of synaptic plasticity by amyloid-beta oligomers [Laurén et al., 2009]
2010	Darwinian evolution of prions in cell culture [Li et al., 2010]
2011	Rapid cell-surface prion protein conversion revealed using a novel cell system [Goold et al., 2011]
2012	Human prion protein binds Argonaute and promotes accumulation of microRNA effector complexes [Gibbings et al., 2012]
2013	The toxicity of antiprion antibodies is mediated by the flexible tail of the prion protein [Sonati et al., 2013]

Prion Diseases

Prions, the infectious agents of PDs, inexorably perforate the brain. Before the onset of clinical symptoms, these diseases have incubation times of more than 30 years in humans [Alpers et al., 1979] and are characterized by a myriad of small vacuoles producing a sponge-like appearance and by astrocytic gliosis in microscopic examinations of the CNS [Zlotnik and Stamp, 1961]. The degree of spongiform degeneration is quite variable and it is believed to be due to prion strains and genetic background, whereas the gliosis correlates well with the degree of neuronal loss [Masters and Richardson Jr, 1978]. So far, sixteen different variants of PDs, also known as transmissible spongiform encephalo-pathies (TSEs), have been reported: 9 in humans and 7 in animals [Liberski, 2012]. The most prominent members of PDs in humans are variant and classical Creutzfeldt-Jakob disease (CJD) [Gibbs et al. 1968] and Kuru [Gajdusek et al., 1966]. A wide range of animal species are affected by TSEs (i.e. sheep and goat [Cuille and Chelle, 1939], deer and elk [Wiliams and Young, 1980] and cattle [Hope et al., 1989]).

The origin of PDs can be classified as either inherited, acquired or as sporadic if a genetic or infectious cause can be excluded. Another pathological hallmark of PDs is associated with accumulation of prions, aggregated PrP^{Sc}, the misfolded isoform of host-encoded cellular prion protein (PrP^C) [Prusiner et al., 1981; Prusiner et al., 1984]. Prions are inimitable in that they defy all conventional methods which routinely and reliably deactivate all known bacteria and viruses [Gordon, 1946, Gibbs jr et al., 1978]. Furthermore, prions lack their own genetic information [Alper et al., 1967].

Although prion diseases share certain morphological and pathophysiological features similar to other progressive neuropathologies (e.g. Alzheimer´s (AD) and Parkinson´s disease) they were considered for a long time as unique in that prions are transmissible [Prusiner, 2012]. This view had to be revised recently by the identification of self-propagating Aβ

conformations in AD which spread by cell-to-cell transmission like prions [Stöhr et al., 2012], transmission of pathological α-synclein initiating Parkinson-like neurodegeneration in nontransgenic mice [Luk et al., 2012], or a prion-like infectious cycle of serum amyloid A [Westermark and Westermark, 2010].

Prion Diseases in Animals

PDs in animals mostly occur as infectious disorders. Neuropathological signs are spongiform vacuolation, astrogliosis and the deposition of PrP^{Sc} in the CNS forming amyloid plaques [Aguzzi, 2006]. Naturally occurring scrapie is the ancient and prototypic form of PDs and has been documented in sheep since 1732 [McGowan, 1922]. Scrapie usually affects animals between the ages of 2 and 5 years and the incubation time varies between 1 to 2 years and is accompanied by behavioural changes, blindness and ataxia [Dickinson, 1976]. Death occurs within a few weeks to 6 months after diagnosis [Aguzzi and Calella, 2009]. Various clinico-pathological phenotypes have been seen which may be due to polymorphisms in sheep PrP. Scrapie is not infectious for humans and no link has been found between CJD [Chatelain et al., 1981].

Chronic wasting disease (CWD) is a TSE in free-ranging captive and occurs predominantly in the US and Canada [Sigurdson & Aguzzi, 2007]. The affected species include deer, elk and moose. The origin of CWD is still unknown. Intracerebral transmission of the scrapie agent induces CWD in elk. CWD is experimentally transmissible to cattle, sheep, goats and other animals. Until now, natural transmission of CWD has not been evident in humans.

It happened in 1986, as the outbreak of an unknown brain disease in cattle shocked Europe [Wilesmith et al., 1988] and became popular in vernacular language as “mad cow” disease or bovine spongiform encephalopathy (BSE). At culmination in 1992, nearly 1’000 cattle were affected weekly [see the BSE Portal on the World Organisation for Animal Health website]. The only way to eradicate the excessive spread ended up in slaughtering of 3.7 mio cattle. The likely cause of the BSE epidemic was considered in meat and bone meal contaminated withinfectious prions. A ban of meat and bone meal in ruminants feed ultimately resulted in a decline of the epidemic [Ducrot C, 2008], although sporadically BSE cases still occur. But that was not all, BSE has also been transmitted by contaminated meat to humans in the form of a new variation of Creutzfeldt-Jacob disease (vCJD) [Bruce ME, 1997], which led to 300 victims, mostly in the UK. The origin of BSE is unknown. Natural transmission of BSE to goats and sheep has been reported.

Several other widespread occurrences in TSEs have been observed in other wild or domesticated species of animals, such as cats, mink [Marsh and Hadlow, 1992] and lemurs.

Prion Diseases in Humans

Sporadic Creutzfeldt-Jacob disease (sCJD) is the most frequent human prion disease, which accounts for roughly 85% of all CJD cases [Aguzzi and Callela, 2009]. It also includes fatal insomnia and variably protease-sensitive prionopathy. The annual incidence is 1-2 cases/million population equally distributed in both sexes with a clinical onset between 55 and 75 years [Brown et al., 1986]. Although different variants of sCJD have been classified, at terminal stage most patients become unresponsive to exterior stimuli due to rapid progressive dementia [Rabinovici et al., 2006]. Neuropathological hallmarks are the presence of spongiform changes and sparse PrP^{Sc}-containing plaques in the CNS [Gambetti et al., 2003]. The etiology of sCJD is unknown. Several hypotheses propose that sCJD is caused by somatic mutations in the prion protein gene (*Prnp*) [Gajdusek, 1977] or suggest that spontaneous conversion of normal PrP^{C} into disease-associated PrP^{Sc} may be the trigger of the disease [Prusiner, 1989]. Polymorphisms in the *Prnp* (i.e. M129V) have been associated with a predisposition to the development of sporadic CJD [Collinge et al., 1991].

Genetic PDs are caused by autosomal, dominantly inherited mutations in the prion protein gene (*Prnp*) [Cohen & Prusiner, 1998]. Several different genetic PDs are classified according to clinical symptoms, although all of them result from mutations in PRNP, including familial (f) CJD, Gerstmann-Sträussler-Scheinker syndrome (GSS) [Gajdusek, 1977] and fatal familial insomnia (FFI) [Medori et al., 1992]. The onset of disease is much earlier though, starting between 30 and 60 years of age. Aquired or transmissible human PDs, which account for only 5% of all human TSEs, have been first discovered in the 1920's in Fore people of Papua New Guinea. Among the Fore people a ritualistic practice was to eat the brain of dead relatives, an attempt to become immortal [Glasse 1967]. The disease was named as Kuru. At its peak, the epidemic killed 1-2% of the population. After banning these rituals the epidemic declined. Pretty soon scientists proved that the etiology of Kuru is the consumption of brain; it is also transmissible to chimpanzees [Gajdusek et al. 1966]. Acquired PDs were next discovered in the mid 1970's when hundreds of young people died of spongiform encephalopathy after receiving prion-tainted growth hormones extracted from human corpses [Koch et al., 1985], neurosurgical instruments [Duffy et al., 1974] or dura mater grafts [Thadani et al., 1988]. The latest finding was in the 1990's, the new variant (v) form of CJD which resulted from prions being transmitted from cattle with BSE to humans via consumption of meat products,

especially the brain [Chazot et al. 1996]. vCJD was shown to be transmitted through blood [Llewelyn et al., 2004].

The Cellular Prion Protein (PrP^C)

The Prion Protein (PrP) is 253 amino acid (aa) in length and encoded by the chromosomal prion protein gene, denoted *Prnp*. *Prnp* belongs to the Prn gene family which also encodes *Prnd,* the doppel protein [Moore et al., 1999] and *Sprn,* the shadoo protein [Watts and Westaway, 2007]. All studied PrP genes from various species comprise three exons. The PrP open reading frame ORF is located within one exon. The other two exons contain promoter and termination sites [Basler et al., 1986]. Interestingly, the sequence from more than 45 PrP genes studied so far shows a high degree of conservation, assuming an important function of PrP through evolution [Wopfner et al., 1999].

Like other membrane-resident proteins, PrP is synthesized in the rough endoplasmatic reticulum and travels through the Golgi apparatus to the cell surface [Harris, 1999]. During its biosynthetic maturation, PrP^C becomes post-translationally modified, including cleavage of the first 22 amino (N)-terminal signal peptide, addition of *N*-linked oligosaccharide chains, formation of a disulfide bond and attachment of a GPI anchor (removing of the last 23 C-terminal aa) which promotes its localisation in lipid rafts. PrP^C contains about 45% α-helix [Pan, 1993] and two short stretches of β-sheet [Riek et al. 1996]. PrP^C has two potential sites for glycosylation (asparagines 181 and 197 in mouse PrP^C) whose differential occupancy results in four different subpopulations of PrP^C: unglycosylated PrP^C, monoglycosylated PrP at N181, monoglycosylated PrP at N197 and diglycosylated PrP^C [Haraguchi et al., 1989]. All of these PrP^C subtypes can be distinguished by Western blotting, because of their distinct molecular weight.

The normal PrP^C is a highly conserved protein that has been identified in all mammals and birds so far, as well as in the frog *Xenopus laevis* [Strumbo et al. 2001], and in fish [Oidtmann et al. 2003; Rivera-Mila et al. 2003]. PrP^C is normally expressed at the surface of neurons, various non-neuronal tissues and leukocytes [Aguzzi and Polymenidou, 2004] and attached by a glycolipid moiety [Stahl et al. 1987].

The long N-terminal part (approximately 100 aa) of PrP^C appears to be unstructured according to *in vitro* NMR studies performed with murine recombinant PrP [Hornemann et al., 1997; Riek et al., 1997]. *In vivo*, PrP^C may be part of a protein complex, in which some yet unidentified proteins could serve as chaperones facilitating the folding and function of PrP. The N-terminal part of PrP contains a tandem repeat of an octapeptide repeat.

In contrast to the N-terminus of PrP, the carboxy terminus has a defined structure, which has been extensively analysed [Riek et al., 1996; Wuthrich and Riek, 2001] and was found to consist of two small β-sheets and three longer α-helices, connected by four loops. Another interesting element of PrP is the highly hydrophobic region that lies between the unstructured and the structured part of PrP. This hydrophobic domain is believed to play an important functional role. Transgenic animals expressing N-terminal deletions of aa 45-121 or 45-134 (but not shorter deleations) confers strong neurotoxicity to PrP *in vivo*. This effect is abrogated by (re-) indroducing WT PrP^C [Shmerling et al., 1998].

Although much has been published and speculated, the function of PrP^C is still a conundrum. Definately, PDs cannot propagate in animals devoid of the *PRNP* gene [Sailer et al., 1994]. However, PrP^C`s conserved expression in different species infers some relevance in the basic physiological processes. PrP^C has been proposed to be involved in several functions: copper and/or zinc ion transport or metabolism [Pauly and Harris, 1998; Watt and Hooper, 2003; Brown, 2001], protection from oxidative stress [Brown, 2001], cellular signalling [Chiarini, 2002; Mouillet-Richard, 2000], membrane excitability and synaptic transmission [Mallucci, 2002; Collinge, 1994], neuritogenesis [Graner, 2000] and apoptosis [Chiarini, 2002; Solforosi, 2004]. These functions could be achieved by interaction of PrP^C with different binding partners [Gauczynski, 2001], such as laminin [Rieger, 1997] or the chaperone BiP [Jin, 2000]. A recent publication by Bremer and co-worker showed that neuronal PrP^C and its regulated proteolysis are required to maintan peripheral myelination [Bremer, 2010].

PrP^C Internalization

GPI-anchored proteins (GPI-AP) are an amalgamation of proteins, carbohydrates and lipids. They are organized in specialized membrane domains or “rafts” at the cell surface. GPI-APs are involved in a range of physiological diseases and thus, endocytosis has been intensively debated. A prominent member of GPI-AP is the cellular prion protein (PrP^C). PrP^C is constitutively endocytosed *in vitro* [Harris 2003; Prado et al. 2004]. Cell culture experiments proved that PrP^C traffics through endocytic compartments and recycles back to the cell surface [Shyng, 1993]. Quite notably, internalization of PrP^C has been reported to be inducible by binding of cupric and zinc ions at the N-terminus and thus may have a physiological function in chelating extracellular copper ions [Pauly, 1998; Lee et al. 2001; Watt and Hooper 2003]. Interestingly, N-terminal PrP^C mutants unable to bind copper or zinc ions do not become endocytosed [Perera, 2001]. The biological role of PrP^C internalization is

unknown. However, this process seems to be crucial for conversion of PrP^{C} to PrP^{Sc} [Borchelt, 1992].

Several internalization processes have been shown to be instrumental in the endocytosis of PrP^{C}. Debated are currently clathrin-dependent, caveolin-dependent and clathrin- and caveolin-independent internalization pathways [Harris 2003; Prado et al. 2004]. Clathrin-mediated endocytosis is the uptake of material into cells by which cargo is packaged into vesicles using a clathrin coat [McMahon and Boucrot, 2011]. This modular process is fundamental to neurotransmission, signal transduction and the regulation of many plasma membrane activities. The clathrin-dependent pathway for PrP^{C} internalization was first described by the Harris group [Shyng, 1994]. It was demonstrated that the N-terminal region of PrP^{C} is essential for its localization in clathrin-coated pits and internalization process [Sunyach et al. 2003]. Further studies supported the clathrin-dependent internalization of PrP^{C} in the presence of cupric ions [Taylor 2005 and Taylor and Hooper 2007]. This process is inhibited by treatment with hypertonic medium which disrupts clathrin lattices.

Although many studies have proposed that PrP^{C} is endocytosed via a clathrin-dependent pathway, other studies have reported that PrP^{C} clusters in raft and/or caveolae-like domains [Ying et al. 1992; Vey et al. 1996; Kaneko et al. 1997; Peters et al. 2003; Sunyach 2003]. Importantly, raft-disrupting drugs inhibit PrP^{C} internalisation [Marella et al. 2002; Peters et al. 2003]. More recent results show that PrP^{C} is either internalized in a clathrin-independent pathway that is associated with Arf6 [Kang et al. 2009] or in a clathrin-dependent pathway [Sarnataro et al. 2009].

In summary, there is no consensus how PrP^{C}'s internalization is regulated.

The Scrapie Prion Protein (PrP^{Sc})

PrP can exist in two different conformational states: a normal (PrP^{C}) and an abnormal or alternative isoform of PrP (PrP^{Sc}). For both states, the primary structure is the same as encoded by the PrP gene. No post-translational modifications differentiate PrP^{C} from PrP^{Sc} [Stahl, 1993]. Differences arise at the level of secondary structure, where α-helical PrP^{C} is converted into a mainly β-sheeted PrP^{Sc} isoform [Caughey et al., 1991; Gasset et al., 1993; Pan et al., 1993]. Through these conformational changes, PrP^{Sc} gains several new physico-chemical properties compared to PrP^{C}, such as partial or full resistance to proteolytic digestion [McKinley et al., 1983] or PI-PLC, respectively, as well as a highly-detergent insolubility which may be due to a higher β-sheet structure [Caughey et al. 1991; Pan et al. 1993]. Incubation of a prion infected brain homogenate with proteinase K under defined conditions

results in a complete digestion of PrP^{C}, but not PrP^{Sc}. PrP^{Sc} loses about 65 aa of its N-terminus and maintains its PK-resisitant part. This trait of PrPSc has been served as a surrogate marker of prion infection because PrP^{Sc} co-purifies with infectivity [Prusiner 1982; Gabizon et al. 1988]. Attempts to purify PrP^{Sc} by fractionation and correlating the mass of the purified protein complexes to the infectivity of the samples, indicates that the most infectious prion particle is composed of 14-28 PrP molecules [Silveira et al., 2005]. Although limited resistance to enzymatic digestion has been proved to be a good tool to detect PrP^{Sc}, not all PrP^{Sc}'s are resistant to protease digestion [Hsiao et al. 1994]. Furthermore, PrP^{Sc} from different prion strains or species differ in their susceptibility to protease digestion [Safar et al., 1998]. Furthermore, PrP^{Sc} has the propensity to polymerize into amyloid-like fibrils and aggregates [Marsh et al., 1984; Prusiner et al., 1983] and accumulation of PrP^{Sc} in the brain causes neurodegeneration.

The existence of prion strains is another puzzling phenomenon in prion biology [Aguzzi et al., 2007]. Prion strains are defined as infectious prion agents that exhibit distinct disease-associated phenotypes such as incubation times, histological lesion profiles and neuronal targeting that persist upon serial transmission rounds [Pattison and Millson, 1961; Bruce and Dickinson 1987; Kimberlin, 1987]. The prion strain phenomenon is explained by the protein-only hypothesis as follows: PrP^{Sc} can obtain different pathological conformations, all of which can cause and transmit disease. This is supported by evdence suggesting that different prion strains have different stabilities against chaotropic salts and heat [Safar et al., 1998] and susceptibility to digestion with PK. In addition, the side of protease digestions can vary with different prion strains [Casalone et al., 2004; Zanusso et al., 2004], suggesting a difference in the accessibility of the N-terminal part of the PrP^{Sc} molecule, supporting the idea that PrP^{Sc} conformation can encode strain phenotypes. Of note, it has been shown that different strains can co-exist within the same individual [Polymenidou et al., 2005; Yull et al., 2006]. However, the experimental proof that conformational variants of PrP^{Sc} represent the biological basis of prion strains is still amiss. Whether the impairment of one or more of PrP^{C}s functions, or the gain of a new function by PrP^{Sc}, is related to the development of disease in not known [Martins et al. 2002; Hetz et al. 2003].

Prion Conversion Reaction

Fundamental events in prion propagation and PDs are the presence and the conformational change of PrP^{C} into PrP^{Sc}. According to the "protein-only" hypothesis, there are two models to explain this event **(Fig. 1)**. One of the theories explaining the conversion reaction claim a

template-directed process [Cohen et al., 1994] **(Fig. 1a)**. Endogenous PrP^{C} acts as a template and is refolded into the pathological isoform upon exogenously introduced PrP^{Sc}. A high energy barrier may prevent spontaneous conversion processes. Sporadic CJD may come about through a very rare spontaneous conversion of PrP^{C} to PrP^{Sc}, giving rise to a template-driven conversion cascade, possibly with the help of a chaperone (designated "protein X") [Telling et al., 1995] or a non-protein molecule such as glucosaminoglycans or short nucleic acids [Priola et al., 2003]. Alternatively, the nucleation-polymeratization hypothesis suggests that PrP^{Sc} exists in a reversible thermodynamic equilibrium with PrP^{C} **(Fig. 1b)**.

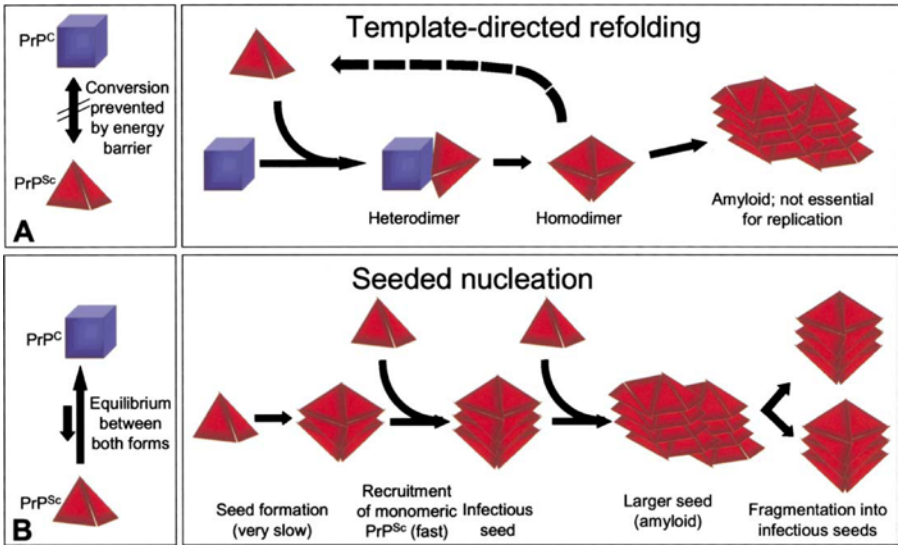

Figure 1. Models for the conversion of normal PrP^{C} into pathological PrP^{Sc}

(a) The "Template-directed refolding model" postulates an interaction between PrP^{Sc} and PrP^{C}, which is subsequently induced to transform itself into PrP^{Sc}. A high energy barrier may prevent spontaneous conversion of PrP^{C} into PrP^{Sc}. **(b)** The "nucleation-polymerization model" proposes that PrP^{C} and PrP^{Sc} are in a reversible thermodynamic equilibrium. Only if several monomeric PrP^{Sc} molecules from a highly ordered seed, can further monomeric PrP^{Sc} entities be recruited and eventually generate larger aggregates with an amyloid structure. Within such a crystal-like seed, PrP^{Sc} becomes stabilized. Fragmentation of PrP^{Sc} aggregates increases the number of nuclei, which can then recruit further PrP^{Sc} and thus replicate the prion agent [Figure and text from Aguzzi and Polymenidou (2004). Mammalian prion biology. One century of evolving concepts. Cell 116:313-27].

Only if several monomeric PrP^{Sc} molecules are organized into higher-ordered seeds, further monomeric PrP^{Sc} can be recruited and eventually aggregate to amyloids. Breaking of PrP^{Sc} aggregates increases the number of seeds, which can recruit further PrP^{Sc} and thus results in replication of PrP^{Sc} [Jarrett & Lansbury jr, 1993]. The seed formation is an extremely slow event. According to the "nucleation hypothesis", the aggregated state and not necessarily the misfolded form of PrP, would be an intrinsic property of infectivity. It is believed that PrP^{C} enters first a metastable intermediate, partially unfolded state, referred to as PrP* [Weissmann,

1991; Cohen et al. 1994] before it interacts with PrP^{Sc} to undergo a conversion. Experimentally, an assumed PrP* -like state is achieved either by denaturation with GdnHCl [Kocisko et al. 1994] or with exposure to sonication [Castilla et al. 2005]. For years, the assistance of an ominous "protein X" was haunted the prion field which facilitates to enter the PrP* state and enables the conversion of PrP^{C} into PrP^{Sc} through PrP^{C} binding. "Protein X" has yet to be identified in animals [Tamgüney et al. 2008].

However, testing these hypotheses needs precise knowledge of the structure of both PrP^{C} and PrP^{Sc}. To date, the 3D NMR resolution structure of mouse, hamster and human PrP^{C} [Riek et al., 1996; James et al., 1997; Hosszu et al., 1999] for example and the study of amyloids has provided some suggestions for a possible conversion mechanism [Lu et al., 2007]. However, the limited amount of PrP^{Sc} and its insolubility compared to PrP^{C} has prevented the generation of a high resolution structure of PrP^{Sc} and the understanding of the conversion process itself.
It should be noted, that both models fail to explain some aspects in PDs, suggesting that a factor might be missing in the equation. How can it be possible that sporadic PDs occur exclusively in elderly patients? If the formation of PrP^{Sc} is a rare and random event, sporadic CJD should occur both in young, as well as in elderly people. This is not the case.

Prion Pathogenesis

The mechanisms underlying prion pathogenesis leading to gliosis, spongiosis and neuronal cell death are not yet understood. Mice devoid of PrP^{C} do not show any signs of neurodegeneration [Büeler et al., 1992] and abolish prion replication upon intracerebral inoculation with prions [Büeler et al., 1993]. Mice expressing a secreted form of PrP^{C} termed "GPI-anchorless" PrP^{C} replicate PrP^{Sc} upon inoculation with prions but do not develop histopathological changes [Chesebro et al., 2005]. In addition, spongiosis and behavioral changes can be reversed by conditionally removing of PrP^{C} selectively in neurons after disease onset [Mallucci et al., 2007]. This illustrates that the expression of membrane bound PrP^{C} is required for cellular toxicity.
Hematopoietic cells are involved in transporting prion infectivity from peripheral entry sites to secondary lymphoid organs in which prions accumulate and/or replicate. Functional FDCs [Montrasio et al., 2000; Mabbott et al., 2003] and B lymphocytes [Klein et al., 1992] are crucial to peripheral prion accumulation. However, it seems that the primary compartment for prion neuroinvasion is nonhematopoietic, because it cannot be adoptively transfered by bone marrow reconstition [Kaeser et al., 2001; Blättler et al., 1997; Klein et al., 1997]. Prions, taken

up by ingestion, are transported by intestinal epithelial cells through the epithelium [Heppner et al., 2001]. Neural entry and transit to the CNS of prions may occur by prion uptake by nerve endings in the intestine. In addition, the vagal nerve and the sympathetic nervous system are involved in the transport of prions to the CNS [Beekes et al., 1996; Glatzel et al., 2001].

Prion Diagnosis

As in other diseases, early diagnosis would be beneficial and increases the chances to cure the disease. Unlike other infectious diseases caused by viruses or bacteria, PDs are difficult to diagnose using conventional methods such as serology or PCR. The diagnosis of PDs is further complicated by the uneven distribution of the prion agent in body tissues, with highest concentrations found in the CNS and very low concentrations in easily accessible body fluids such as blood and urine [Aguzzi & Glatzel, 2005]. Compared to other fields in diagnostics, presymptomatic diagnosis in PDs is almost impossible. The earliest possible diagnosis is based on clinical signs and symptoms after the disease has considerably progressed. Definite diagnosis of PDs is determined *post mortem* by immunohistochemistry.

The discovery by Stanley Prusiner and co-workers, in which misfolded PrP^{Sc} is the disease causing agent of prion diseases, as well as the resistance of PrP^{Sc} against proteolytic degradation [McKinley et al., 1983], stood for a turning point in prion research and diagnosis. These remarkable findings identified PrP^{Sc} as a surrogate marker of prion infection. Even thirty years after its first description, detection of PK-insensitive prion protein is the gold standard for prion diseases and is the basis for all the currently available detection methods [Aguzzi and Polymenidou, 2004].

The most common techniques for measuring PrP^{C} and PrP^{Sc} in brain samples are either done by Western blotting [Inoue et al., 2005] or by ELISA [Grathwohl et al., 1997] after PK digestion. After degradation of PK-sensitive PrP, the remaining resistant form can be detected. ELISA enables simmultanous analysis of larger number of samples than Western blotting, which represents a major advantage. However, to measure PrP^{C} and PrP^{Sc} from a huge variety of different sources at the same time, the assay has to be done in a homogeneous phase. A popular choice for homogeneous assays is Förster/Fluorescence Resonance Energy Transfer (FRET).

In addition to PK treatment the CDI (conformational dependent immunoassay) assay uses the differential binding of antibodies to native or denatured PrP^{Sc}. The detection antibody recognises a conformation-dependent epitope. It only becomes exposed in the infectious form upon denaturation while it is always exposed in the non-infectious form (PrP^{C}) [Safar et al.,

2005]. Another approach to detect PrP^{Sc} is called PMCA (protein misfolding cyclic amplification), in which PrP^{Sc} can be amplified. Here, PrP^{Sc}-containng brain homogenate is diluted in normal brain homogenate and after various incubation and sonication cycles, amplified PrP^{Sc} can be measured [Castilla J et al., 2005]. Although PMCA is a very sensitive method, PK-resistant material can be formed in the absence of prions and thereby leading to false positive results.

Luminescent conjugated polymers (LCPs) are able to bind with striking affinity to a variety of amyloids. The interaction is measured by characteristic spectral changes specific to distinct amyloids upon binding [Sigurdson et al., 2007].

Prion Drug Treatment

So far no efficient treatments against prion diseases are available [Appleby and Lyketsos 2011], although many compounds that inhibit prion propagation have been identified in prion-infected cultured cells [Korth et al., 2001] and in animal models [Pocchiari et al., 1987]. These include polysulphated polyanions [Caughey and Raymond 1993], polyamines [Supattapone et al. 1999], tetrapyrroles [Caughey et al. 1998], polyene antibiotics [Pocchiari et al. 1987], tetracyclic antibiotics [Forloni et al. 2002] and tricyclic compounds [May et al. 2003]. Polyanions interact and stabilize PrP^{Sc} as shown for Congo red [Ingrosso et al., 1995] and prolong incubation times in rodent models upon co-inoculation with prions [Caspi et al., 1998].

Prion Bioassays

The classical method for measuring prions *in vivo* consists of inoculating test material into susceptible indicator animals [Cuille and Chelle, 1939; Gordon, 1946; Chandler, 1963]. End-point dilutions of the test material allow precise prion titer determination [Prusiner, 1978]. These experiments require a very large number of indicator animals. In addition, these bioassays require observation periods which often span the entire life of indicator animals. In early studies of scrapie using sheep and goat, incubation periods of one to three years were required. The discovery of experimental transmission of scrapie from sheep to mice ushered in a new era of prion disease research [Chandler, 1961]. The incubation periods were shortened to four to five month. With the generation of transgenic mice that overexpress PrP genes, an animal model was found with even shorter incubations times [Carlsen et al., 1994]. However, this common technique is expensive and time consuming. The introduction of the prion organotypic slice culture assay (POSCA) by Jeppe Falsig et al. 2008 has eliminated

some of the concerns listed above [Falsig et al., 2008]. This method allowed a dramatic acceleration of prion replication *ex vivo*.

The discovery that mouse neuroblastoma cells (N2a) propagate prions derived from sheep with scrapie and humans with CJD [Kingsbury et al., 1984; Race et al., 1987], enabled the use of cultured cells to study prions. The scrapie cell assay in end-point format (SCEPA) is the most common solid-phase *in vitro* prion assay [Klohn et al., 2003]. It enables the quantification of the prion titer in prion-susceptible cells after PK digestion and reduced the time of the experiment down to three weeks. This assay has been assessed by exposing cells to serial dilutions of prion-infected mouse brain homogenates. The dilution rate which yields to a negative outcome in a dot blotting assay for PrP^{Sc} has been determined to be the infectivity level. The application spectrum of this prion assay can be extended to other cell lines and to the use of different prion strains serving as inoculum. [Mahal et al., 2007]. To achieve accurate and precise measurement of a large variety of different samples, the SCEAPA has to be done in a homogeneous phase, which is much faster to do than heterogeneous assays. A popular method for homogeneous assays is Fluorescence Resonance Energy Transfer (FRET).

Förster/Fluorescence Resonance Energy Transfer (FRET)

Principles and Requirements of FRET

FRET is a distance-dependent and non-radiative energy transfer from a donor fluorophore to a light-absorbing acceptor molecule [Selvin et al., 1994] and was first described by Theodor Förster in the late 1940s [Förster, 1946; Förster, 1948]. FRET occurs at distances beyond orbital overlap and below radiative transfer interactions, between an excited donor fluorophore and a ground-state acceptor at distances of 1-20 nm [Geissler et al., 2010]. In compliance with the resonance condition, the luminescence energy of the donor must be equal to the absorption energy of the acceptor **(Fig. 2)**. Due to FRET, the intensity of the donor fluorescence decreases while the intensity of the acceptor fluorescence increases. The FRET efficiency of this energy transfer is inverserly proportional to the sixth power of the distance between the donor and acceptor molecule ($E_{FRET} \sim r^{-6}$) which makes FRET extremely sensitive to small distances [Stryer & Haugland, 1967]. The distance at which the energy transfer is 50% is called the Förster distance or Förster Radius [Förster, 1948].

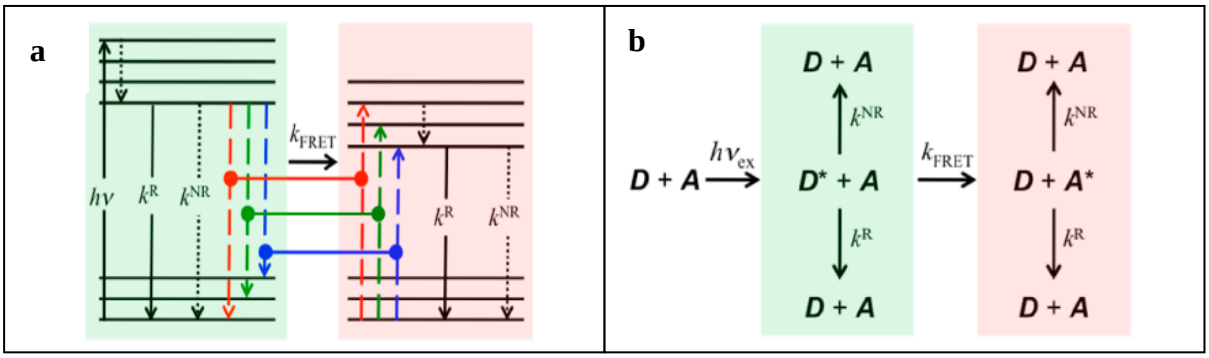

Figure 2. Principle of donor (green background) and acceptor (red background) interaction in FRET

a) Energy-level diagram representing excitation of the donor (hυ) followed by inner relaxation (dotted arrow), followed by radiative decay (k^R), non-radiative decay (k^{NR}), or FRET (k_{FRET}). The energy resonance condition [ΔE(donor) = ΔE(acceptor)] is represented by the colored lines connecting donor and acceptor transitions. After FRET, the acceptor is in an excited state, followed by raditive or non-radiative decay to its ground-state. b) Different energy pathways after donor excitation ($hυ_{ex}$) leading to radiative (k^R) or non-radiative (k^{NR}) decay of the donor or acceptor in case it is excited by FRET (k_{FRET}). D, D* and A, A* indicate the ground or excited state of the donor and acceptor, respectively. Figures and text from Geissler et al., 2013.

Currently, lanthanide chelates are predominantly used as donor fluorophores in FRET applications. Unlike formerly used organic dyes, they have unique properties. One of their characteristics is their extremely long excited-state lifetimes (up to several milliseconds) which enable time-resolved (TR) measurement of the acceptor emission. This trick decreases the effect of autofluorescence as well as direct acceptor excitation and makes FRET a particular sensitive technique. Another one is that their emission spectra are narrow and well separated and their Stokes' shifts are long [Hemmilä and Laitala, 2005]. Several different lanthanides (Europium, Terbium, Samarium, Dysprosium) are available with unique spectral properties and a large variety of acceptor molecules.

The Europium chelate [www.PerkinElmer/LANCE] is composed of an emitting Europium cation (Eu^{3+}) coordinated by an aromatic ligand, which serves both as a photo-collecting antenna and as a protective shield towards interacting solvent molecules. Because of the indirect excitation of the Eu^{3+} through the coordinated ligand, the excitation and emission wavelengths of the complex are at different energy levels referring a large Stokes' shift [Hemmilä, 1999].

Terminology and FRET Assays in Prion Biology

FRET assays can be categorized into four different classes. They are either competitive or non-competitive and are performed either in a homogeneous or in a heterogeneous phase. Non-competitive assay formats are defined as the recognizing agent bound to the analyte is

the source of the FRET signal. Thus, in non-competitive FRET assays the signal increases with increasing analyte concentration. In competitive assays, the signal created by agent is not bound to the analyte. Typically, non-competitve assays are considered to have a higher sensitivity than competitive ones [Wild et al. 2005]. In heterogeneous assays, the analyte is physically bound to a solid-phase. The advantage in this assay format is to remove free label or interfering factors by a washing step before measurement. This is not the case in homogeneous assays which have no separation step and are often called “mix and measure” assays. Homogeneous assays are very popular when the number of samples is large and/or the speed of the assay is important. Heterogeneous assays are considered to be more sensitive.

Recently, a Terbium-based FRET assay was introduced in prion biology by Karapetyan et al., 2013. Because PrP^{C} is necessary for PrP^{Sc} replication, they developed a homogeneous assay which enables the detection of PrP^{C} at the surface of living cells. By screening for compounds which down regulate cell surface expression for PrP^{C}, they established an unique drug screening platform which could also be applied to treat Alzheimer's disease [Karapetyan et al., 2013].

AIMS OF THE THESIS

The focus of the current study was to develop FRET-based immunoassays which enable the detection of PrP^{C} and PrP^{Sc} in high-throughput applications **(Fig. 3)**. The aim is to use this novel platform to perform RNAi, substance and drug screenings.

More specifically the aims were:

Part I **Development of a sandwich ELISA which discriminates between PrP^{C} and PrP^{Sc}**

To assess whether the FRET technology can be applied to detect PrP^{C} and PrP^{Sc} in cell lysates, the first goal was to develop a sandwich ELISA which discriminates between both PrP isoforms. More specific aims were:

(i) To generate chronically prion-infected cells and determination of PK-resistant material by SCA and Western blotting.

(ii) Because PrP^{Sc} resembles repeated aggregates of misfolded PrP^{C}, detection of PrP^{Sc} with the same antibody twice should be tried [Pan et al., 2005] otherwise PK digestion of cell lysates and denaturation of PrP^{Sc} should be considered.

(iii) Among the anti-PrP POM antibody library the best ELISA antibody combination should be identified by the detection limit of PrP^{Sc} and by the signal-to-noise ratio. By calculating the Z' factor for the PrP^{Sc} sandwich ELISA, the feasibility for further development into a homogeneous FRET-based application with high-throughput potential should be determined.

To further validate the PrP ELISA, results should be compared and correlated with two other prion assays, the SCA and the protein misfolding assay. Furthermore, the PrP ELISA should be applied to answer the question whether LCP treatment influence prion replication in cerebellar slice culture tissues.

Part II **Development of FRET-based immunoassays which detect recPrP, PrP^{C} and PrP^{Sc}**

The goal of this project was to establish TR-FRET-based high-throughput methods for detection and quantification of various PrP species.

(i) The first aim was to detect recPrP in a homogeneous phase in a 384-well plate format by FRET. To achieve this aim, the best FRET antibody pair has to be determined according to the limit of detection for recPrP and to the signal-to-noise ratio.

(ii) The second aim was to determine the amount of PrP^{C} and PrP^{Sc} in prion-infetced cell lysates and brain homogenates by FRET. Therefore, best lysis, digestion and denaturation conditions for PrP^{C} and PrP^{Sc} have to be evaluated. Various POM antibody combinations should be tested and validated according to the limit of detection for PrP^{C} and PrP^{Sc} and to the signal-to-noise ratio. By calculating the Z' factor for each PrP FRET assay, the feasibility for automatisation by robotics at a high-throughput level should be determined.

(iii) The third aim was to detect PrP^{C} on the surface of living cells in the 384-well plate format. In cell titration experiments, best FRET antibody combination should be determined according to the limit of detection for PrP^{C} and to the signal-to-noise ratio. The feasibility to monitor changes of PrP^{C} cell surface expression by FRET should be tested. The principle that the FRET signal intensity depends on distance should be applied to study the internalisation of PrP^{C} in living cells. If this is possible, siRNA treatment should be done to study genes involved in the internalisation of PrP^{C}.

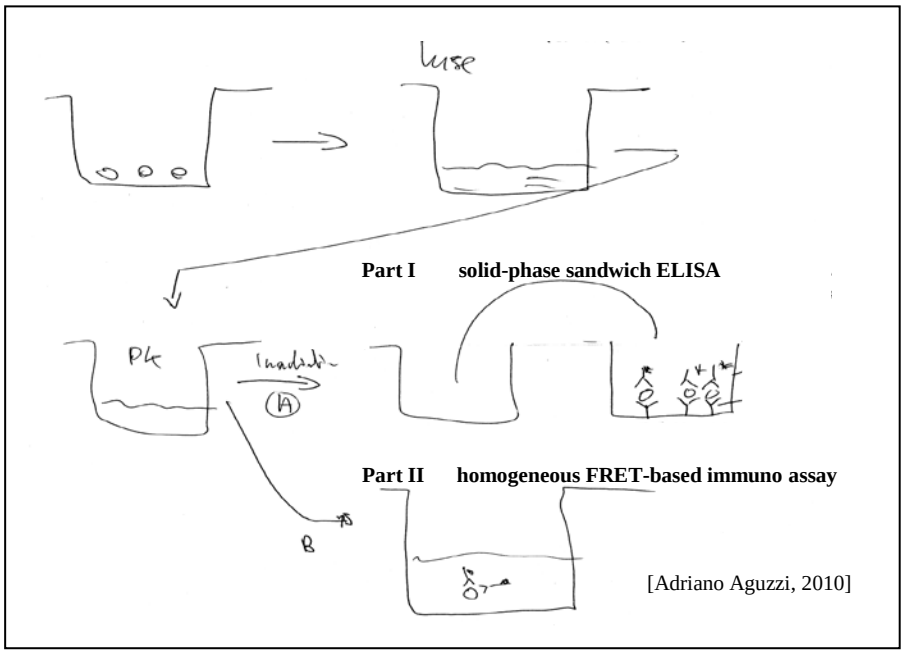

Fig. 3. Aims of the thesis

To discriminate between normal PrP^{C} and infectious PrP^{Sc}, samples are lysed and digested with proteinase K (PK). After PK inactivation, PrP^{C} and PrP^{Sc} are detected by a solid-phase sandwich ELISA **(Part I)** or by a homogeneous FRET-based immunoassay **(Part II)**.

PART I RESULTS

PrP^{C} and PrP^{Sc} Enzyme-Linked Immunosorbent Assay (ELISA)

Principle of the Sandwich ELISA

An ELISA is an analytical test which uses antibodies to detect a substance [Crowther, 2001]. The substance, usually an antigen in liquid solution, is immobilized on a solid support either non-specifically via adsorption or specifically by catching via a particular antibody to the surface. A sandwich ELISA is a solid-phase enzyme immunoassay which needs at least two antibodies, a catching and a detection antibody. Usually, a polystyrene microtiter plate is coated with a specific catching antibody which binds the antigen on the plate. By adding the detection antibody a complex is formed with the antigen. The detection antibody can be directly linked to an enzyme or indirectly via a second antibody conjugated with an enzyme. The addition of the enzyme's substrate produces a signal which is proportional to the antigen-enzyme complex. Between each step, the plate is typically washed with a mild detergent buffer to remove unbound and unspecific sample [Crowther, 2001] **(Fig. 4a)**.

To develop a sandwich ELISA which detects PrP^{C} and PrP^{Sc} from various biological samples, I used our in-house PrP targeting POM antibody library [Polymenidou et al., 2008; Sonati et al., 2013]. More than 15 different in-house monoclonal antibodies are available for PrP detection **(Fig. 4b)**.

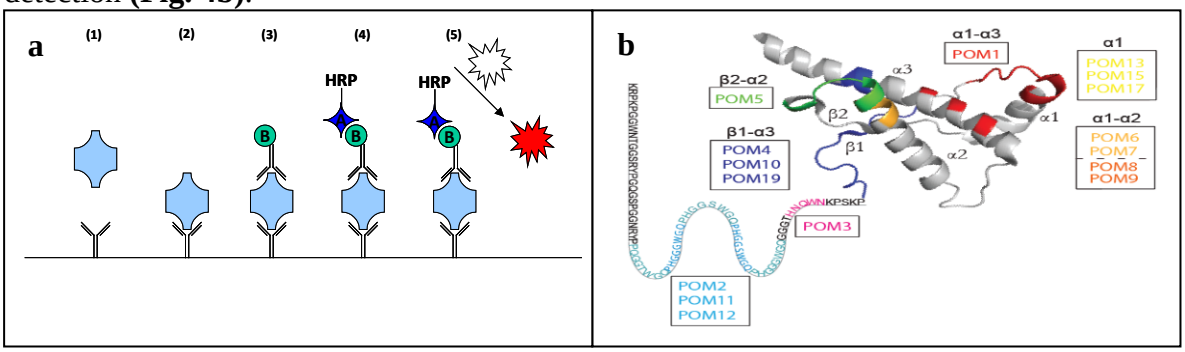

Figure 4. Principle of the solid-phase sandwich ELISA and anti-PrP POM antibody library

(a) Principle of a sandwich ELISA. A clear 96-well microtiter plate is coated with the capture antibody and sample is added (1). Any antigen within the sample binds to the capture antibody (2). Detection antibody with a biotin tag is added and binds to immobilized antigen (3). Avidin-HRP conjugate is added and binds to the biotinylated detection antibody. HRP enzyme substrate is added and converts to a detectable signal (4) and (5). **(b)** Schematic illustration of PrP and its POM antibody epitopes. The POM1 and POM19 antibody recognises PK-resistant epitopes at the C-terminus of PrP. The POM2 antibody has four binding epitopes [Figure was taken from Sonati et al., (2013). The toxicity of antiprion antibodies is mediated by the flexible tail of the prion protein. Nature 501:102-106].

In order to develop an ELISA that discriminates between PrP^{C} and PrP^{Sc} from prion-infected cell lysates, various parameters were tested. First, a prion infectivity protocol was established for several different murine cell lines. Prion infectivity was measured from various prion strains by the scrapie cell assay (SCA) and a time course analysis of prion-infection was done. To detect PrP^{Sc} by ELISA, cell lysis conditions, proteolytic digestion and its inactivation, as well as a denaturation step was tested.

Prion Infectivity Protocol for Murine Cell Lines

To infect cells with prions, I used a protocol which is used in the SCEPA [Klohn et al., 2003]. Prion susceptible cells were co-cultured with prions originating from brain homogenates of terminally sick mice. Several cell splits are necessary to get rid of the initial inoculum. Two different murine cell lines were tested, namely neuroblastoma-derived N2aPK1 and hippocampal CAD cells. Hpl PrP-deficient (Hpl KO) cells were used as negative controls. All cell lines were infected with two different prion strains: RML and Me7. To determine PrP^{Sc} in lysates, cells were digested with PK at different concentrations. PK inactivation was done by heating. PrP^{C} and PrP^{Sc} detection was assessed by Western blotting using the POM1 antibody **(Fig. 5a)**. In the presence of 5 to 20 μg/ml PK no PrP^{C} was detectable in non-infected N2a cells. In contrast, RML-infected N2a cells (N2aRML) digested with even 10 μg/ml PK showed a weak signal for PrP^{Sc}. Prion infectivity was determined by SCEPA **(Fig. 5b)**. Here, 20'000 non-infected cells (N2a, CAD, Hpl KO) were either inoculated with RML or Me7 prion strain with prion titers ranging from 10^{-3} to 10^{-8}. After every third day, cells were harvest from the flaks and diluted 1 to 10. This process was repeated two times. No initial inoculum was detected in Hpl PrP KO cells after three 1:10 cell splits. Both cell lines showed different properties in prion replication. Me7-infected N2a cells showed a lower replication rate of prions compared to RML-infected N2a cells. In contrast, both prion strains replicated at a higher level in CAD cells. These results are in line with earlier published reports [Mahal et al., 2007]. According to literature, prion replication in cells decreases after several cell splits. For that, prion titer of RML-infected N2a cells was monitored from three to 20 1:10 cell splits. Prion titer decreased after 20 splits about 1 log unit **(Fig. 5c)**. For the further experiments, I decided to use N2a cells infected with the RML prion strain at a concentration of 10^{-4}. N2aRML cells were used only to the 10^{th} cell passage.

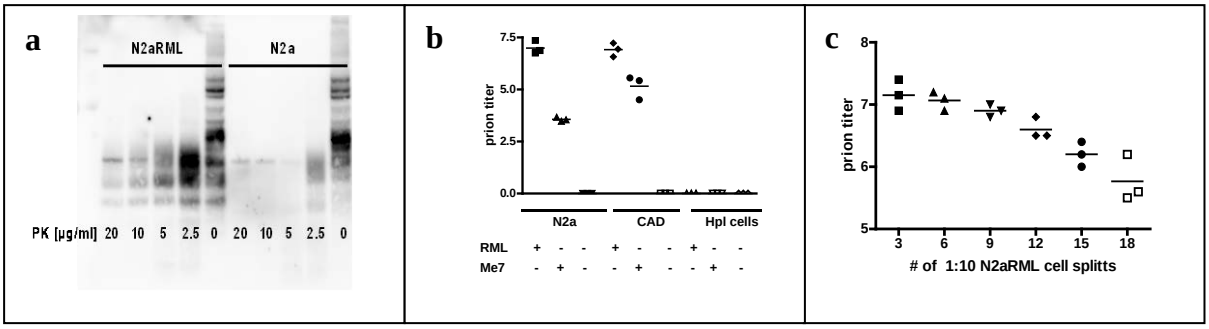

Figure 5. Western blot analysis, scrapie cell assay (SCA), and prion titer time course analysis

(a) The Western blot shows the PrP^{C} and PK-resistant PrP^{Sc} levels of N2a and N2aRML-infected cells. PrP^{C} levels of non-infected N2a cells disappeared in the presence of 5 µg/ml PK. PrP^{Sc} is still detectable at a PK concentration of 10 µg/ml. **(b)** Prion titers of RML- or Me7-infected N2a or CAD cells from three different biological samples are shown. **(c)** Summarized are the prion titers of N2a cells infected with 10^{-4} RML during 18 cell splits. Shown are biological triplicates.

Cell Lysis Conditions

In a first set of experiments, I tested various cell lysis conditions, such as the concentration of different detergents as well as temperature. In a clear 96-well plate, 20'000 non-infected and RML-infected N2a cells were plated and digested in TBS buffer in the presence of 0.3, 1.5 and 3% of either Tween20 or TritonX100 at 37°C or 4°C for 30 min. Protein concentration was assessed by Bradford assay **(Fig. 6)**. The digestion with Tween20 and TritonX100 was more efficient in N2a cells at 37°C and at the highest detergent concentration used than at 4°C with the same concentrations **(Fig. 6a/c)**. In N2aRML-infected cells, lysis was more efficient at 4°C compared to 37°C **(Fig. 6b/d)**.

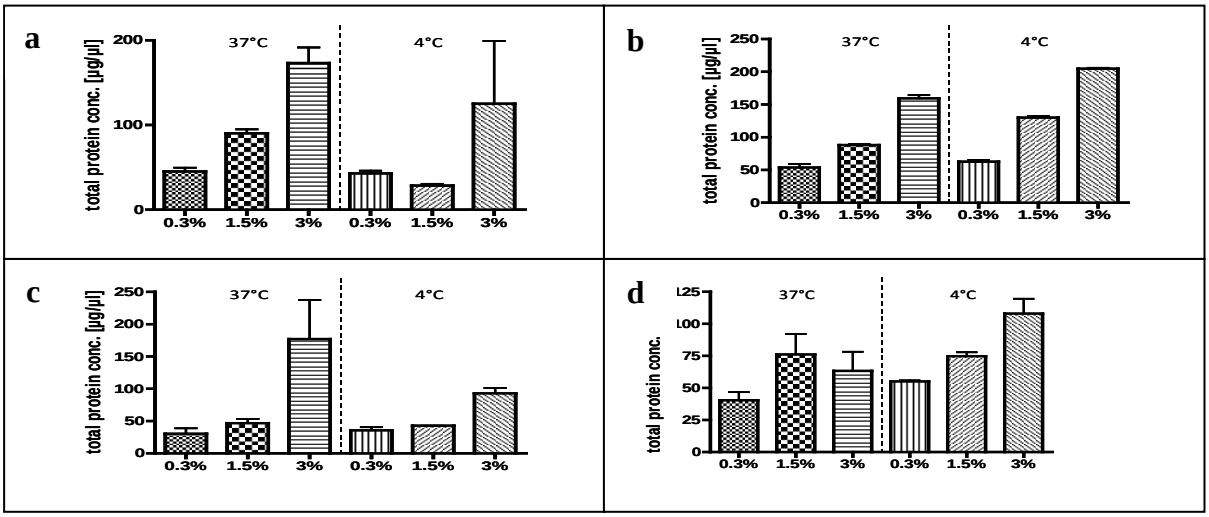

Figure 6. Cell Lysis conditions

In **(a)** are shown cell lysis conditions of Tween20 in N2a cells at two different temperatures. In **(b)** for N2aRML cells. The same experiments were done with TritonX100 in N2a **(c)** and N2aRML cells **(d)**. Shown are biological duplicates.

Proteinase K (PK) Digestion and its Inactivation

The gold standard assay for assessing the detection of PrP^{Sc} relies on the resistance to digestion with proteinase K (PK) [Bolton et al., 1982]. The native PrP^{C} protein is sensitive to hydrolysis by proteases (PK, trypsin, SV-8), PrP^{Sc} only partially. However, denaturation by boiling in sodium dedecylsulfate (SDS) or β-mercaptho-ethanol rendered PrP^{Sc} susceptible to proteolytic digestion [McKinley et al., 1983]. The relative resistance of PrP^{Sc} to PK depends on the activity of PK [McKinley et al., 1983], on lysis conditions [Madec et al. 1997; Oesch et al 1994], on the concentration of non-PrP contaminants and prion strains.

The first goal was to combine cell lysis and PK digestion in a single step. For that, PK enzyme was titrated in the presence of N2aRML cell lysate under different lysis conditions in a clear 96-well plate. Normal N2a cell lysate was used as a negative control. Various ionic and non-ionic detergents at various concentrations and different combinations were tested **(Fig. 7)**. The lysis and digestion was performed at 37°C for 30 min. The detergent influences the PK resistance of PrP^{Sc}, either by enhancing or diminishing signal intensity. Best lysis and digestion conditions were found with TBST (Tris-HCl pH 7.5 + 1.5% Triton X100) for 30 min at 37°C on a shaking platform (600 rpm) **(Fig. 7c)**. Cell lysates were subjected to digestion with various concentrations of PK. PrP^{C} and PrP^{Sc} content was detected by sandwich ELISA with POM1 as catching and biotinylated-POM19 as detection antibody. Digestion of 50 µg total protein concentration with 10 µg/ml PK in a reaction volume of 50 µl (corresponding to 1 mg/ml total protein concentration) was found to ensure complete and consistent removal of PrP^{C} in N2aRML cell lysates.

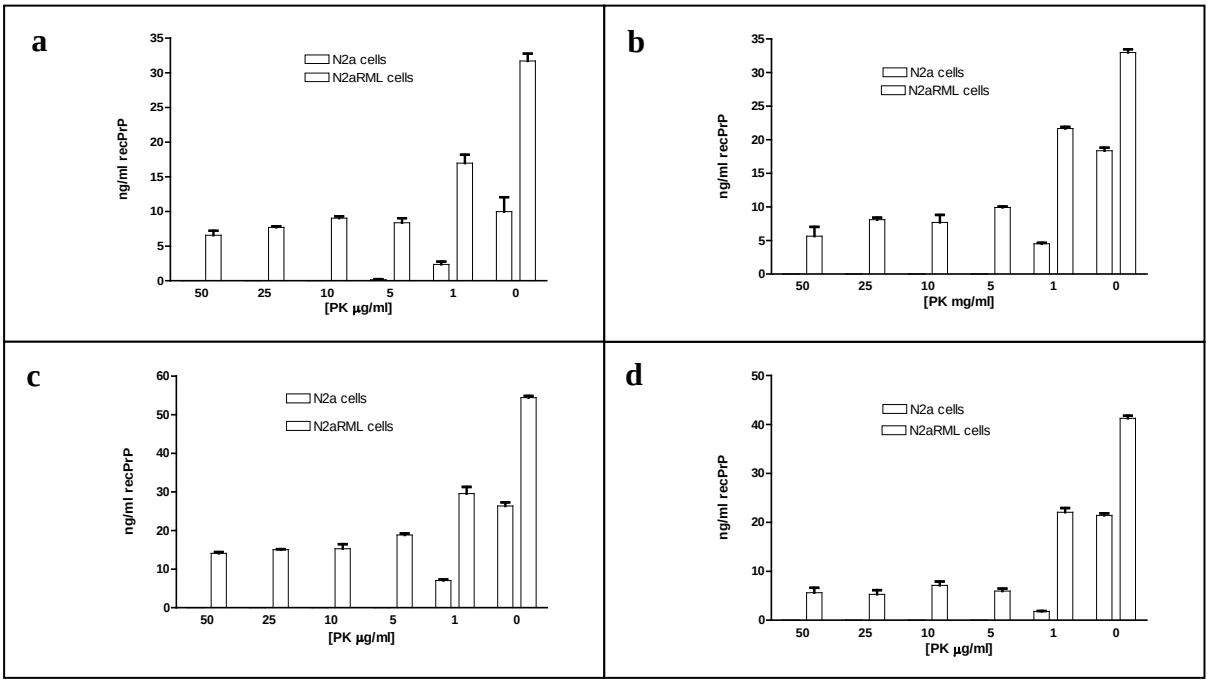

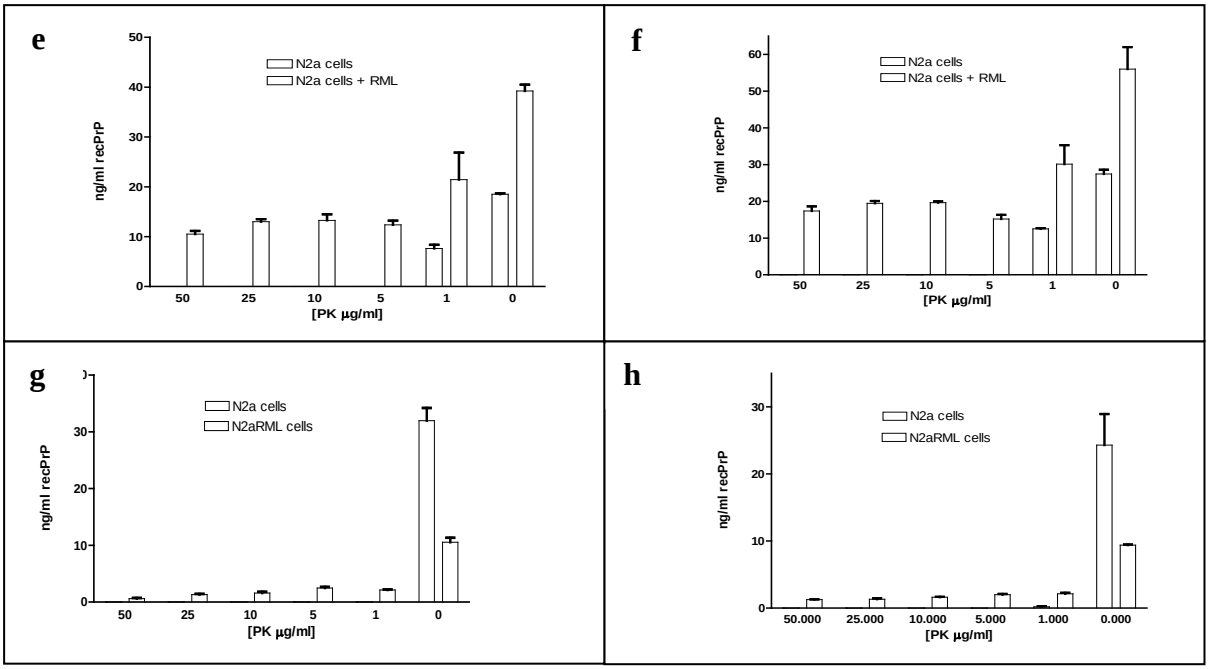

Figure 7. Cell lysis conditions and PK titration in a single step (opposite page)

In all experiments, N2a and N2aRML cells were digested with the same concentrations of PK ranging from 0 to 50 µg/ml. At the same time, cell lysis occurred in the presence of various detergents at different concentrations, such as **(a)** Tween20 1.5%, **(b)** Tween20 3%, **(c)** TritonX 1.5%, **(d)** TritonX 3%, **(e)** Tween20/TritonX 1.5%, **(f)** Tween20/TritonX 3%, **(g)** SDS 1.5%, **(h)** SDS 3%. Digestion with saponin (not shown) gave similar results as digestion with SDS. All experiments were performed at 37°C during shaking. Shown are triplicates.

One way to inactivate PK is by heating the samples at 95°C for ten min, which is suitable for small sample sizes, for example in Western blotting experiments [Bolton et al., 1982]. This procedure is inapplicable in ELISA experiments when working in the 96-well plate format. Here, PK's activity was halted by the cysteine proteinases inhibitor phenylmethylsulfonyl fluoride (PMSF). To determine PK inactivation, PrP-deficient Hpl cell lysate was digested with 10 µg/ml PK for 30 min at 37°C. Different concentrations of PMSF were either added or not for 10 min and thereafter spiked with recPrP for 10 min. Results in **Fig. 8** showed that 2 mM or higher concentrations of PMSF were sufficient to block the activity of PK. For all further experiments, 10 µg/ml PK was inactivated by 2 mM PMSF for 10 min at room temperature during stirring.

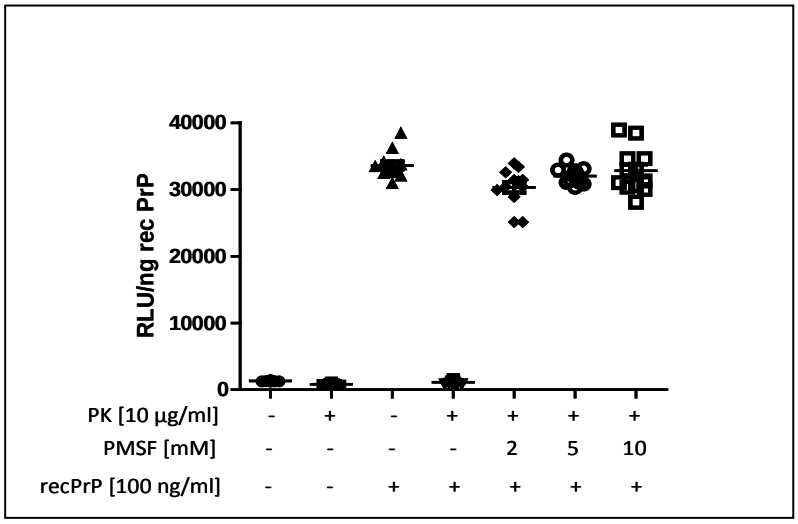

Figure 8. PK inactivation by addition of PMSF

Hpl cell lysate was digested with a constant concentration of 10 µg/ml PK for 30 min at 37°C during shaking. The PK inhibitor PMSF was added at different concentrations for 10 min. To show PK inactivation, samples were spiked with recPrP and incubated for further 10 min. POM1 was used as coating antibody, biotinylated POM19 antibody as primary one. Shown are hexaplicates.

Denaturation of PrP^{Sc} with Guanidinium Thiocyanate (GdnSCN)

Attempts to detect PrP^{Sc} by ELISA after proteolysis with only PK digestion were not sufficient. Detection of PrP^{Sc} can be enhanced by including a denaturation step which loosens the aggregated state of the PrP^{Sc} particles and therefore unmasks some PrP epitopes. The effect of the chaotropic salt GdnSCN (guanidinium (Gdn), thiocyanate (SCN)) was explored on a recPrP standard curve. GdnSCN was diluted 1:1 in $NaHCO_3$ to an end concentration ranging from 0.2 to 3 M and then incubated with recPrP for 10 min at room temperature. Samples were transferred into a POM1-coated plate and detection was done via biotinylated-POM19 antibody. An increase in RFU was observed for up to 0.5 M GdnSCN. The signal decreased with increasing GdnSCN concentrations **(Fig. 9)**, presumably by interfering with both antibodies. For all following experiments, samples were denatured with 3 M GdnSCN and diluted with 0.1 M $NaHCO_3$ pH 8.9 to an end concentration of 0.5 M GdnSCN.

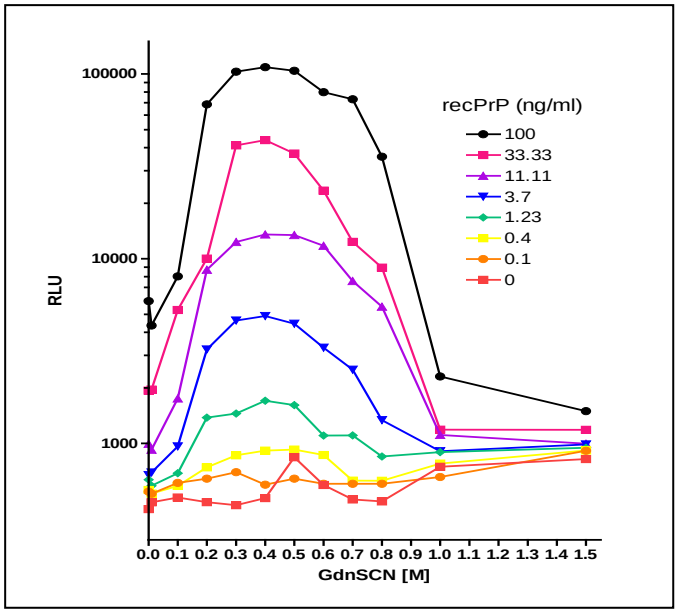

Figure 9. Titration of the denaturation agent GdnSCN

Increasing concentrations of GdnSCN/$NaHCO_3$ were added to recPrP at the indicated concentrations and incubated for 10 min at room temperature. Samples were transferred onto a POM1-coated plate and detected with biotinylated POM19 antibody. Shown are monoplicates.

Antibody Titration

Forced through the conformational change of PrP^C to PrP^{Sc}, the C-terminal part of PrP^{Sc} becomes protease resistant. Therefore, only protease-insensitive POM-epitopes, mainly located at the C-terminus of PrP, enable the detection of PrP^{Sc} by sandwich ELISA. The first choice was the POM1/POM19 antibody pair, many times used in PrP^{Sc} Western blot experiments. Both POM1 and POM19 were tested either as coating or as biotinylated primary antibody. Titration experiments were performed at a constant amount either with recPrP or N2a cell lysate. Better results were found when using POM1 as coating antibody.

At a POM1 concentration of 400 ng/ml, the saturation point was reached for recPrP **(Fig. 10a)** as well as PrP^C from crude cell lysate **(Fig. 10b)**. Titration experiments for biotinylated POM19 antibody with recPrP and N2a cell lysate are shown in **Fig. 10c** and **d**. The concentration of POM1 as coating antibody was kept constant at 400 ng/ml. For all further experiments, biotinylated POM 19 antibody was used at a concentration of 1 µg/ml.

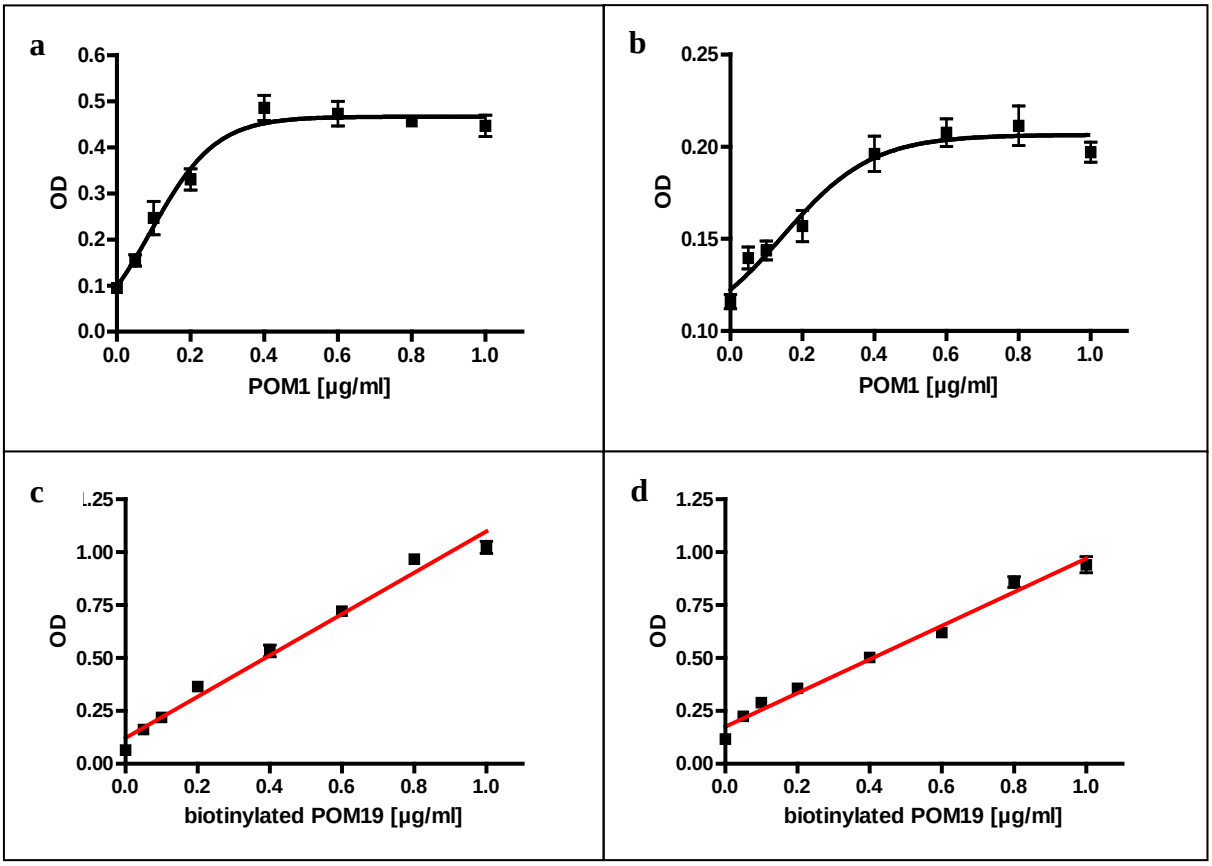

Figure 10. Titration of coating and primary biotinylated POM antibodies

To determine the optimal concentration of the coating antibody, a clear 96-well plate was coated overnight with different concentrations of POM1 antibody in coating buffer. Test samples were either recPrP (5 ng/ml) **(a)** or N2a cell lysate (300 µg/ml) **(b)**. Biotinylated POM19 was kept constant at a concentration of 400 ng/ml. In **(c)** and **(d)** the detection of recPrP and PrP^{C} in cell lysates, respectively, with the primary POM19 antibody are shown. Shown are the mean of hexaplicates ± standard deviations.

Limit of Detection (LOD) for recPrP and PrP^{Sc} Detection

To estimate the detection limit (LOD) of recPrP, a 96-well plate was prepared with recPrP serially 1:1 diluted in Hpl PrP KO cell lysate. The LOD for recPrP was determined at a concentration of 1.5 ng/ml (**Fig. 11a)**. When denatured with GdnSCN, LODs were obtained for concentrations lower than 0.5 ng/ml. To determine the LOD of PrP^{Sc}, crude N2aRML cell lysate at an initial concentration of 100 µg/ml was serially 1:1 diluted in normal N2a cell lysate at a constant concentration of 100 µg/ml in the presence or absence of PK. A statistically significant result for PrP^{Sc} detection from RML-infected N2a cells was found for 6 µg/ml total protein concentration **(Fig. 11b)**.

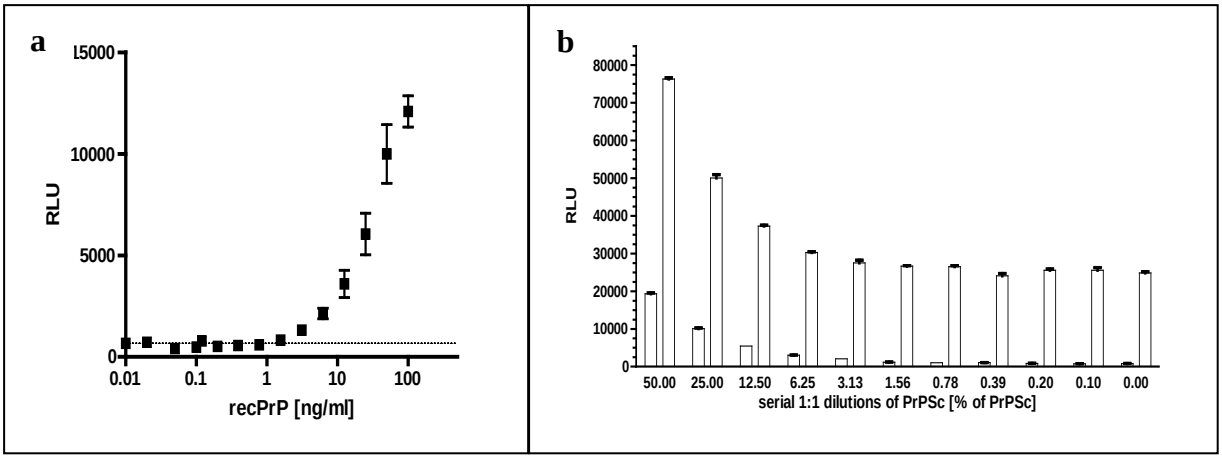

Figure 11. LOD for recPrP and PrP^{Sc}

(a) End point titration curve of recPrP. Dashed line represents detection limit of recPrP. Error bars represent standard deviations from 6 replicate wells. **(b)** Titration curve of PrP^{Sc} (N2aRML) spiked with PrP^{C} (N2a) in the presence or absence of PK. Error bars represent standard deviations from 6 replicate wells.

Validation of the PrP ELISA

To judge whether the PrP^{Sc} ELISA can be developed to a FRET-based high-throughput screening assay, the Z' factor was measured. The Z'-factor is defined in terms of four parameters: the means (μ) and standard deviations (σ) of both the positive (p) and negative (n) controls (μ_p, σ_p and μ_n, σ_n) **(Fig. 12)**. RML- and non-infected N2a cells were digested with 10 µg/ml PK and inactivated with 2mM PMSF. Protein cell lysate was denatured with 3M GdnSCN and neutralized by $NaHCO_3$ to an endconcentration of 0.5 M. Cell lysates were transferred into a POM1-coated 96-well plate. Biotinylated POM19 was used as primary antibody. The %CV values for N2a (n=44) was 18.88% and for N2aRML (n=44) 6.98%. A Z'-factor of 0.58 was obtained, which corresponds to an excellent assay. The Z'-factor is large enough to warrant further attention and to establish a homogeneous FRET based assay for detection of recPrP, PrP^{C} and PrP^{Sc}.

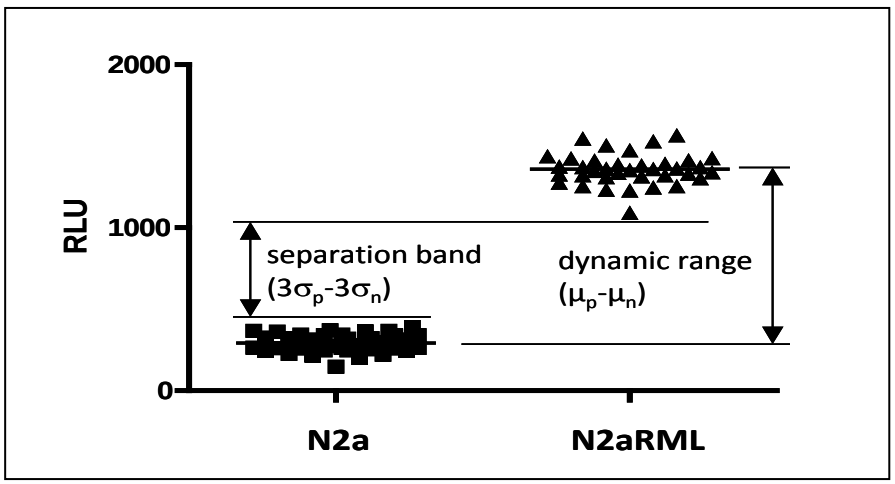

Figure 12. Determination of the Z'-factor of the PrP ELISA (opposite page)

Calculation of the Z factor, separation band and dynamic range. Error bars represent standard deviations from 44 replicate wells.

Detection of PrP^{Sc} with the same Coating and Primary POM Antibody by ELISA

PrP^{Sc} occurs as aggregates of PrP^{C}. We reasoned whether the same POM antibody could be used as coating as well as primary antibody to detect higher aggregated PrP^{Sc}. The reason for that is that the same epitope may occur several times in the aggregated isoform. The first choice was the POM1 and POM19 antibodies. Both antibodies were tested in normal and RML infected cell lysates under various lysis conditions in the presence of PK. Control experiments were done in the absence of PK. Under these conditions, neither the POM1 and POM19 antibody nor another member of the POM antibody family enabled the detection of PrP^{Sc} **(Fig. 13)**.

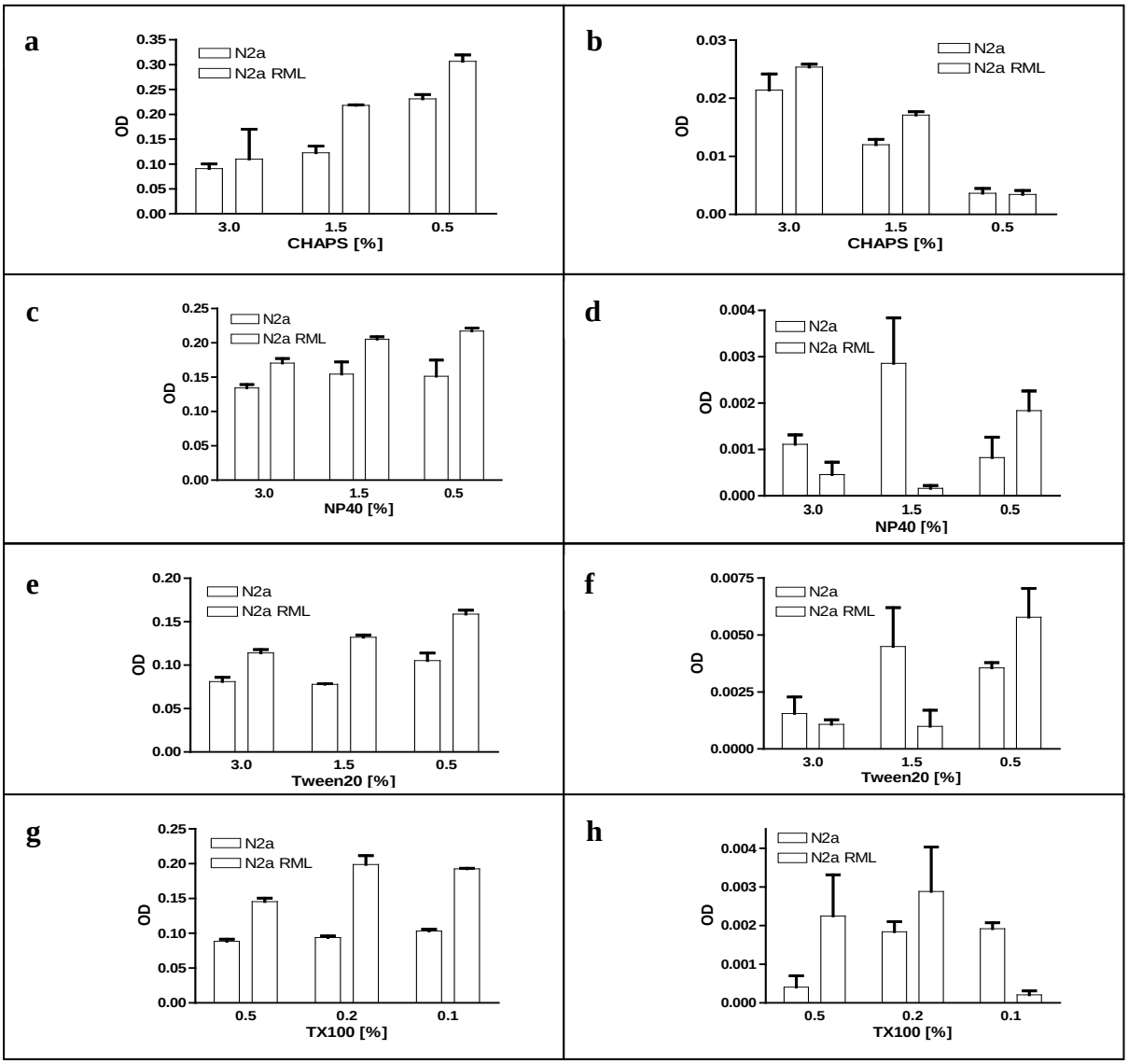

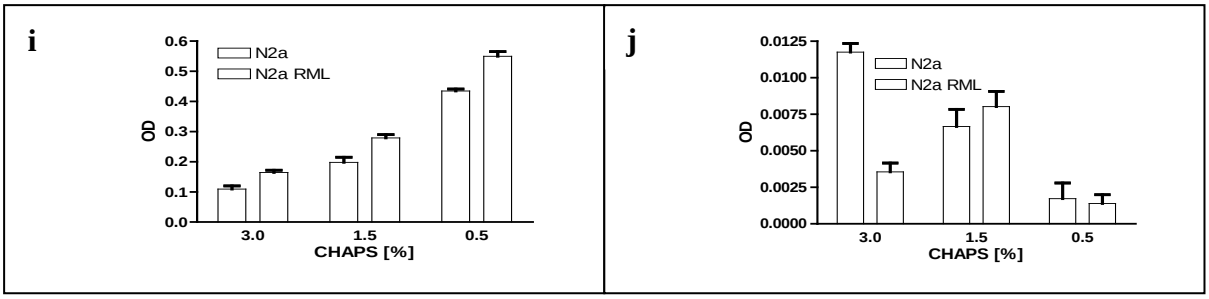

Figure 13. Dectetion of PrP^{Sc} with the same POM antibody twice (opposite page)

PrP^{C} and PrP^{Sc} was detected with the POM1 antibody as capture and primary antibody without **(a)** and after PK **(b)** with CHAPS, NP40 **(c** and **d)**, Tween20 **(e** and **f)** and TritonX100 **(g** and **h)**. PrP^{C} and PrP^{Sc} was detected with the POM19 antibody as capture and primary antibody without **(i)** and after PK **(j)** with CHAPS, NP40 **(k** and **l)**, Tween20 **(m** and **n)** and TritonX100 **(o** and **p)**.

Detection of N-GPI-PrP^{C}

The use of the same antibody twice as coating and detecting antibody is possible to detect PrP^{C}. Here, the ELISA was used to detect and quantify N-GPI-PrP^{C} expressend in transgenic mice. The N-GPI-PrP^{C} is a deletion mutant of the prion protein which mainly comprises the octapeptide repeat at the N-terminus and the GPI anchor (PrPΔ144-225). The N-GPI-PrP^{C} level was monitored from brain homogenates of animals at different ages (day 68 to day 76) and detected either with the POM2/POM2 **(Fig. 14a)**, the POM2/POM11 **(Fig. 14b)** or the POM11/POM2 (**Fig. 14c)** ELISA antibody combinations. The POM2 epitope occurs four times, whereas the POM11 epitope is two times present within the octapeptide repeat region of PrP. In control experiments, recPrP titration curves were used. In all three experiments, an age-dependent increase in N-GPI-PrP^{C} levels could be monitored. Spiking experiments of recPrP in Hpl PrP KO cell lysates confirmed the data found for N-GPI-PrP^{C} detection **(Fig. 14d)**.

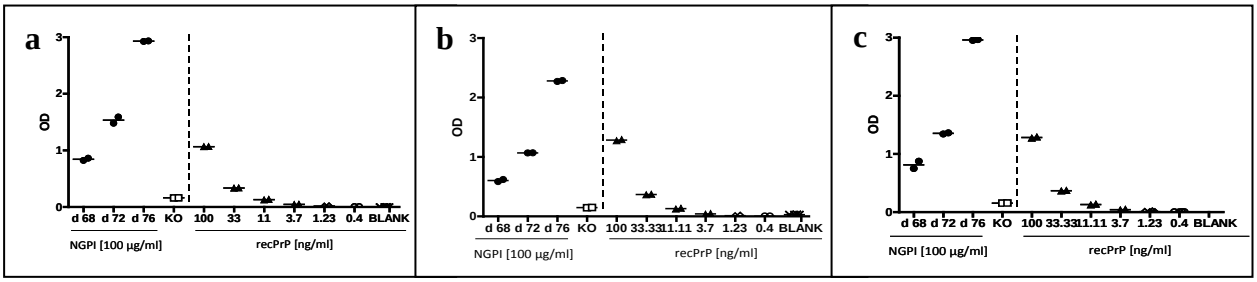

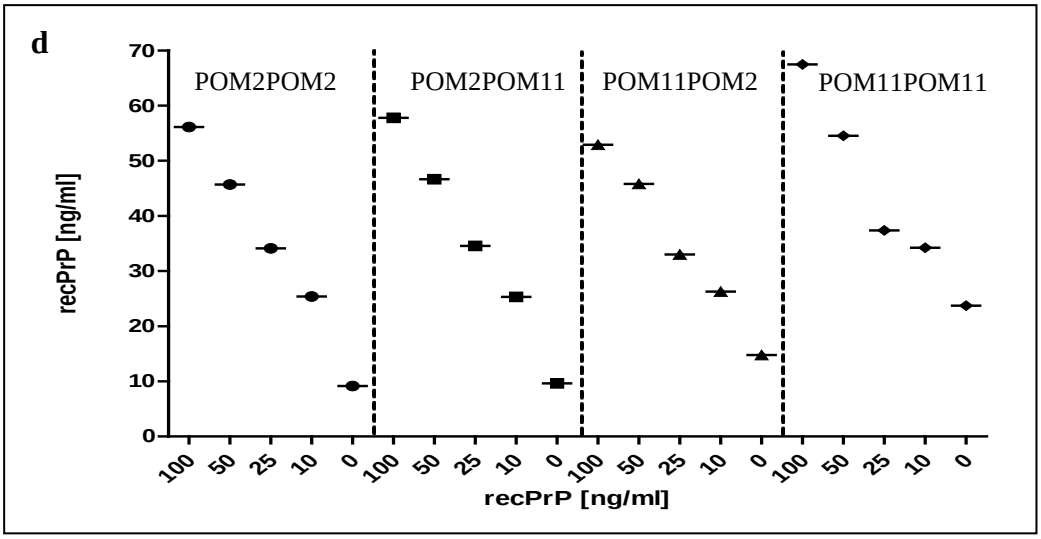

Figure 14. Dectetion of NGPI-PrP^C and recPrP with N-terminal POM antibodies

N-GPI-PrP^C was detected with POM2/POM2 **(a)**, POM2/POM11 **(b)** and POM11/POM2 **(c)** in mice at the age of 68 day (d68) to 76 days (d76). KO = knock out PrP brain homogenate. In **(d)**, the detection of recPrP is shown, spiked with Hpl KO cell lysate using the same antibody combinations.

PTAA Drug Treatment of Prion-Infected Tissue Cultures

The Prion Organotypic Slice Culture Assay (POSCA)

In collaboration with Ilan Margalith the effect of PTAA on prion replication and prion infectivity was studied *ex vivo* [Margalith et al., 2012]. We used the POSCA, a cerebellar slice culture system introduced by Jeppe Falsig [Falsig and Aguzzi, 2008; Falsig et al., 2008]. The POSCA is a flexible tool which allows the manipulation of the tissue such as compound treatment via culture media as well as specific cell type depletion or addition.

The experimental setup is summarized in **Fig. 15**. Cerebellar organotypic slices were produced from 11 day old PrP^C-overexpressing tga20 mice and inoculated with RML prions. At day 21, the PTAA drug treatment started. The drug was administered in the slice culture media three times per week. PrP^{Sc} was measured by ELISA after PK digestion and denaturation.

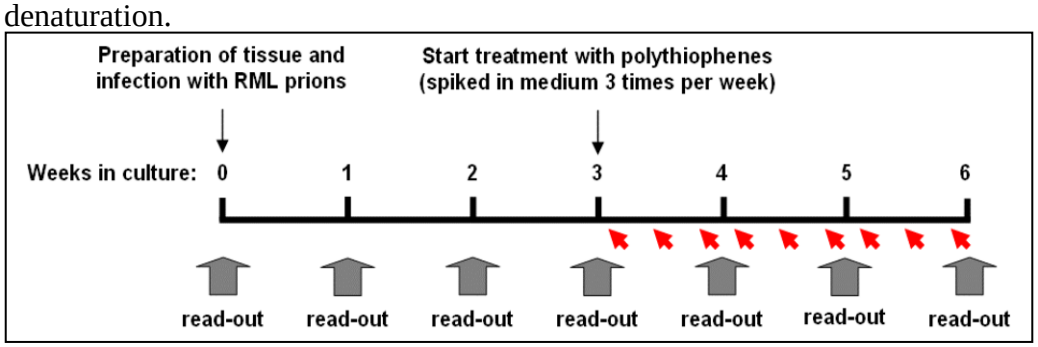

Figure 15. Experimental set up. PTAA treatment of RML-infected cerebellar tissue cultures.

Total PrP expression (PrP^C + PrP^{Sc}) was obtained without digestion. PrP^C expression was calculated by the subtraction of total PrP from PK-digested one. PTAA-treated, chronically infected cerebellar slice cultures have less PK-resistant material than untreated cultures **(Fig 16a)**. The decrease in PrP^{Sc} load depends on PTAA concentration and strongly correlated with the SCEPA and MPA data **(Fig 16c** and **d)**. At the concentration of 60 µg/ml PTAA, no PK-resistant PrP could be detected by ELISA. Calculated PrP^C expression levels were relatively constant and showed no statistically significant difference except for slices treated with 60 µg/ml PTAA, which showed a significant reduction in PrP^C levels **(Fig 16b)**.

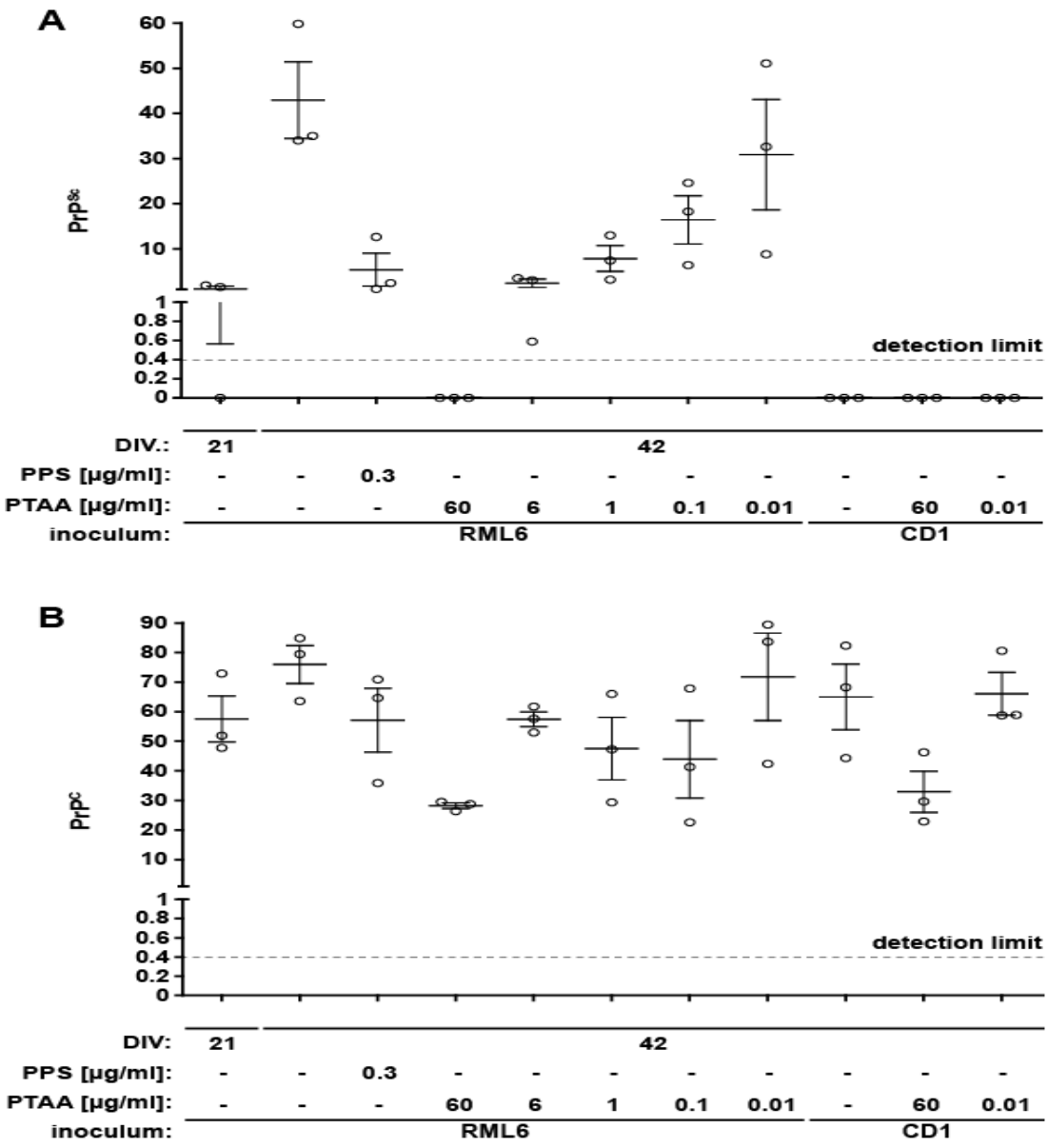

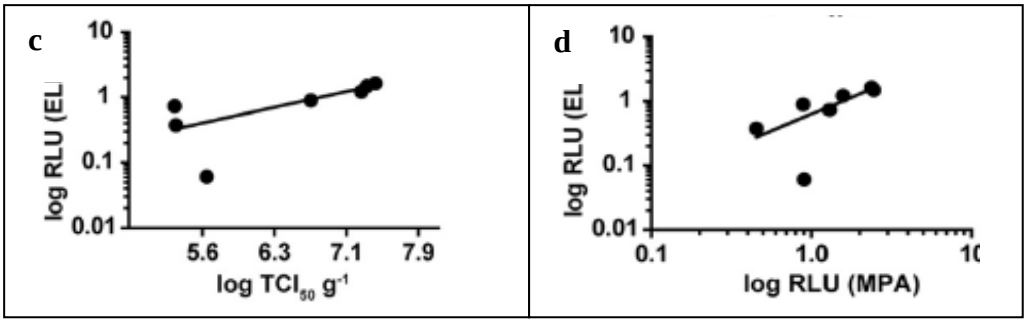

Figure 16: PTAA treatment of COCS decrease PK-resistant material measured by ELISA.

(a) PrP^{Sc} levels of COCS brain homogenates are shown. Each dot represents the average value of technical duplicates for one COCSBH. Error bars represent the mean ± SEM of biological triplicates. All data were normalized to protein concentration of the corresponding sample. P-values represent difference to control and are shown in Table 3. **(b)** The calculated PrP^{C} levels of COCS brain homogenates are shown. P-values represent difference to control and are shown in Table 4. **(c)** Correlation diagram to show the relationship between the SCEPA and ELISA data. **(d)** Correlation diagram to show the relationship between the MPA and ELISA data. Figures are taken from Margalith et al., 2012.

In the next set of experiments, we wanted to monitor the effects of PTAA treatment in a time-course analysis. Prion-infected slices were prepared in biological duplicates and the tissue was harvested at 7, 19, 21, 28, 35, 42, 45, 49 and 56 DIV. In parallel, prion-infected cultures were treated at a constant concentration of 10 µg/ml PTAA and administrated from day 7, 19, 21, 28 and 35. All cultures were harvested at 42 DPI and PrP^{Sc} and PrP^{C} levels were determined by ELISA. PK-resistant PrP in untreated tissue could be detected at 21 DIV and increased during the course of the experiment. Treatment with 10 µg/ml PTAA from day 28 kept the level of PK-resistant PrP at the level of the corresponding time point in untreated tissue, whereas treatment started from day 35 resulted in a decrease of detectable PK-resistant PrP. It cannot be excluded, however, that PTAA treatment induces a modification of PrP aggregates that interferes with the ELISA assay. PrP^{C} levels of the cerebellar tissues are shown in **Fig. 17c**. PTAA treatment started at either time-point decreased PrP^{C} levels about two fold. This confirms that PTAA treatment might affect prion accumulation by reducing the amount of PrP^{C} or of a transition intermediate to PrP^{Sc}.

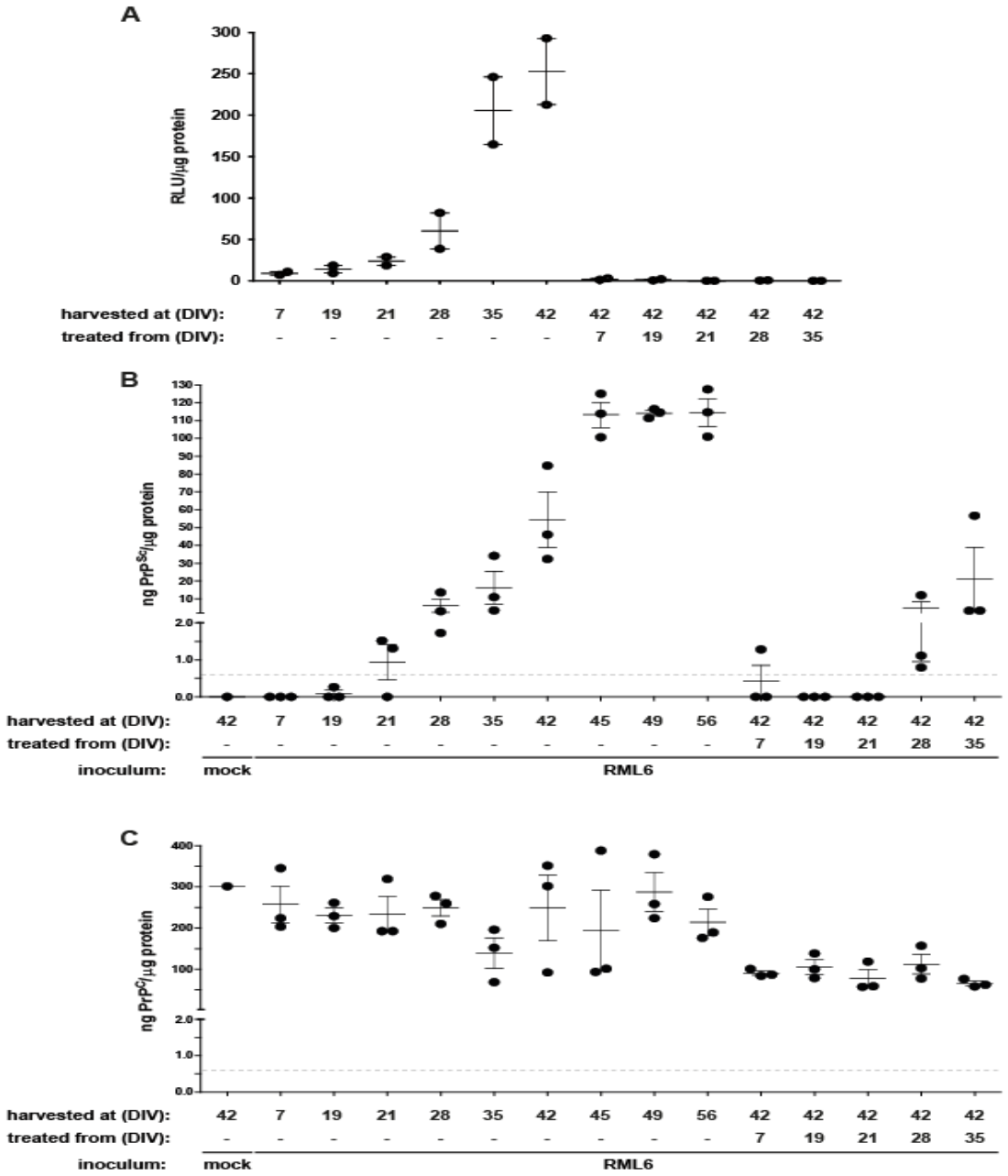

Figure 17. PTAA inhibits prion accumulation in RML6-infected slice cultures from different time points

(a) MPA of homogenates from RML6 infected slices harvested at days 7, 19, 21, 28, 35 and 42 DIV. PTAA was administered at a concentration of 10 µg ml^{-1} at the time of medium change freshly into the medium from days 7, 19, 21, 28 or 35 DIV. Slice cultures were harvested at 42 DIV and analyzed for PrP aggregates. Each dot represents the average value of technical triplicates for one slice culture homogenate. Error bars represent the mean ± SEM of biological duplicates. All data were corrected for non-infectious brain homogenates obtained from CD1 mice as negative control (mock) and represented as the ratio between relative light units (RLU) and protein concentration for each sample. P-values are shown in Table 5. **(b)** Sandwich ELISA of the same homogenates as in (A) analysed for PrP^{Sc}. The data are represented as biological triplicates. The signal for the negative control (mock) is shown as single replica. **(c)** Sandwich ELISA of the same homogenates as in (A) analysed for PrP^{C}. The ELISA was developed by chemiluminescence. The detection limit of 600 pg ml^{-1} (dashed line) was determined as the mean background levels plus three times SD. Figures taken from Margalith et al., 2012.

Table 2 (Data taken from Margalith et al., 2012)

Statistical analysis of data shown in Figure 16a using a one-way ANOVA with Tukey's multiple comparison test.

Figure 16a	**p-value**	**95% c.i. of difference**
untreated (21 DIV)	$p < 0.001$	-41.79(-66.96 to -16.62)
PPS 0.3 μg/ml	$p < 0.001$	37.56(12.39 to 62.73)
PTAA 60 μg/ml	$p < 0.001$	42.94(17.77 to 68.11)
PTAA 6 μg/ml	$p < 0.001$	40.57(15.40 to 65.74)
PTAA 1 μg/ml	$p < 0.001$	35.09(9.917 to 60.26)
PTAA 0.1 μg/ml	$p < 0.001$	26.51(1.36 to 51.70)
PTAA 0.01 μg/ml	$p = 0.450$	12.11(-13.06 to 37.28)

Table 3

Statistical analysis of data shown in Figure 16b using a one-way ANOVA with Tukey's multiple comparison test.

Figure 16b	**p-value**	**95% c.i. of difference**
PTAA 60 μg/ml	$p < 0.05$	47.70(0.65 to 94.75)

Table 4

Statistical analysis shown in Figure 17 using a one-way ANOVA with Tukey's multiple comparison test.

Fig. 17a	p-values	95% c.i. of difference
7 DIV	ns	-9(-108.8 to 90.80)
19 DIV	ns	-13.86(-113.7 to 85.94)
21 DIV	ns	-23.77(-123.6 to 76.03)
28 DIV	ns	-60.36(-160.2 to 39.44)
35 DIV	$p < 0.001$	-205.5(-305.3 to -105.7)
42 DIV	$p < 0.001$	-252.8(-352.6 to 153.0)
From 7 DIV	ns	-2.11(-101.9 to 97.68)
From 19 DIV	ns	-1.26(-101.1 to 98.54)
From 21 DIV	ns	0(-99.80 to 99.80)
From 28 DIV	ns	-0.49(-100.3 to 99.30)
From 35 DIV	ns	-0.04(-99.84 to 99.75)

Fig. 17b	p-values	95% c.i. of difference
7 DIV	n/s	0(-38 to 38)
19 DIV	n/s	-0.09(-38 to 38)
21 DIV	n/s	-0.95(-39 to 37)
28 DIV	n/s	-6.2(-44 to 32)
35 DIV	n/s	-16(-54 to 21)
42 DIV	$p < 0.001$	-54(-92 to -17)
45 DIV	$p < 0.001$	-113(-151 to -76)
49 DIV	$p < 0.001$	-114(-152 to -76)
56 DIV	$p < 0.001$	-114(-152 to -77)
From 7 DIV	n/s	-0.43(-38 to 37)
From 19 DIV	n/s	0(-38 to 38)
From 21 DIV	n/s	0(-38 to 38)
From 28 DIV	n/s	-4.6(-42 to 33)
From 35 DIV	n/s	-21(-59 to 17)
42 DIV vs. from 7 DIV	$p < 0.001$	54(16 to 92)
42 DIV vs. from 19 DIV	$p < 0.001$	54(17 to 92)
42 DIV vs. from 21 DIV	$p < 0.001$	54(17 to 92)
42 DIV vs. from 28 DIV	$p < 0.01$	50(12 to 87)
42 DIV vs. from 35 DIV	n/s	33(-4.5 to 71)

Fig. 17c	p-values	95% c.i. of difference
7 DIV	ns	44(-174 to 261)
19 DIV	ns	71(-146 to 289)
21 DIV	ns	67(-151 to 284)
28 DIV	ns	52(-165 to 270)
35 DIV	ns	162(-55 to 380)
42 DIV	ns	53(-165 to 270)
45 DIV	ns	107(-110 to 325)
49 DIV	ns	14(-203 to 232)
56 DIV	ns	88(-130 to 305)
From 7 DIV	ns	211(-6.6 to 428)
From 19 DIV	ns	196(-22 to 413)

From 21 DIV	$p < 0.05$	223(5.7 to 441)
From 28 DIV	ns	189(-28 to 407)
From 35 DIV	$p < 0.05$	236(18 to 453)
42 DIV vs. from 7 DIV	ns	158(59 to 376)
42 DIV vs. from 19 DIV	ns	143(-74 to 361)
42 DIV vs. from 21 DIV	ns	170(-47 to 388)
42 DIV vs. from 28 DIV	ns	136(-81 to 354)
42 DIV vs. from 35 DIV	ns	183(-34 to 400)

Statistical analysis using a one-way ANOVA with Tukey's multiple comparison test was done by Ilan Margalith. Unless stated otherwise, time points are compared to the non-infected COCS. For 42 DIV vs. From 7 DIV, for instance, the value obtained for COCS harvested at 42 DIV is compared to the value obtained for COCS harvested at 42 DIV with treatment from 7 DIV.

DISCUSSION

PrP^{C}/PrP^{Sc} Sandwich ELISA

In order to establish a sandwich ELISA which detects PrP^{Sc} from cell lysates I first developed a protocol to efficiently infect cells with prions. For that purpose, infection of two different cell lines with two different prion strains was compared. First, murine neuroblastoma N2a cells were infected with RML and Me7 prions, respectively. Infectivity titers were assessed by SCA. The data showed that N2a cells replicated RML prions more efficiently compared to the Me7 prion strain and had therefore a higher prion titer of 7.5 compared to 5 for Me7. CAD cells were able to replicate both prion strains with a prion titer between 6 and 7. This is in accordance with the literature [Klohn, 2003; Mahal et al. 2007]. The presence of PrP^{Sc} in RML-infected cells was determined by PK digestion and assessed by western blotting. A concentration of 5 µg/ml PK is sufficient to eliminate PrP^{C} in non-infected N2a cells. Prion-infected cells in culture showed a decreased prion titer over several cell splits. For that reason, prion infectivity in RML-infected N2a cells was monitored over 18 cell splits. As shown in Fig. 2c, a ten-fold reduction of prion titer could be determined during the cell splits. Therefore, chronically RML-infected N2a cells were only used from passage 3 to 9 in all experiments.

Next, I combined cell lysis and PK digestion in a one step procedure. Lysates from RML-infected cells were exposed to several detergents at different concentrations and were tested in the presence of various PK concentrations for 30 min at 37°C. Best cell lysis and digest conditions were found when 1.5% TritonX100 was used in the presence of 10 µg/ml PK. A concentration of 5 mM PMSF was identified as best condition to halt the action of PK.

I was not able to detect PrP^{Sc} from RML-infected N2a cell lysates after cell lysis and PK digestion, presumably because the binding epitopes were buried inside the aggregates. Therefore, cell lysates had to be denatured after lysis and proteolytic digestion. This was done by GdnSCN which was diluted with $NaHCO_3$ to obtain different GdnSCN concentrations. An end concentration of 0.3 to 0.5 M GdnSCN did not interfere with the ELISA antibodies. Therefore, cell lysates were denatured with 3 M GdnSCN and diluted six times with $NaHCO_3$. Several POM antibody combinations were tested. Best results were found when using POM1 as capture antibody at a concentration of 0.4 µg/ml per well and biotinylated-POM19 antibody at a concentration of 1 µg/ml for detection.

The detection limit for recPrP was determined at a concentration of 40 ng/ml. PrP^{Sc} was detected from 6 µg/ml total RML-infected cell lysate. In organotypic slice cultures, PrP^{Sc} was detected 19 weeks after inoculation with prions which corresponds to a limit of detection of about 400 ng/ml recPrP. However, it will require highly purified PrP^{Sc} to precisely determine the sensitivity.

Aggregated PrP^{Sc} contains hidden epitopes while other epitopes might be present more than once. The number of epitopes for binding depends on the composition of aggregated PrP^{Sc}. Theoretically, it might be possible to use the same POM antibody twice, as capture and detecting antibody, to detect PrP^{Sc} [Pan et al., 2005]. However, PrP^{C} dimers have also been reported in cells [Priola et al., 1995]. None of the tested POM antibodies showed increased binding avidity to PrP^{Sc}. Therefore, if some aggregated PrP^{Sc} is present in the cell lysate it is not possible to dectect it under the tested conditions with the same antibody used as capturing and detection antibody.

PTAA Drug Treatment of Prion-Infected Slices

We have previously shown that LCPs interact with amyloids and PrP^{Sc} [Sigurdson et al., 2007]. The fluorescence spectra formed by PrP^{Sc}-LCPs complexes allows differentiation of different prion strains. Theses findings prompted us to test whether the stability of PrP^{Sc} aggregates and their infectiousness may be affected by interactions with PTAA, a member of the LCP family.

In this study [Margalith et al., 2012], the established ELISA was used to detect PK-resistant material in PTAA-treated prion-infected cerebellar slice culture tissues. In PTAA-treated cultures, less PK-resistant material could be detected by ELISA than in untreated cultures in a PTAA concentration dependent manner. The operating characteristics of the ELISA have been further evaluated against two other assays: SCEPA and MPA (misfolding protein assay [Novartis]). The ELISA results are perfectly in line with the parallel observations of decreased prion infectivity in the SCEPA and decreased prion aggregates in the MPA and further point towards a decreased prion load in PTAA-treated tissue. Of note, a good correlation between the entities measured by MPA, SCEPA and ELISA indicates that the same entity is being affected by PTAA which results in a decrease of measurable PrP^{Sc} aggregates and infectivity. Treatment with 60 µg/ml PTAA resulted in a prion load of cultures that lies below that of tissue harvested at 21 DIV.

In addition, we performed PTAA treatment in a time-resolved manner and investigated PrP^{C} and PrP^{Sc} levels by ELISA. This analysis revealed that PTAA treatment is most effective if initiated before 21 days post-infection. PTAA treatment started at 28 or 35 DIV resulted in an amount of PK-resistant material that was similar or lower than at the time of treatment start and further indicates that PTAA interferes with prion replication within the tissue and possibly transforms pre-existing prions into a form that is less efficiently detected. It is not clear, however, how this anti-prion seeding effect is achieved.

OUTLOOK

The established ELISA assay has been validated for the detection of PrP^{C} and PrP^{Sc} in cell lysates and in extracts of brain tissue cultures. Discrimnation of both isoforms was done by PK digestion. This method also enables the determination of total PrP concentractions by subtracting PK digested from non-digested samples. However, the PrP ELISA has some automation but no high-throughput potential because of the following reasons: solid phase ELISA requires washing steps and is normally performed in 96-well plates.

Therefore, I used the data obtained from the ELISA experiments as basis to develop homogeneous phase TR-FRET assays which are amenable for automated high-throughput applications because they are running in 384-well plates obviating washing steps.

PART II RESULTS

PrP Time-Resolved Fluorescence Resonance Energy Transfer Assays

Overview of FRET-Based PrP Assays

In order to establish a FRET-based PrP assay I utilized the LANCE technology developed by PerkinElmer [www.perkinelmer.com/LANCE] as well as the Ruthenium-based system introduced by Roche [www.roche-diagnostics.ch]. In homogeneous phase FRET technologies of the LANCE format, one PrP-directed POM antibody is conjugated with the donor fluorophore Europium chelate (Eu), whereas the other POM antibody is labelled with an acceptor fluorophore allophycocyanin (APC) [Kronick, 1986]. When Eu and APC are in close proximity by virtue of the biomolecular interaction, a fluorescence resonance energy transfer (FRET) is detectable upon fluorescence emission of APC. The level of light emitted from the acceptor fluorophore is proportional to the degree of donor-acceptor complex formation. I established different PrP FRET-based assays which are summarized in **Figure 18a-c**.

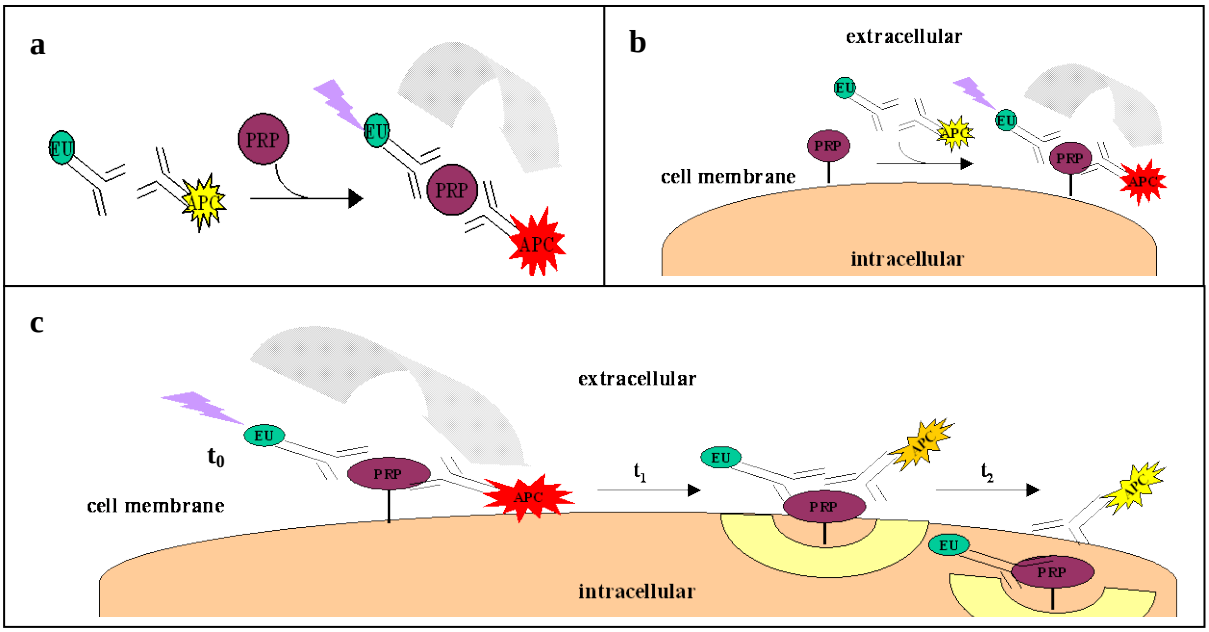

Figure 18. Overview of FRET-based PrP assays

Model systems used for PrP FRET detection assays. The POM antibody library allows the versatile tagging of PrP either at its N- or C-terminal region or at both termini simultaneously. Two POM antibodies conjugated with Eu and APC, respectively, were used to generate a FRET signal if the tandem pair is in close proximity. Finally, the energy transfer of Europium chelate-labelled POM antibody to APC-labelled POM antibody is evaluated in a HTRF (without washing) and/or TR-FRET (after washing) mode. Different types of PrP-based FRET assays were established. **a)** Detection and manipulation of recPrP, PrP^{C} and PrP^{Sc} by HTRF/TR-FRET **b)** Detection and manipulation of PrP^{C} expression on the surface of intact cells by HTRF/TR-FRET. **c)** Measurement and manipulation of PrP^{C}'s endocytosis by HTRF/TR-FRET.

FRET Calculation and Parameters

The Wallac EnVision multilabel reader (PerkinElmer) was applied for all FRET experiments using protocols installed by the manufacturer. A nitrogen laser device with an excitation pulse of 337.1 nm excites Europium (Eu), which activates APC in a distance-dependent manner. Fluorescence emissions are monitored both at 615 nm for Eu and at 665 nm for allophycocyanin (APC). The collected fluorescence data is corrected by both background and spectral overlap between Eu and APC channel. The resulting Net FRET signal is the number of APC counts depending on FRET events. Each well is calculated as:

$$\text{Net FRET signal} = (\text{counts} - \overline{\text{APC blank}})_{\text{APC channel}} - P\,(\text{counts} - \overline{\text{buffer}})_{\text{Eu channel}}$$

$$P = \frac{(\overline{\text{Eu blank}} - \overline{\text{buffer}})_{\text{APC channel}}}{(\overline{\text{Eu blank}} - \overline{\text{buffer}})_{\text{Eu channel}}}$$

counts	raw counts in APC and Eu channel
APC blank	all reagents except Eu in APC channel
Eu blank	all reagents except APC in APC and Eu channel
buffer	all reagents except APC and Eu in APC and Eu channel
P	proportionality factor which defines spectral overlap compensation of FRET results

Various measurement conditions affect the signal and were tested, including integration time, time delay, measurement height as well as different types of plates suitable for FRET applications. For all PrP time-resolved (TR) FRET measurements, an integration time of 100 or the standard 400 μs were used after a time delay ranging from 50 to 100 μs. Depending on assay format, FRET parameters such as time delay and integration time are mentioned in each set of experiments.

Dynamic Range of the Wallac EnVision Multilabel Reader for Europium Measurements

In order to determine the dynamic range, sensitivity and precision of the EnVision reader for Eu-FRET applications, aqueous solutions of Eu standards were prepared. To increase signal intensity, EU standards ranging from 0.1 pM to 10 nM were dissolved in the DELFIA® enhancement solution (PerkinElmer Life Sciences) **(Fig. 19a)**. For the measurement settings, I employed 100 flashes over 400 μs at 100% light intensity using a 100 μs time delay after each flash. The fluorescence emission intensity increased with approximately linear correlation (R^2 = 0.9993) to the Europium concentration ranging from 0.1 to 100 pM **(Fig. 19b)**. The coefficients of variation (CV) for the triplicate measurements were below 7% for all measured concentrations. The CV is a normalized measure of sample dispersion and therefore a term of

pipetting accuracy. CV values lower than 20% are acceptable. By preparing a clear 96-well plate with six different concentrations of Europium in the DELFIA® enhancement solution from 0 to 1 pM, I obtained a limit of detection (LOD) for Eu^{3+} of 0.05 pM **(Fig. 19c)**. The Eu standard measurements were also used to calculate the molarity of Eu-coupled biomolecules (see below).

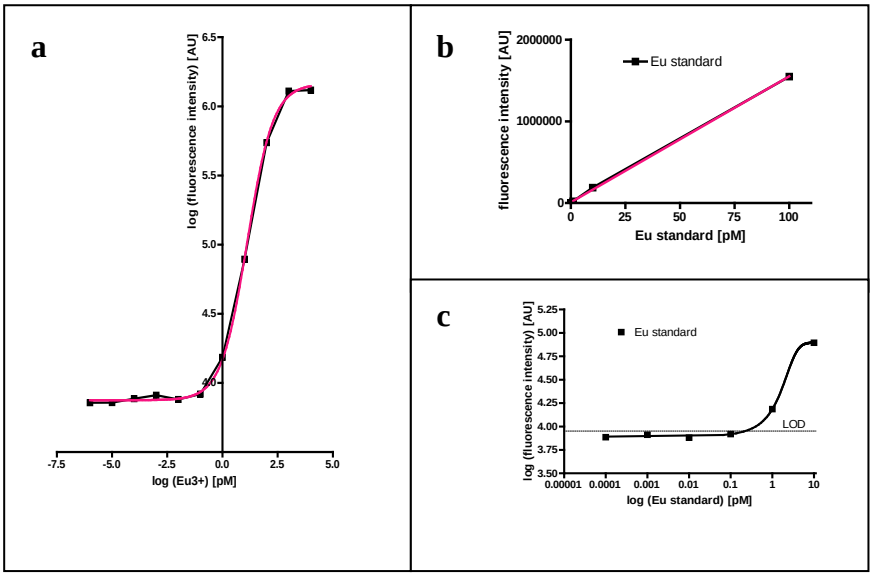

Figure 19. Dynamic range of the Wallac EnVision multilabel reader for Eu^{3+} chelate

A Eu standard solution was diluted to the indicated concentrations in the DELFIA® enhancement solution. In a clear 96-well plate, 200 µl per well of the indicated Europium solution was manually pipetted in triplicates. The fluorescence was measured at 615 nm. **(a)** This figure shows the dynamic range of the Envision reader from 10^{-6} to 10^{4} pM $Eu3^{+}$. The sigmoidal regression curve (in red) gives a R^2 value of 0.9994. **(b)** A linear correlation (R^2 = 0.9993) to the Eu concentration ranging from 0.1 to 100 pM was found. The limit of detection (LOD) of Europium standard is 0.05 pM. Shown are standard deviations of triplicates.

Measurement Time of the Wallac EnVision Multilabel Reader and Signal Stability

The Wallac EnVision multilabel reader combines standard FRET technology with time-resolved (TR) measurement of long-lived fluorescence. By introducing a time delay between excitation and fluorescence measurement, this technique allows the clearance of all non-specific short-lived background fluorescence. This is shown in **Fig. 20a**. For the EnVision reader the overall measurement time is the sum of the plate transports (in and out), the exposure time and the time window. For a 50 µs exposure time and a time window of 100 µs per 96-well plate this adds up to 65 s. The exposure time settings are typical instrument settings as recommended by the device manufacturers for average HTS applications. Moreover, the specific signal over background net FRET signal generated remains detectable for at least 48h when the plate is stored at 4°C (**Fig. 20b)**.

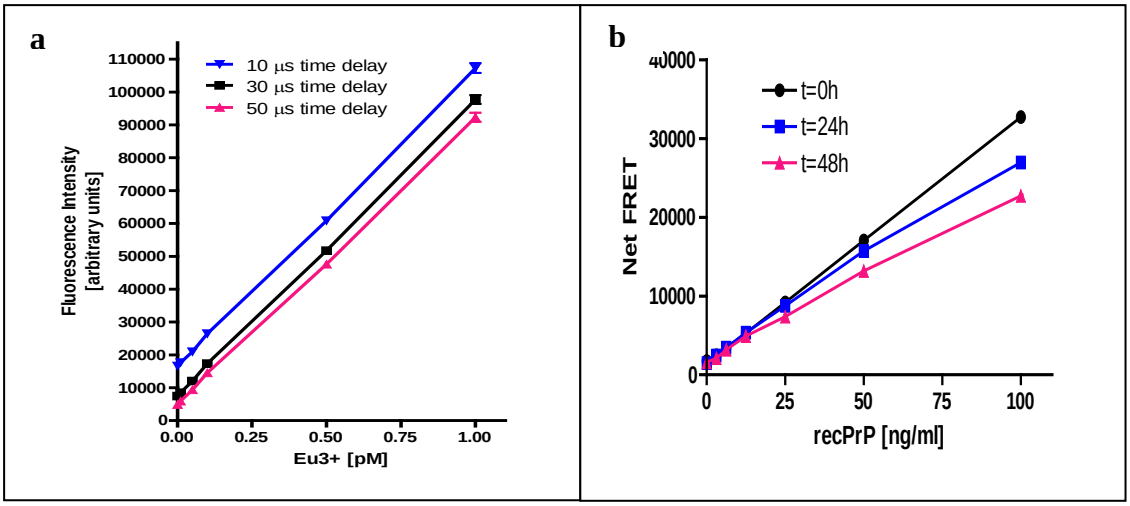

Figure 20. Time Delay and Stability of the FRET signal

(a) Detection of Eu standard solution with TR fluorescence measurement. Eu standard solution from 0 to 1 pM was pipetted into a clear 96-well plate. This plate was measured for three different time delays. The time window was kept constant. **(b)** To test FRET signal stability over time, serially diluted recPrP ranging from 0 to 100 ng/ml was detected by the FRET antibody combination POM1Eu/POM19APC and measured at day 0 (t=0 h), day 1 (t=24 h) and day 2 (t=48 h).

Preparation and Characterization of FRET Antibody Tandem Pairs

Based on the goal to detect PrP via a homogeneous FRET immunoassay, several POM antibodies (POM1, 2, 3, 5, 6, 7, 10, 11, 15, and 19) as well as the antibody 3F4, which is an antibody directed against the amino acids 109-112 of the human prion protein [Bolton et al., 1991], were coupled either to the donor fluorophore Eu or to the acceptor fluorophore APC. In **Fig 21**, the coupling steps are exemplarily shown for POM1-Eu and POM19-APC. Native full length POM antibodies were dialyzed in Eu or APC coupling buffer, respectively, at 4°C over night. In preliminary experiments, POM antibodies were conjugated with a 4 or 1.5x molar excess of fluorophore, respectively. In a later set of experiments, the molar excess of Europium was increased for all coupling reactions from 10x to finally 24x to achieve a higher Eu^{3+}/antibody ratio. APC was constantly kept at a 1.5x molar excess to POM antibodies. Removal of uncoupled Eu chelate or APC was done either by size exclusion chromatography (SEC) **(Fig. 21a)** or Protein G column, respectively. Purity of conjugated antibodies was assessed by Coomassie gels for all labelled antibodies **(Fig. 21a** and **Fig. 21d)**.

The absorbance of APC-coupled antibodies was routinely monitored by Nanodrop measurements at a wavelength of 650 nm **(Fig. 21c)**. Protein concentration was assessed at a wavelength of 280 nm **(Fig. 21c)**. To determine the molarity of POM1-Eu conjugates, antibodies were pre-incubated with 0.1 M HCl for 10 min to liberate Europium from the antibody and compared to a Eu standard curve according to the manufacturer guideline (not

shown). POM antibodies with a good labelling ratio of Eu^{3+}/IgG of 6-7 and APC/IgG of 1.5 were used in FRET experiments.

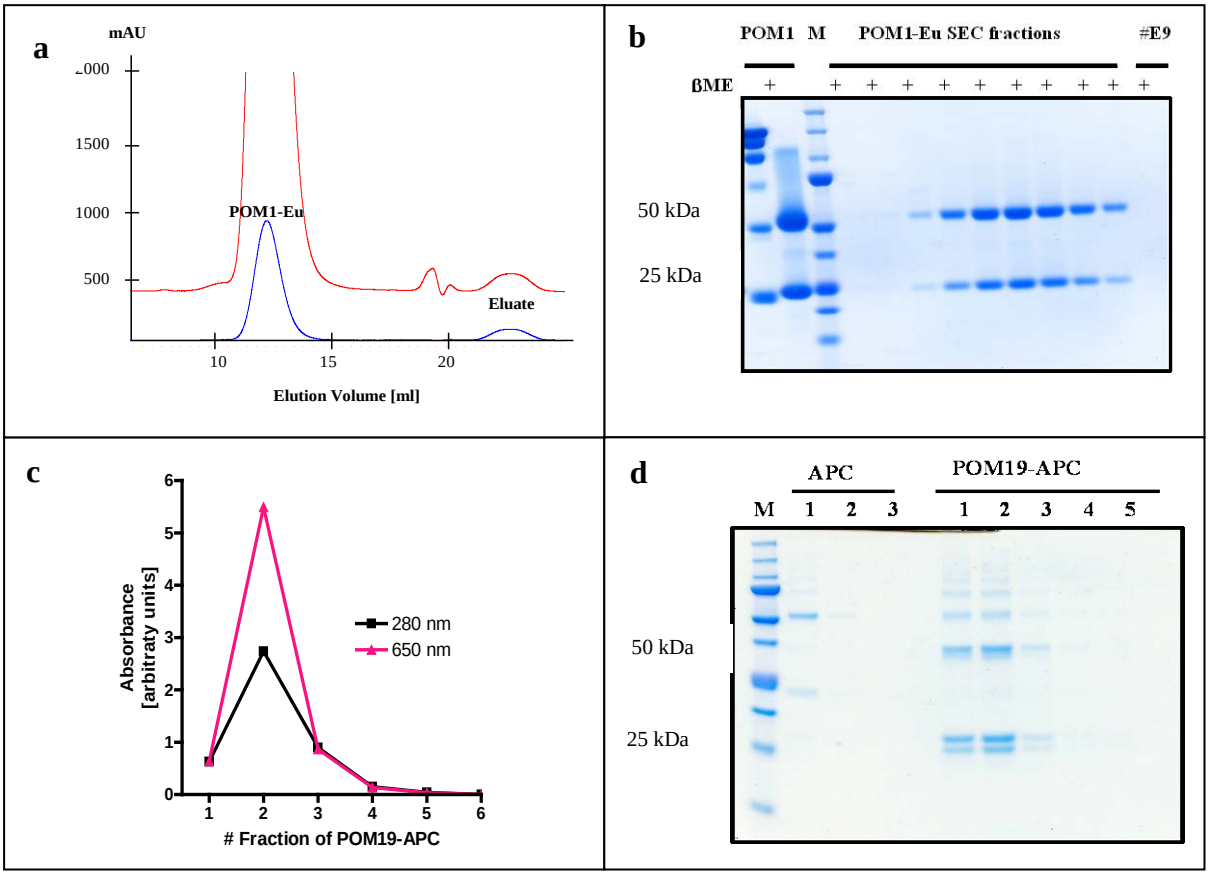

Figure 21. Conjugation of POM1 with Europium chelate and POM19 with APC

(a) Elution profile of Eu-coupled POM1 antibodies separated by SEC. UV light at A_{280nm} (blue curve) and A_{215nm} (red curve) monitor the fractionation. The peak after 12 ml elution volume contains labelled POM1Eu antibodies, the smaller peak arising after 22.5 ml elution buffer represents the free Eu chelate. **(b)** Fractions containing POM1Eu and eluate (#E9) were collected and equal volumes of protein were loaded onto a Coomassie gel in the presence of β-mercaptoethanol (βME) (reducing conditions). Samples only containing Eu-conjugated POM1 were pooled and used for experiments. As control, native POM1 was used. **(c)** Shown is the absorbance at 280 nm (black curve) and at 650 nm for APC (red curve) for each POM19APC fraction. **(d)** Equal volumes of fractions (#1-6) containing APC-labelled POM19 antibodies from the Protein G column purification step were loaded onto a Coomassie gel under reducing conditions. M: protein marker in kDa. Experiments in **Fig. (a)**, **(b)** and **(d)** were performed by Rita Moos and Irina Abakumova.

Development of a Homogeneous recPrP TR-FRET Assay

In the LANCE format, the fluorescence emissions of the Eu chelate (615 nm) and APC (665 nm) are measured separately in two steps. The suitability of the EnVision for LANCE measurements was tested in the following two biological assay setups: First, a FRET system was established to detect recPrP in solution using POM antibodies conjugated either with Eu or APC.

To estimate the dynamic range and sensitivity of the Wallac EnVision multilabel reader for complexes between recPrP and FRET antibody pairs, recPrP was 1:1 diluted in Hpl PrP KO cell lysate at a starting concentration of 128 ng/ml. Hpl PrP KO cell lysate was used as blank. Different FRET antibody pairs were tested. The best results were found with the POM1-Eu/POM2-APC FRET antibody pair **(Fig. 22)**. The LOD gave a value of less than 100 pg/ml recPrP. It seems that a concentration higher than 100 ng/ml recPrP reaches a saturation plateau. Excellent S/N ratios as well as Z' factors were found **(Table 5)**. Therefore, the EnVision supported a robust HTS-suitable format for recPrP (Z' value of above 0.5) with a POM1-Eu concentration of 2.5 nM combined with 5 nM POM2APC.

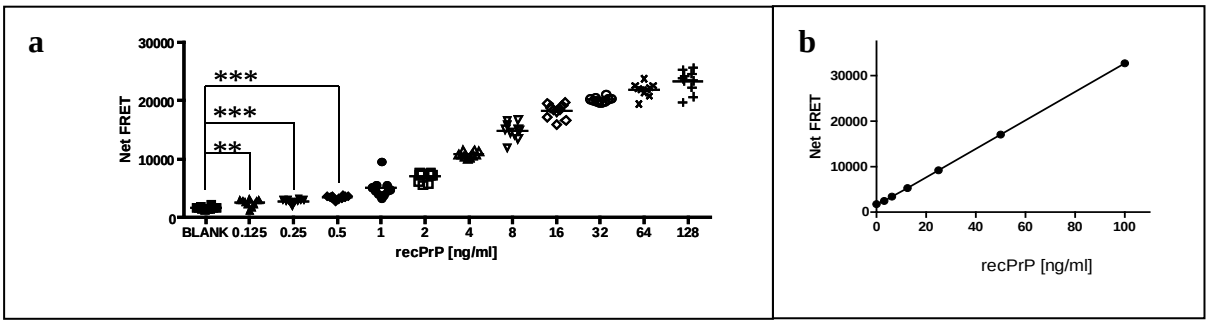

Figure 22. Titration of monomeric recPrP, LOD, dynamic and linear range

(a) RecPrP was serially diluted 1:1 in PrP-deficient Hpl cell lysate (BLANK). Net FRET signal was detected with 2.5 nM POM1Eu and 5nM POM2APC in 1x LANCE® buffer. Shown are means ± standard deviations from hexaplicates. **(b)** Linearity of FRET signal to analyte concentration was found in the range of 0-100 ng/ml recPrP with the POM1Eu/POM19APC FRET antibody pair.

recPrP [ng/ml]	BLANK	0.125	0.25	0.5	1,00	2,00	4,00	8,00	16,00	32,00	64,00	128,00
%CV	13,24	24,74	12,20	8,14	33,31	11,41	4,70	9,55	6,86	2,14	5,28	8,16
S/N		3,72	7,66	11,67	2,89	8,52	20,79	10,32	14,41	46,32	18,73	12,16
z'		0,90	0,95	0,96	0,76	0,90	0,94	0,86	0,89	0,96	0,91	0,85

Table 5. FRET assay performance for recPrP detection

Coefficient of variance (%CV) shows the extent of variability in relation to the mean of the samples. A %CV value lower than 20 is acceptable. The signal to noise (S/N) ratio indicates the potential sensitivity of the assay. Values higher than 20 are not unusual in FRET assays of the LANCE® format. The Z factor (Z') is another important indicator of assay variability. Values higher than 0.5 are necessary for high throughput applications.

To further validate the recPrP-based TR-FRET assay, various other experiments were addressed to characterize this assay in more detail. Enzymatic digestion of recPrP with PK is shown in **Fig. 23a**. A constant amount of 100 ng/ml monomeric recPrP was incubated with PK in the range of 0 to 2.5 µg/ml PK. A clear decrease in FRET signal intensity dependent on increasing PK concentrations was found. As a negative control and to determine the background of the assay, PrP-deficient Hpl cell lysate was utilized. Similar results were found for tryptic digestion (not shown). In another approach, a constant amount of recPrP was pre-incubated with different concentrations of unlabelled full length POM1 and POM19 antibody. FRET signal was detected with the POM1Eu/POM19APC FRET antibody pair. The higher the concentration of the blocking antibodies, the lower the FRET signal. As control, unlabelled full length POM2 was used, which had a minor effect on the FRET signal intensity **(Fig. 23b)**. In a next experiment, recPrP was pre-incubated with either full length or single chain POM2 antibodies at various concentrations. Single chain POM2 antibody weakly interfered with the FRET signal upon POM1Eu/POM19APC labelling compared to full length POM2 **(Fig. 23c)**, presumably because of less steric interactions.

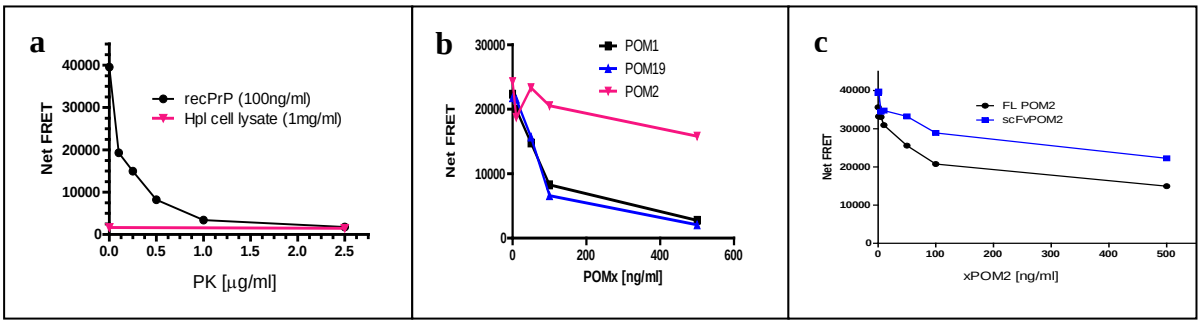

Figure 23. Characterization of biochemical recPrP TR-FRET assay

(a) RecPrP`s PK sensitivity is shown. A constant concentration of 100 ng/ml recPrP was digested with an increasing concentration of PK at 37°C for 30 min. Inactivation of PK was done by heating at 95°C for 5 min. PrP-deficient Hpl cell lysate was used as negative control. **(b)** By pre-incubating a constant amount of recPrP with different concentrations of unlabelled full length antibodies, either POM1 or POM19, the FRET signal was dose-dependent blocked upon addition of the FRET antibody pair POM1Eu/POM19APC. In a control experiment, pre-incubation of unlabelled full length POM2 antibody had only a weak effect on the FRET signal when using the same FRET antibody pair for detection. **(c)** A difference in blocking FRET signal was found when comparing unlabelled full length POM2 antibody with unlabelled single chain POM2 antibody.

I was wondering, whether the biochemical recPrP FRET assay could also be applied to discriminate between monomeric and fibrillic recPrP. Therefore, I generated fibrillic recPrP in the presence of GdnHCl by thermal shaking for 48 h [Apetri et al., 2005]. Monomeric and fibrillar recPrP was subjected to proteolytic digestion, either with PK or trypsin. In **Fig. 24a**, PK digested recPrP was detected by the C-terminal POM1Eu/POM19APC FRET pair. No

fibrillic recPrP was detectable under these conditions. The same results were found when monomeric and fibrillic recPrP was digested with trypsin and detected with the same antibodies **(Fig. 24b)**. Aggregated recPrP was only detectable by the N-terminal POM2Eu/POM2APC FRET antibodies after trypsin digestion. It seems that trypsin digestion loosens the aggregated state or makes buried epitopes accessible and enables the detection of recPrP **(Fig. 24c)**.

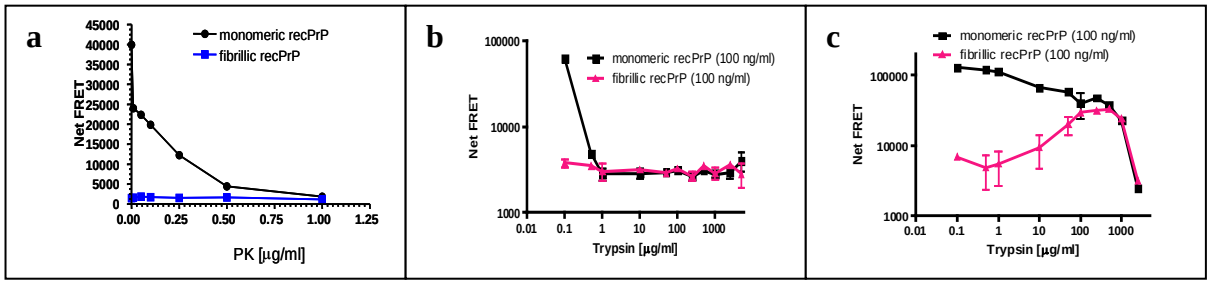

Figure 24. Detection of monomeric and fibrillic recPrP after proteolytic digestion

Monomeric and fibrillic recPrP detection by **(a)** POM1Eu/POM19APC after PK or **(b)** POM1Eu/ POM19APC or **(c)** POM2Eu/POM2APC after trypsin digestion. Shown are standard deviations of biological triplicates.

Development of a Homogeneous PrP^C TR-FRET Assay

The most common methods for detection and measuring cellular PrP involve Western blot analysis or various types of ELISAs [Kretzschmar et al., 1996]. These are time-consuming assays and inherently have a low throughput performance. The sensitivity and efficacy of the established biochemical recPrP FRET assay prompted an investigation in more complex environments. Therefore, to more directly and rapidly analyse PrP from crude cell lysates and brain homogenates, the influence of some detergents on the FRET signal intensity was tested in recPrP solutions. TritonX-100 (TX100) and Brj35 had a strong influence on the FRET signal intensities at the tested concentrations **(Fig 25 a/b)**.

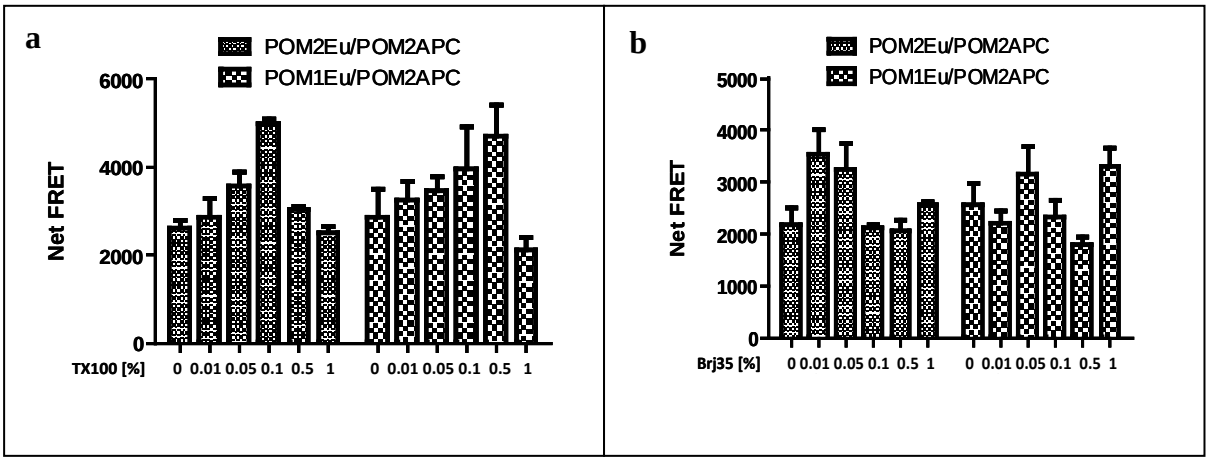

Figure 25. Titration experiments of detergents for cell lysis optimisation (opposite page)

(a) Titration of TritonX100 (TX100) in a recPrP solution. Detection of PrP^C was done either with POM2Eu/POM2APC or POM1Eu/POM2APC. **(b)** Titration of Brj35 in a recPrP solution. Detection of PrP^C was done either with POM2Eu/POM2APC or POM1Eu/POM2APC

Next, the sensitivity for PrP^C detection by FRET technology was determined in spiking experiments. PrP^C expressing N2a and PrP KO cells were lysed in 50 mM TrisHCl pH 7.4 and 0.5% TX100 for 60 min on a rotating shaker. Protein concentration was determined by Bradford assay. An initial total protein concentration of 1 mg/ml of N2a cell lysate was serially diluted 1:1 in 1 mg/ml Hpl cells lysate. PrP^C was detected by the POM1Eu/POM2APC FRET antibody pair. The detection limit for PrP^C was determined at a total protein concentration of 16 µg/ml **(Fig. 26a)**. A linear range for PrP^C detection of non-spiked N2a cell lysate was found in the range of 50 to 1000 µg/ml **(Fig. 26b)**.

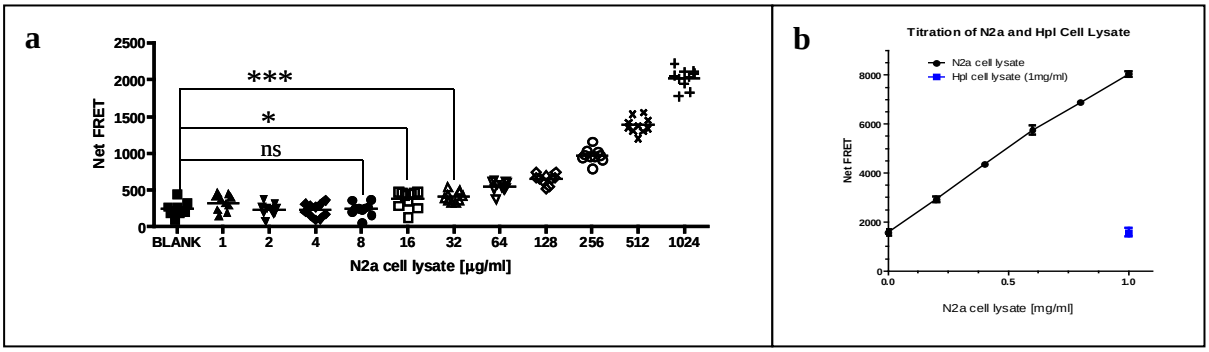

Figure 26. Characterization of PrP^C-based FRET assay

(a) Crude N2a cell lysate was serially diluted 1:1 in PrP-deficient Hpl cell lysate (BLANK). Net FRET signal was detected by 2.5 nM POM1Eu and 5nM POM2APC diluted in 1x LANCE® buffer. Shown are means ± standard deviations from hexaplicates. *: $p < 0.05$; ***: $p < 0.001$. In **(b)**, linear correlation ($R^2 = 0.9917$) ranging from 0.05 to 1 mg/ml of PrP^C to total protein concentration was found. Net FRET signal was detected by POM1Eu and POM19APC diluted in 1x LANCE® buffer.

I further validated the homogeneous PrP^C FRET assay by performing enzymatic proteolysis experiments in order to show the degradation of PrP^C. N2a cell lysate was digested with different concentrations of PK for 30 min at 37°C. PK was inactivated by heating to 95°C for 10 min and PrP^C levels were monitored by POM1Eu/POM2APC FRET antibodies **(Fig 27a)**. In another series of experiments, N2a cell lysate was digested with trypsin and inactivated by 5 mM PMSF **(Fig 27b)**. Inactivation of trypsin was shown by spiking the samples with recPrP for 15 min. PrP^C was detected by the POM1Eu/POM2APC FRET pair **(Fig. 27c)**. In both proteolysis experiments, PrP^C levels decreased as a function of enzyme concentration. To confirm that PMSF inactivates the action of trypsin, PrP^C was detected from digested N2a cell lysate by a FRET antibody pair which binds to trypsin-resistant epitopes at the C-terminus

(Fig. 27d). Hpl PrP KO cell lysate was used as a negative control in all experiments. The sensitivity and specificity of the cell lysate-based TR-FRET assay was controlled by an antibody blocking experiment **(Fig. 27e)**. By pre-incubating crude cell lysate with unlabelled holo antibody POM2 (mAB) or single chain POM2 antibodies (scFv), a concentration-dependent decrease in PrP^C signal intensity was found as function of unlabelled antibody after labelling with POM2Eu/POM2APC **(Fig. 27e)**, demonstrating the specificity of the homogeneous FRET assay.

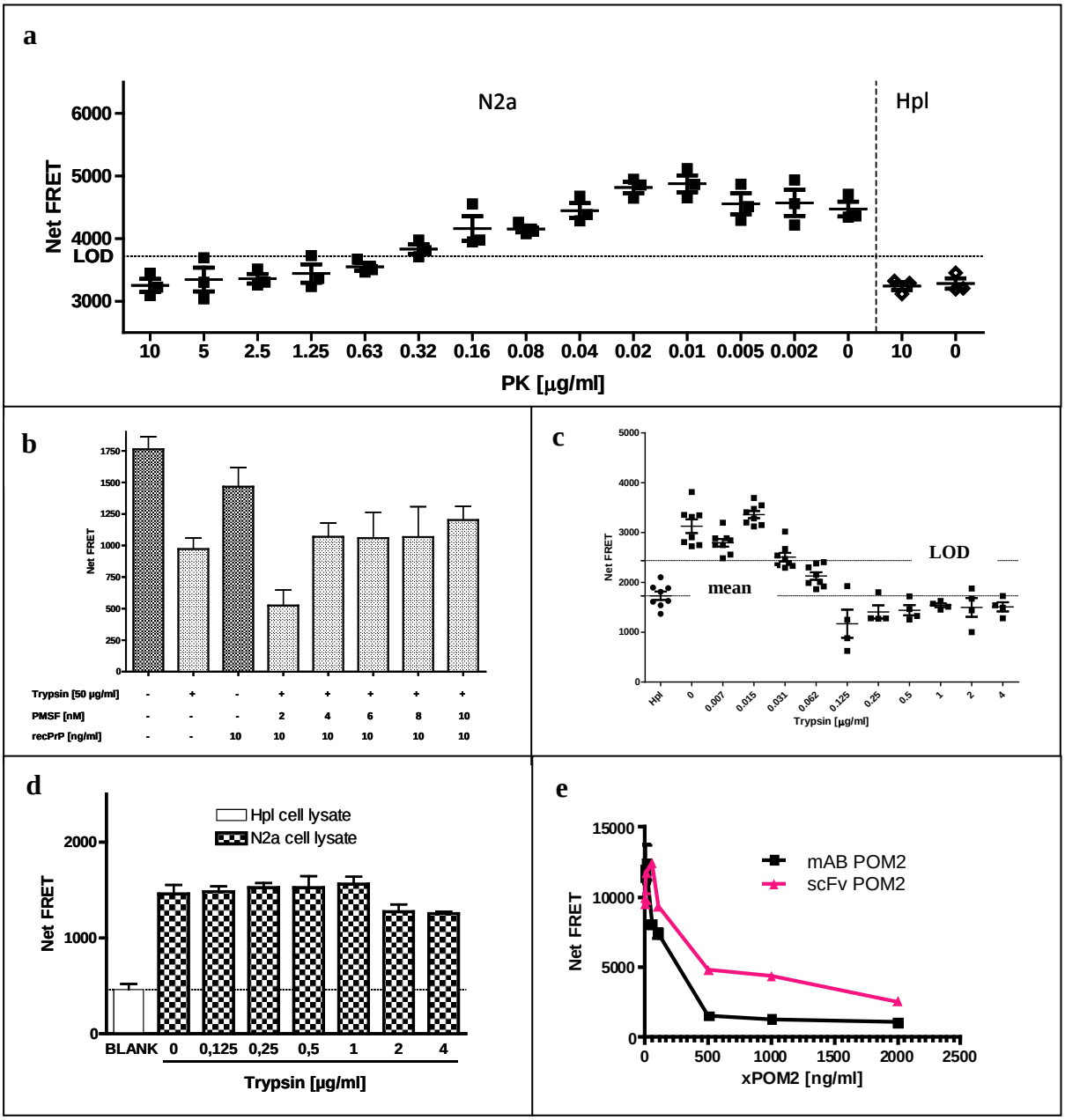

Figure 27. Characterization of PrP^C-based FRET assay

To validate the PrP^C FRET assay, N2a cell lysate was digested with two different proteinases, PK **(a)** and trypsin **(b)** - **(d)**. The catalytic activity of both enzymes was inhibited by heating **(a)** or by addition of the proteinase inhibitor PMSF **(b)** - **(d)**. **(e)** Blocking of FRET antibody epitopes of crude cell lysate by pre-incubation with full length or single chain unlabelled POM2 antibodies. FRET measurement was done with POM2Eu/POM2APC.

Development of a Homogeneous PrP^{Sc} TR-FRET Assay

The strategy to discriminate between PrP^{C} and PrP^{Sc} from unfractionated cell lysates and brain homogenates is done by enzymatic proteolysis and is outlined in **Fig. 28**. The gold standard procedure to discriminate between both PrP isoforms is PK digestion, which completely degrades PrP^{C}, but patially PrP^{Sc}. However, other proteolytic enzymes, such as trypsin [Yam et al., 2010], can also be used for discrimination.

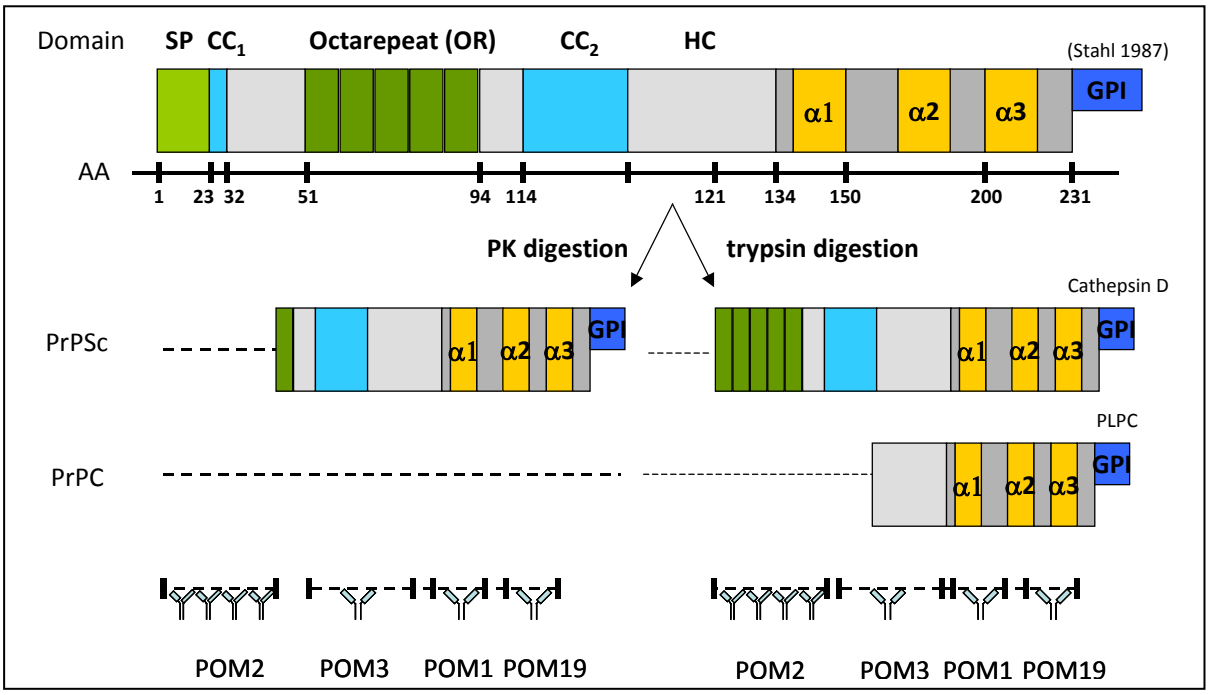

Figure 28. Overview of PrP's domains, size, digestion fragments and POM antibody binding sites
The unstructured N-terminal domain of PrP consists of an octarepeat region. The structured C-terminal domain contains the sequence for the GPI anchor. Both regions contain post-translational glycosylation sites. The numbers describe the position of the amino acids (AA). The proteinase K (PK) and trypsin resistant cores of PrP^{Sc} are shown. The epitopes recognized by the POM antibodies are also indicated. SP signal peptide, CC charged cluster, OR octarepeat, HC hydrophobic core.

In order to discriminate between both PrP isoforms, I performed PK titration experiments starting from 0 to 32 µg/ml and used the same dilution (10^{-3} equal 0.01% [lab nomenclature]) for all samples **(Fig. 29a** and **b)**. PK action was halted by 2 mM PMSF. As control, PrP KO BH as well as non-digested CD1 BH was used. Results in **Fig. 29a** and **b** showed a PK concentration-dependent decrease of FRET signals in CD1 and 22L samples after POM1Eu/19APC detection, respectively. In a follow up experiment, different dilutions of 22L BH from 10^{-2} to 10^{-5} was applied to a constant concentration of PK. Only a very high concentration of 10^{-2} diluted 22L BH, PrP^{Sc} could significantly discriminated by PK digestion from PrP knockout samples ($PrP^{-/-}$) **(Fig. 29c)**.

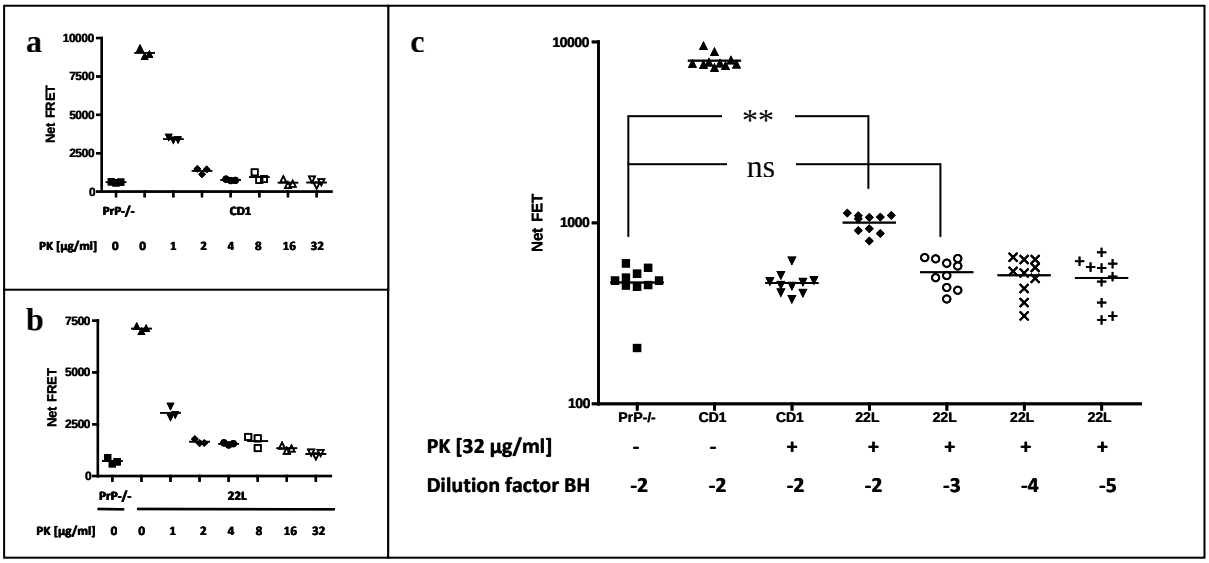

Figure 29. Detection of PrP^{Sc} in BH after PK digestion

Shown are PK titration experiments of non-infected (CD1) **(a)** and prion-infected (22L) BH **(b)**. PrP KO (-/-) BH was used as negative control. Samples were digested for 30' at 37°C during shaking. PK was inactivated with 2mM PMSF for 10' at RT during shaking. FRET detection was done with POM1Eu/POM19APC. Shown are triplicates. **(c)** Different dilution of 22L BH was subjected to a constant concentration of 32 µg/ml PK for 30' at 37°C. PK was inactivated with 2 mM PMSF and detected with POM1Eu and POM19APC. Shown are decuplicates. **: $p < 0.01$.

In contrast to PrP^{C}, the immunoreactivity of PrP^{Sc} is improved by denaturation, because buried epitopes become accessible [Serban D 1990]. To exclude interactions of denaturation/neutralisation agents with FRET antibodies, recPrP was added to different ratios of denaturation/neutralisation buffer for 10' at RT and labelled with POM1Eu/POM19APC. As summarized in **Fig. 30a**, 0.1 N NaOH pH 12.3 or 0.3 M NaH_2PO_4 pH 4.3 completely diminished the FRET signal intensity, compared to a ratio of 3/2 of 0.1 N NaOH/ 0.3 M NaH_2PO_4 which had only a marginal effect on the FRET signal intensity. This ratio was used to denature PrP^{Sc} in further experiments. The use of GdnSCN was not successful **(Fig. 30b)**. With these findings, I next used crude brain homogenate (10^{-3}) infected with 22L prions and denatured/neutralised with different concentrations of NaOH and NaH_2PO_4. Here, total PrP was determined without discrimination of PrP^{C} and PrP^{Sc}. Compared to untreated BH, a 1:1 ratio of denaturation/neutralisation with 0.1 N NaOH and 0.3 M NaH_2PO_4 almost doubles FRET signal intensity (**Fig. 30c**).

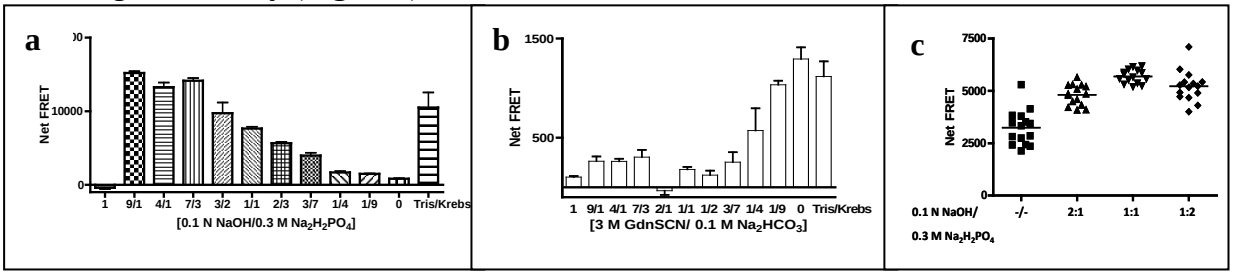

(a) RecPrP, pre-labelled with POM1Eu/POM19APC, was exposed to different ratios of 0.1 M NaOH and 0.3 M NaH_2PO_4. Shown are triplicates ± SD. **(b)** The same experiment was performed with different ratios of 3M GdnSCN and 0.1 M $NaHCO_3$. Shown are triplicates ± SD. **(c)** Prion-infected BH (22L) was diluted to 10^{-3} and exposed to 0.1 N NaOH for 10 min at room temperature during shaking (750 rpm). The action of NaOH was neutralised with 0.3 M NaH_2PO_4. Detection was done with POM19Eu/POM1APC. Time delay/window: 100 µs/400 µs. Shown are 15-plicates.

To determine the limit of detection of PrP^{Sc}, 10% brain homogenates of 22L prion infected mice were prepared and serially diluted 1:10 in PrP KO brain homogenate. PrP^{Sc} levels were determined after PK digestion and denaturation with the POM1Eu/POM19APC FRET antibody pair. PrP^{Sc} was detectable at a brain homogenate dilution of 10^{-5} **(Fig. 31)**.

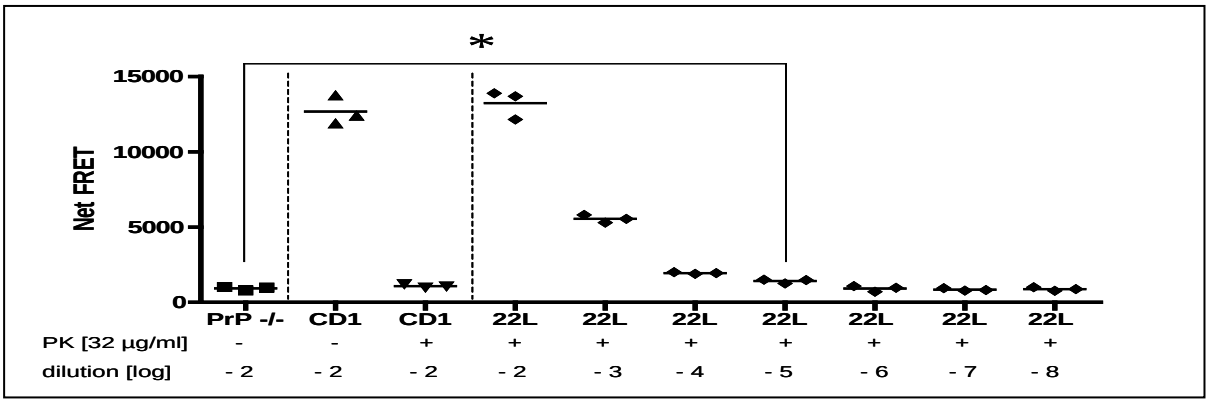

Figure 31. PrP^{Sc} detection in 22L-infected murine brain homogenates

PrP^{Sc} was detected after proteolytic digestion with PK, denaturation with 0.1 N NaOH and neutralization with 0.3 M NaH_2PO_4. PrP WT CD1 brain homogenate was used as control. A prion titer of 10^{-5} was detectable. *: $p < 0.05$. PrP $^{-/-}$: PrP knock out brain homogenate.

Development of a Heterogeneous PrP^C Cell Surface TR-FRET Assay

In a first set of experiments I examined whether the FRET assay could be applied to monitor the presence of PrP^C on the cell surface of living N2a cells. To test this idea, different numbers of intact N2a cells were seeded in 96-wells one day before the experiment. For FRET detection of PrP^C on intact cells, different tandem antibody combinations were used and co-incubated in Tris/Krebs buffer at 4°C for 30 min. **Fig. 32 a** and **b** illustrates graphs showing the cell surface PrP^C expression of living N2a cells directly after labelling **(Fig. a)** or after **(Fig. b)** washing out the non-reactive labelling antibodies as a function of cell number. PrP knock-out cells (Hpl PrP KO) lacking expression of PrP were used as negative controls.

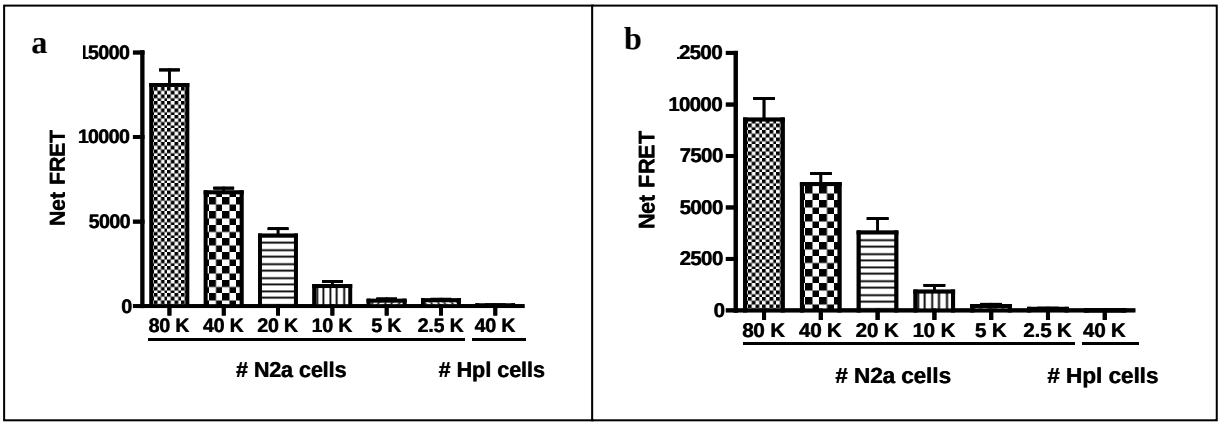

Figure 32. PrP^C detection at the cell surface of living cells as a function of cell number

Using equimolar mixtures of FRET antibody pair POM2Eu/POM2APC, PrP^C was detected as a function of cell number before **(a)** and after **(b)** a washing step at the surface of intact N2a cells. Hpl PrP KO cells were used as negative controls. Mean ± SD are shown from triplicates. K = 1000.

Surprisingly, not all used FRET antibody combinations worked. A correlation of signal-to-cell number ratio was found for the N-terminal POM2Eu/POM2APC antibody pair, even without a washing step. This indicates that the FRET signal generated by the bound antibodies is directly proportional to the amount of PrP^C expressed on the surface of living N2a cells. This also proves that the used antibodies are not degraded or cleaved from the cell surface during labelling. The second tested tandem antibody pair, C-terminal directed POM1Eu/POM19APC, did not work (not shown). A reason could be that steric hindrances interact with their target epitopes and therefore become inaccessible for binding. The reduction of the FRET signals before and after the washing step resulted most likely from the removal of non-binding antibodies. POM2Eu/POM2APC FRET signals from $PrP^{0/0}$ Hpl cells are negligible and disappear after a washing step with Tris/Krebs buffer. In a further experiment, N2a cells were seeded in a 384-well plate from 32’000 to 0 one day before the experiment. In **Fig. 33a** and **b**, results are shown for the POM2Eu and POM1APC in HTRF and TR-FRET mode, respectively. In HTRF mode, a number of 500 cells are clearly detectable. The results are even more robust in the TR-FRET mode after removing unbound FRET antibodies by washing. For other FRET antibody combinations such as POM1Eu/POM2APC and POM2Eu/POM2APC, respectively, less robust results were found in the HTRF mode (**Fig. 33c** and **d**).

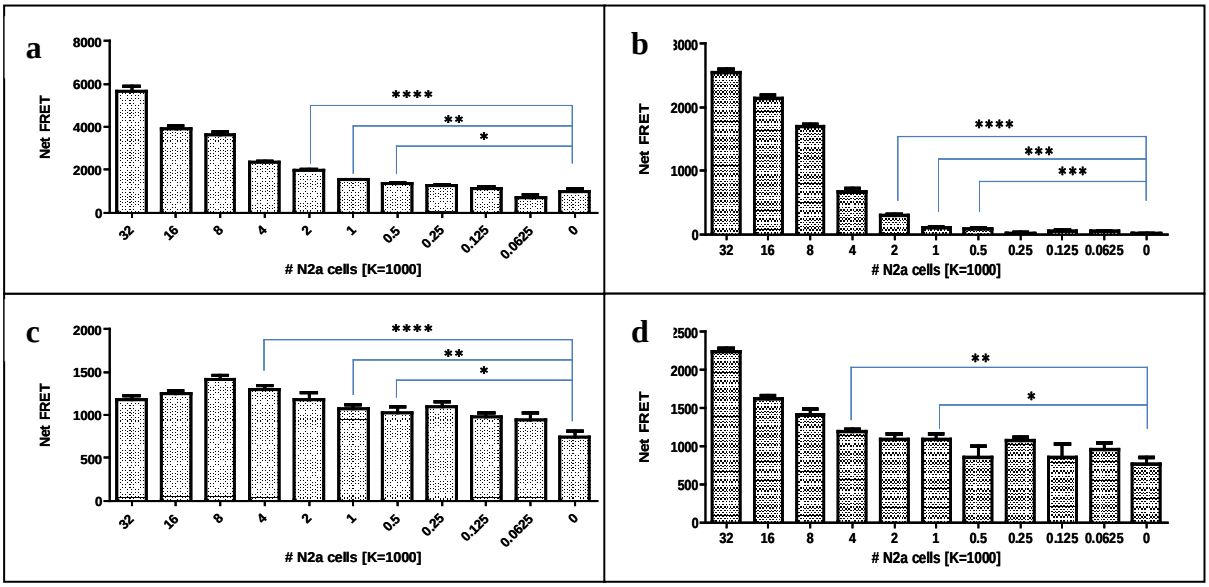

Figure 33. Detection of PrP^C on the cell surface of living N2a cells

Cell surface detection of PrP^C in the 384-well format. **(a)** POM2Eu/POM1APC in HTRF and **(b)** in TR-FRET mode. **(c)** POM1Eu/POM2APC in HTRF and **(d)** POM2Eu/POM2APC in HTRF mode. Shown are triplicates. *: $p < 0.05$; **: $p < 0.01$; ***: $p < 0.001$.

The N-terminal octarepeat of PrP contains four POM2 antibody binding sites [Polymenidou et al., 2008]. To prevent a binding preference for either POM2Eu or POM2APC labelled antibodies, equimolar concentrations were used in titration experiments **(Fig. 34)**. Briefly, 20'000 (20K) N2a cells were seeded in 96-wells one day before starting the experiment. Equimolar antibody concentrations ranging from 1-17.5 nM were diluted in Tris/Krebs buffer. Cell labelling was done at 4°C for 30 min. Immediately after an included washing step with Tris/Krebs buffer, FRET signals were measured. Concentrations as low as 2.5 nM for the Eu-Donor and APC-acceptor POM2 antibody were sufficient to get a large and specific signal for each fluorophore on intact N2a cells **(Fig. 34a** and **b)**. The detected FRET signal reached a plateau at about 7.5 nM for each POM2 FRET tandem antibody, suggesting the saturation of specific recognition sites of the conjugates **(Fig. 34c)**.

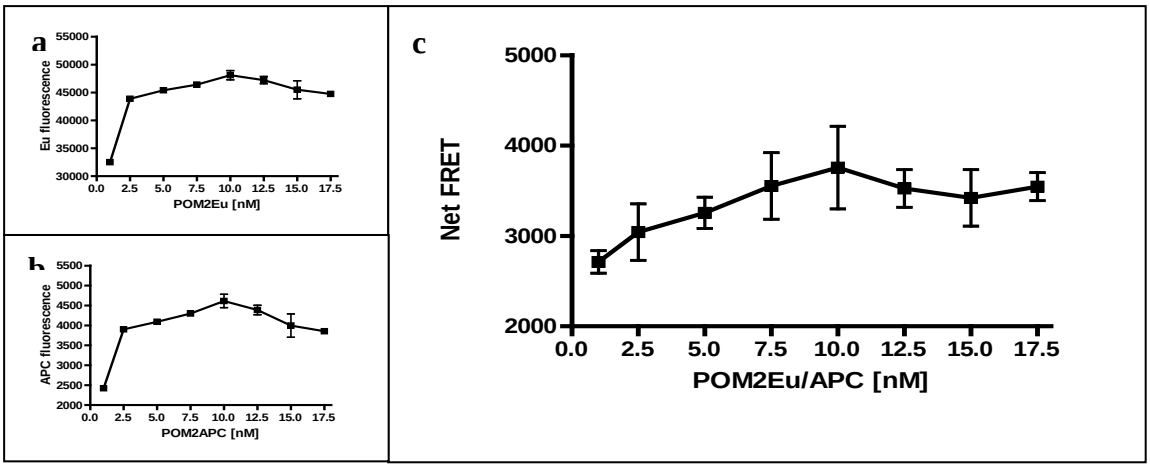

Fig. 34. Titration experiments of POM2Eu/POM2APC conjugated antibodies at the surface of living N2a cells (opposite page)

The fluorescence of the donor (POM2Eu) **(a)** and the fluorescence of the acceptor (POM2APC) **(b)** were measured separately for each channel in the titration experiments. Net FRET signals are shown in **(c)**. Each point represents the mean ± SD of sixplicates.

Next, I did binding studies of POM2Eu/POM2APC antibodies at the surface of viable N2a cells. For that, an equimolar concentration of 2.5 nM was used for both antibodies. FRET signals were measured at different time points directly or after a washing step **(Fig. 35)**. Without washes, antibody saturation seems to reach a plateau after 2 hrs, in contrast, FRET signals stay constant over the measured time after washing out unbound antibodies. For the following experiments, POM2Eu and POM2APC tandem antibodies were used at 2.5 nM concentrations and the cell surface labelling procedure was done at 4°C for 30 min.

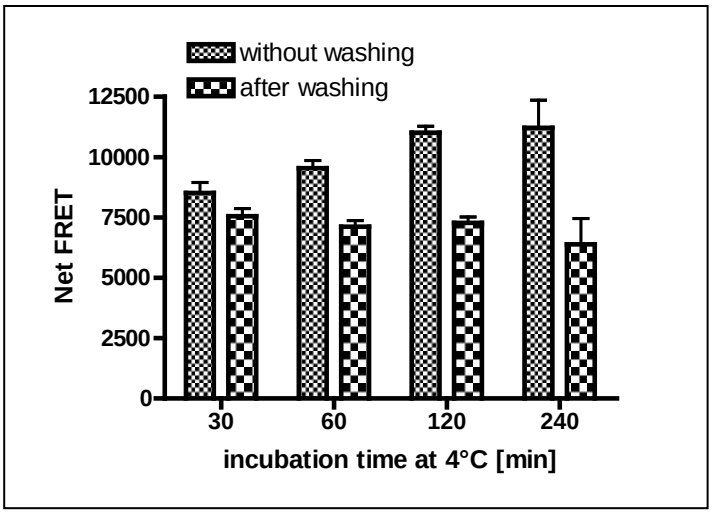

Figure 35. Binding studies of POM2Eu/POM2APC FRET antibodies on the surface of living N2a cells.

Binding of the FRET antibody pair was performed at 4°C. One day before, 40'000 N2a cells were plated into 96-well plates. FRET signals were measured at different time points without and after washing out unbound antibodies. Each bar represents the mean ± SD of sixplicates.

Only unspecific FRET signals were observed when cocultering mono-labelled intact N2a and Hpl cells in the same wells for 18 hours. Both cell lines were each incubated with both POM1-Eu and POM2-APC antibodies, respectively. The coupling procedure was performed at 4°C for 30 min. To remove unbound antibodies, the cells were washed two times with pre-warmed cell culture medium. All possible "Eu-APC"-cell culture combinations were tested and Net FRET signals were measured at two different time points t=0 and t=18h **(Fig. 36 a** and **b)**.

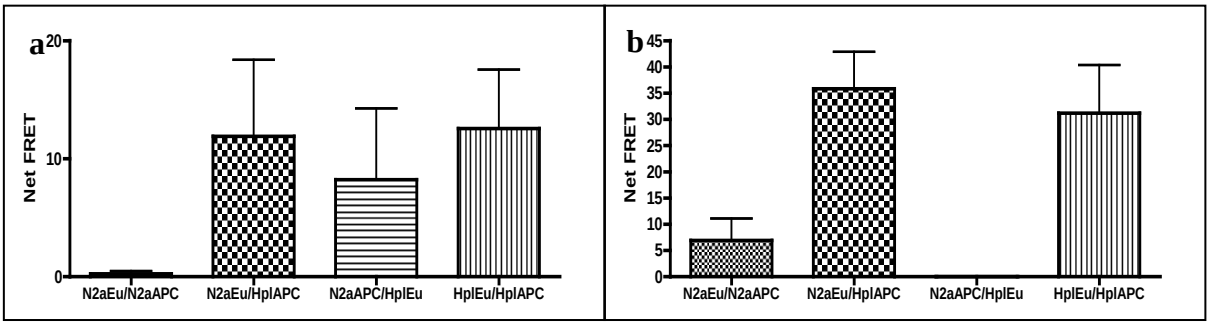

Figure 36. Mono-labelled cell co-culturing experiments

For the cell culture experiments, cells were pre-incubated either with POM1-Eu (N2aEu or HplEu) or POM2-APC antibodies (N2aAPC or HplAPC) at 4°C for 30 min. After removal of unbound antibodies by a washing step, 20'000 mono-labelled N2a cells were co-cultured either with 20'000 mono-labelled N2a or Hpl cells. As a control experiment, HplEu and HplAPC were cocultured. Net Fret signals were immediately measured after plating the cells (t=0) **(a)** or after 18 hours **(b)**.

Next, I wanted to control the cell surface levels of PrP^C pharmacologically. To that aim, N2a cells were treated with Brefeldin A (BFA). BFA is a compound that prevents trafficking of proteins from the endoplasmatic reticulum to the Golgi apparatus [Nebenfuhr, 2002] and downregulates the expression of PrP^C at the cell surface. For this experiment, 40'000 N2a cells were incubated with different concentrations of BFA in cell culture medium for 18 hrs. After washing, FRET signals were detected with equimolar mixtures of POM2Eu/POM2APC in Tris/Krebs buffer. Again, the FRET signals are dependent on the number of PrP^C at the cell surface **(Fig. 37)**.

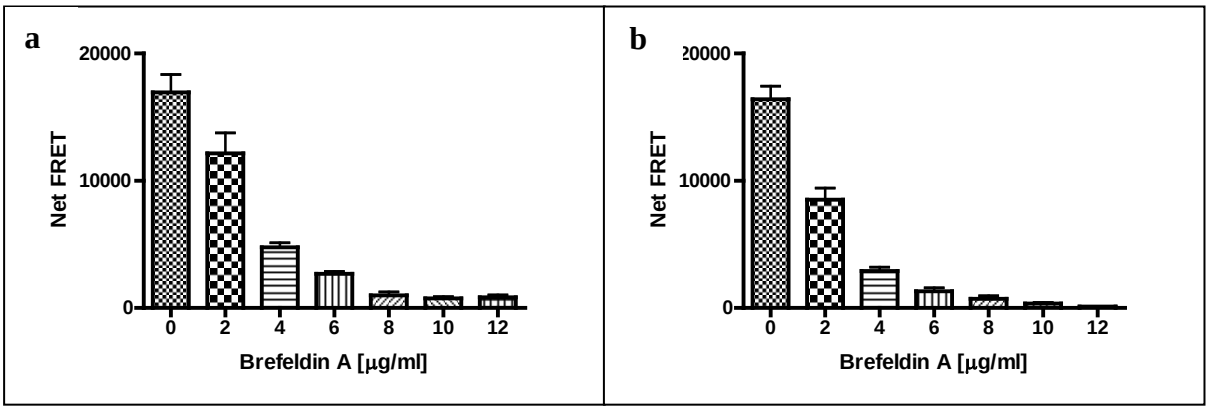

Figure 37. Detection of cell surface PrP^C after BFA treatment

The Figures show a dose-response for BFA treatment in **(a)** without and in **(b)** after a washing step.

The release of a protein from intact cells into the medium with phosphatidylinositol phospholipase C (PI-PLC) is considered for the presence of a phosphatidyl-inositol-containing glycolipid anchoring the protein to the cell surface [Low MG, 1987]. PrP^C is anchored to the cell surface by a GPI glycolipid [Stahl N, 1987] and can be released by PI-PLC digestion. To extend the cell surface studies, I approached PI-PLC to deplete PrP^C from

the plasma membrane of intact cells. For that, living N2a cells were digested with increasing concentrations of PI-PLC at 4°C for 30 min. Increasing PI-PLC concentrations significantly increased PrP^C in cell culture media **(Fig. 38a)**, however, a significant PrP^C decrease on the surface of living N2a cells could not be detected. These experiments confirm that binding of antibody relies on the presence of the extracellular prion protein, such that only cell surface protein can be detected.

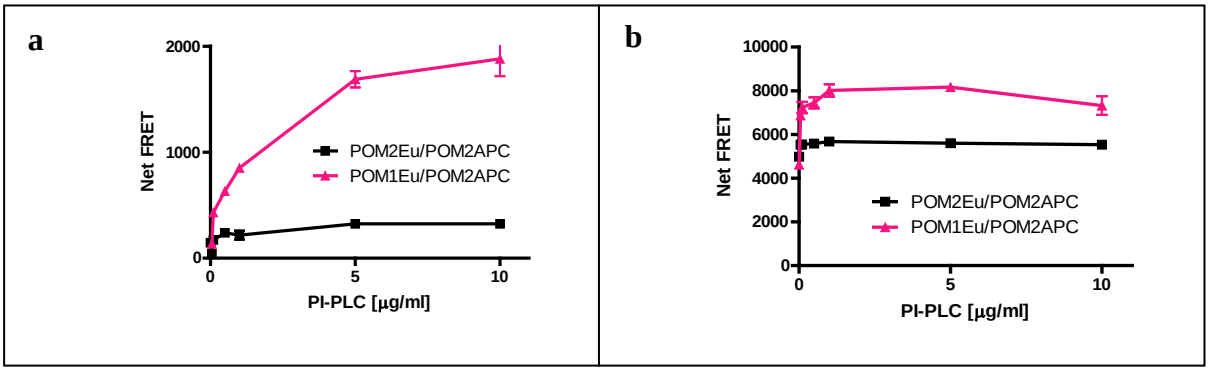

Figure 38. PI-PLC digestion of living N2a cells

Digestion of intact N2a cells with PIPLC at 4°C, **(a)** cleaved PrP^C in cell culture media, **(b)** cell surface expression of PrP^C.

I was wondering, whether PrP^C cell surface detection by different FRET antibody combinations depends on a single double-stained PrP^C molecule or two or more mono-labelled PrP^C molecules forming a higher molecular complex. For that reason, intact POM2Eu/APC FRET-labelled N2a cells were exposed to different detergents, which loosens cell membrane structure. Each detergent extremely decreased the FRET signal **(Fig. 39)**, assuming that complex membrane structures are mainly responsible for the FRET signal rather than single PrP^C molecules distributed over the whole cell surface.

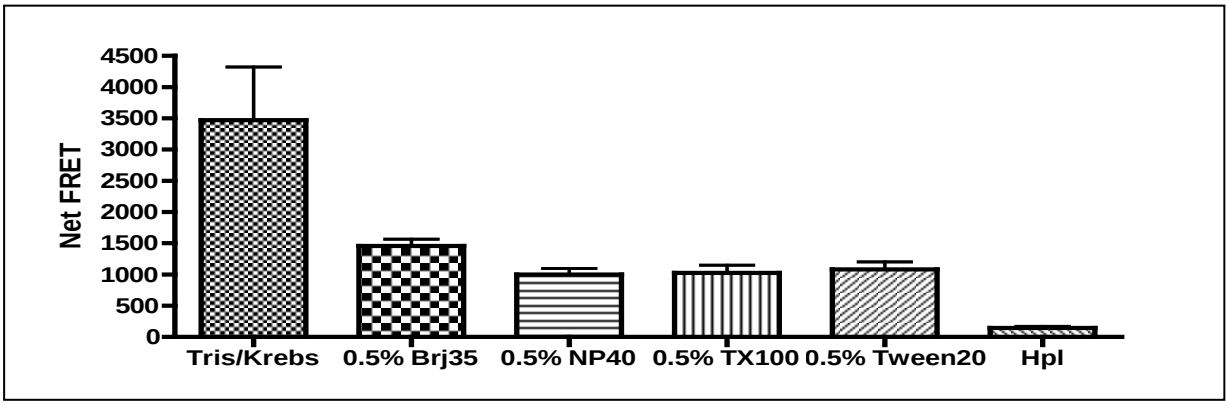

Figure 39. Membrane disruption of intact FRET-labelled N2a cells

One day before, 40K N2a cells/well were plated onto a 96-well plate. Next day, the cells were labelled with 2.5 POM2Eu and 5 nM POM2APC for 30' at 4°C. After removing non-reactive antibodies, cells were exposed to 0.5% Brj35, NP40 TritonX100 for 30' at 4°C.

Interfering PrP^C Cell Surface FRET Signals with Prions

According to the "prion-only" hypothesis, PrP^{Sc} needs PrP^C as a template for its propagation [Prusiner, 1982]. I was wondering whether I can show such an interaction by FRET. To do so, PrP^C of non-infected N2a cells was labelled with POM1Eu/POM19APC or POM1Eu/POM2APC FRET antibodies at 4°C and washed with Tris/Krebs buffer. Labelled cells were exposed to different concentrations of either prion-infected (RML BH), non-infected (CD1 BH) or PrP-KO ($PrP^{-/-}$) brain homogenates. Brain homogenates were diluted in cell culture medium and experiments were performed for 30 min at 37°C or in a control experiment at 4°C **(Fig. 40)**. Clear differences in FRET signal intensities were detected at 37°C **(Fig. 40a** and **c)** compared to 4°C, where the signals were quite similar **(Fig. 40b** and **d)**. It seems that interactions of PrP^C and PrP^{Sc} occur at higher temperatures. Differences in FRET signal intensities were also observed between the two different FRET antibody combinations. Higher FRET signals were observed with the POM1Eu/POM19APC FRET antibody pair. An explanation could be that upon binding of PrP^{Sc} to PrP^C, POM1 and POM19 epitopes become closer to each other and therefore the FRET signal is increasing **(Fig. 40a)**. Using the POM1Eu/POM2APC FRET antibody pair, a decreasing FRET signal was monitored. However, whether conformational changes are responsible for the different FRET signals can only be proved when repeating these experiments with purified PrP^{Sc}.

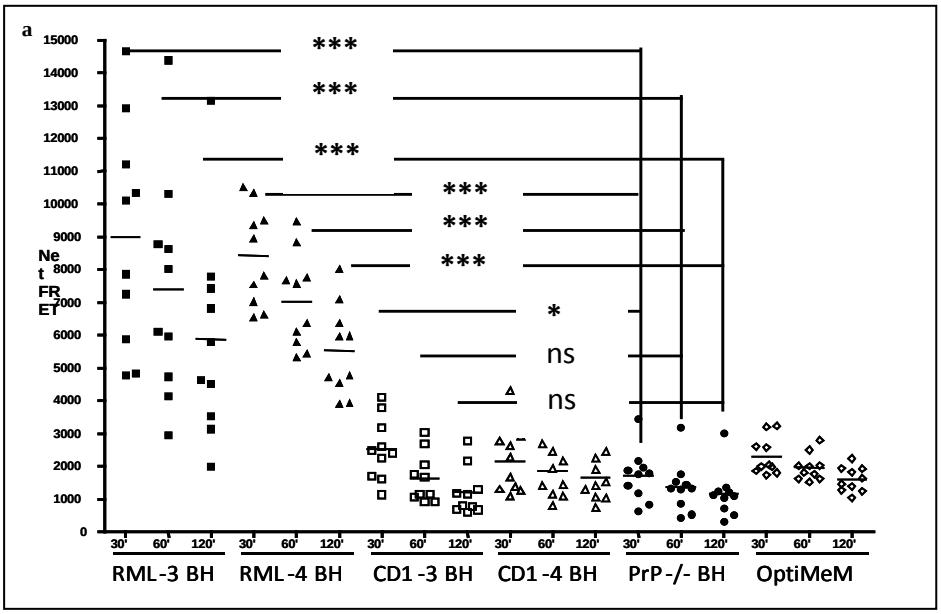

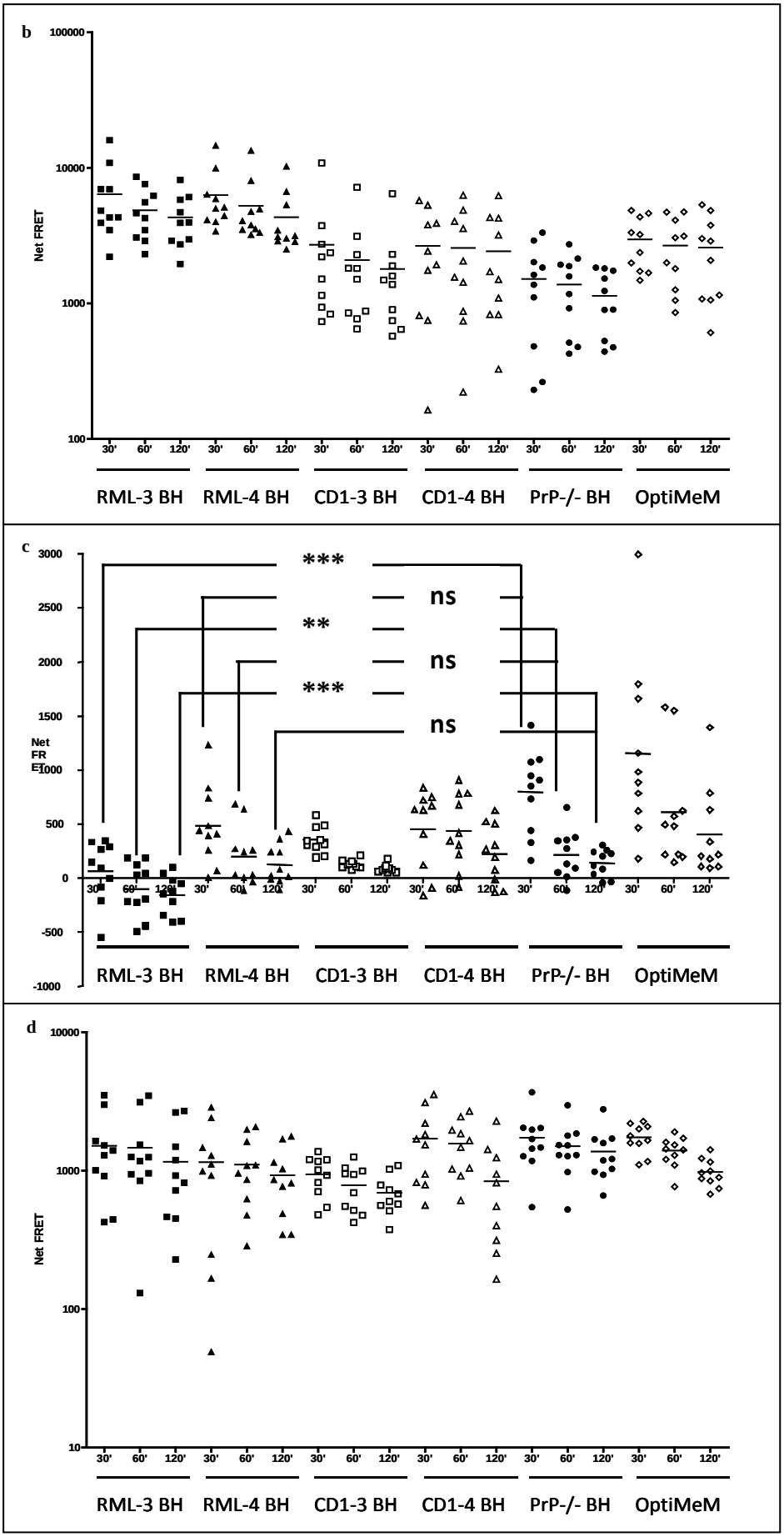
b
Net FRET
100000
10000
1000
100
30' 60' 120' 30' 60' 120' 30' 60' 120' 30' 60' 120' 30' 60' 120' 30' 60' 120'
RML-3 BH
RML-4 BH
CD1-3 BH
CD1-4 BH
PrP-/- BH
OptiMeM
c
Net FRET
3000
2500
2000
1500
1000
500
0
-500
-1000
***
**
***
ns
ns
ns
30' 60' 120' 30' 60' 120' 30' 60' 120' 30' 60' 120' 30' 60' 120' 30' 60' 120'
RML-3 BH
RML-4 BH
CD1-3 BH
CD1-4 BH
PrP-/- BH
OptiMeM
d
Net FRET
10000
1000
100
10
30' 60' 120' 30' 60' 120' 30' 60' 120' 30' 60' 120' 30' 60' 120' 30' 60' 120'
RML-3 BH
RML-4 BH
CD1-3 BH
CD1-4 BH
PrP-/- BH
OptiMeM

Figure 40. FRET-PrP^C cell surface blocking experiments (opposite page)

PrP^C on the surface of N2a cells was labelled either with POM1Eu/POM19APC **(a/b)**, POM1Eu /POM2APC **(c/d)** or POM2Eu(24x)/POM2APC (not shown). Cells were washed and thereafter exposed to 10^{-3} or 10^{-4} in OptiMEM diluted brain homogenates (BH). Experiments were performed either at 37°C **(a/c)** or 4°C **(b/d)**. OptiMEM media without any supplements was included as an additional control. *: $p < 0.05$; **: $p < 0.01$; ***: $p < 0.001$.

Development of a Heterogeneous PrP^C endocytosis TR-FRET Assay

It has been shown that PrP^C, located on the cell surface, is constitutively internalised and recycles back to the plasma membrane [Harris DA, 2003; Prado MA, 2004] within 60 min [Shyng SL, 1993; Harris DA, 2003]. This cycling process is inducible by copper or zinc ions [Pauly PC & Harris DA, 1998; Watt NT & Hooper NM, 2003; Lee KS, 2001] and is believed to be necessary for conversion of PrP^C to PrP^{Sc} [Borchelt DR, 1993].

We therefore wondered whether the FRET technology could also be used to measure PrP's endocytosis. In a first set of experiments, living cells were preincubated only with one of the two FRET antibodies at 4°C and thereafter exposed for different time points at 37°C. After several washing steps to remove unbound antibodies, the cells were labelled with the second FRET antibody at 4°C for 30 min. In a control experiment (no internalization) the same FRET antibody pair was used and all incubation times were performed for the same time period but at 4°C for 30 min. Low temperature prevents all energy-driven internalization processes [Goldenthal K, 1984] and only a marginal amount of PrP^C became endocytosed at 4°C. Incubation at 37°C led to a decrease in cell surface PrP^C expression, presumably because of internalisation **(Fig. 41)**.

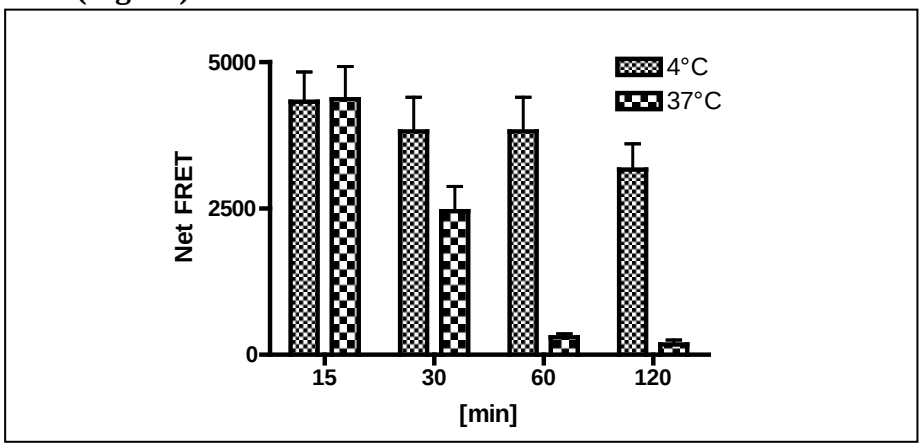

Figure 41. Kinetics of PrP^C on intact murine N2a cells

N2a cells were incubated with POM1Eu at 4°C for 30 min, washed and exposed to 37°C for various time points in cell culture medium. After each time point, POM2APC was added and the FRETsignal was measured. To block endocytosis of PrP^C, all steps were performed at 4°C.

PrP^C Cell Surface Detection of Human Cells with TR-FRET

Next, we decided, in collaboration with Prisca Liberali and Lucas Pelkmans (Institute of Molecular Life Sciences, University of Zürich), to elucidate genes involved in the endocytosis of human PrP^C in cells. This should be done with a treatment of siRNAs which interfere with the expression of specific genes with complementary nucleotide sequence [Elbashir et al., 2001]. To monitor toxic effects of siRNA treatments, an alamarBlue viability assay was established.

AlamarBlue Cell Viability Assay

AlamarBlue is the commercial trademark of resazurin which is used as an indicator of cell viability in mammalian cell cultures [Anoopkumar-Dukie et al., 2005]. It is a blue dye, itself weakly fluorescent until it is irreversibly reduced to the pink colored and highly red fluorescent resorufin [Bueno C et al., 2002]. To assess whether the alamarBlue assay could be used to monitor the cell viability of cells, cell titration experiments were performed. One day before the start of the experiment, different numbers of N2a cells ranging from 32'000 to 0 were plated into a 384 well plate. Cells were incubated for 12 h with alamarBlue and the fluorescent signal was read with a Paradigm fluorescent reader. The fluorescent signal depends on the number of living cells **(Fig. 42a)**. In the same experiment the cell surface expression of PrP^C was determined by FRET. A good correlation of cell viability versus cell surface PrP^C expression was found **(Fig. 42 insert)**. I used HeLa cells to do a time course analysis. Different amounts of cells were cultured for three days and after each day, the viability was measured **(Fig. 42b-d)**. Cell death was induced by co-culturing HeLa cells with staurosporine (STS), a compound that activates caspase-3 [Chae et al., 2000] **(Fig. 42e-g)**.

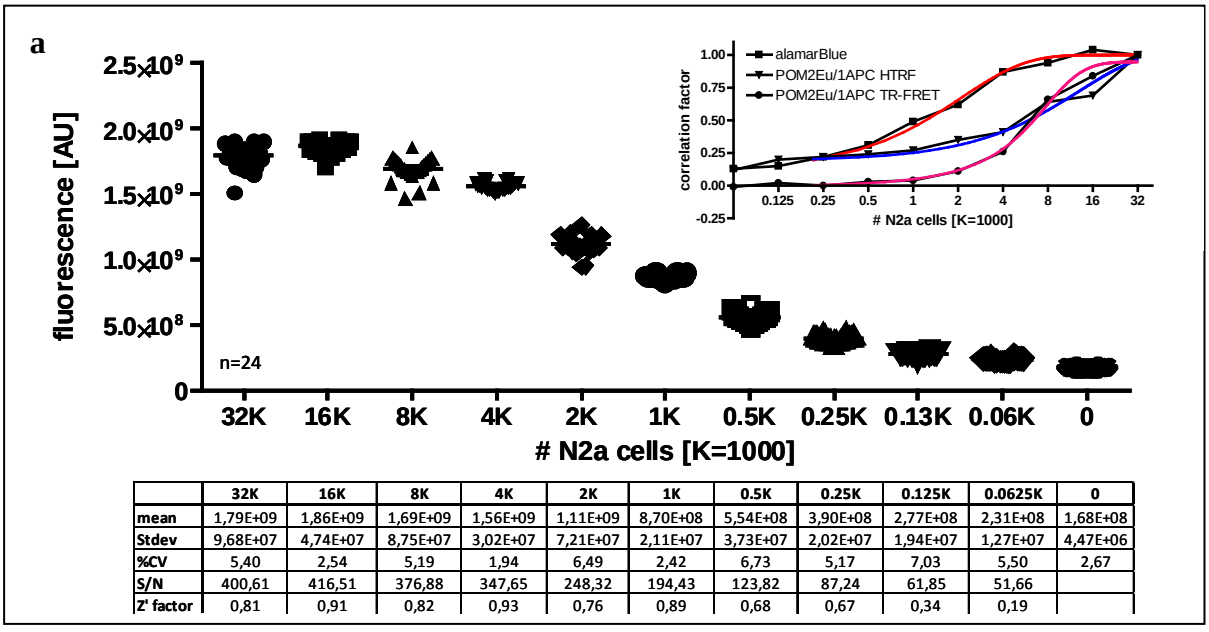

	32K	16K	8K	4K	2K	1K	0.5K	0.25K	0.125K	0.0625K	0
mean	1,79E+09	1,86E+09	1,69E+09	1,56E+09	1,11E+09	8,70E+08	5,54E+08	3,90E+08	2,77E+08	2,31E+08	1,68E+08
Stdev	9,68E+07	4,74E+07	8,75E+07	3,02E+07	7,21E+07	2,11E+07	3,73E+07	2,02E+07	1,94E+07	1,27E+07	4,47E+06
%CV	5,40	2,54	5,19	1,94	6,49	2,42	6,73	5,17	7,03	5,50	2,67
S/N	400,61	416,51	376,88	347,65	248,32	194,43	123,82	87,24	61,85	51,66	
Z' factor	0,81	0,91	0,82	0,93	0,76	0,89	0,68	0,67	0,34	0,19	

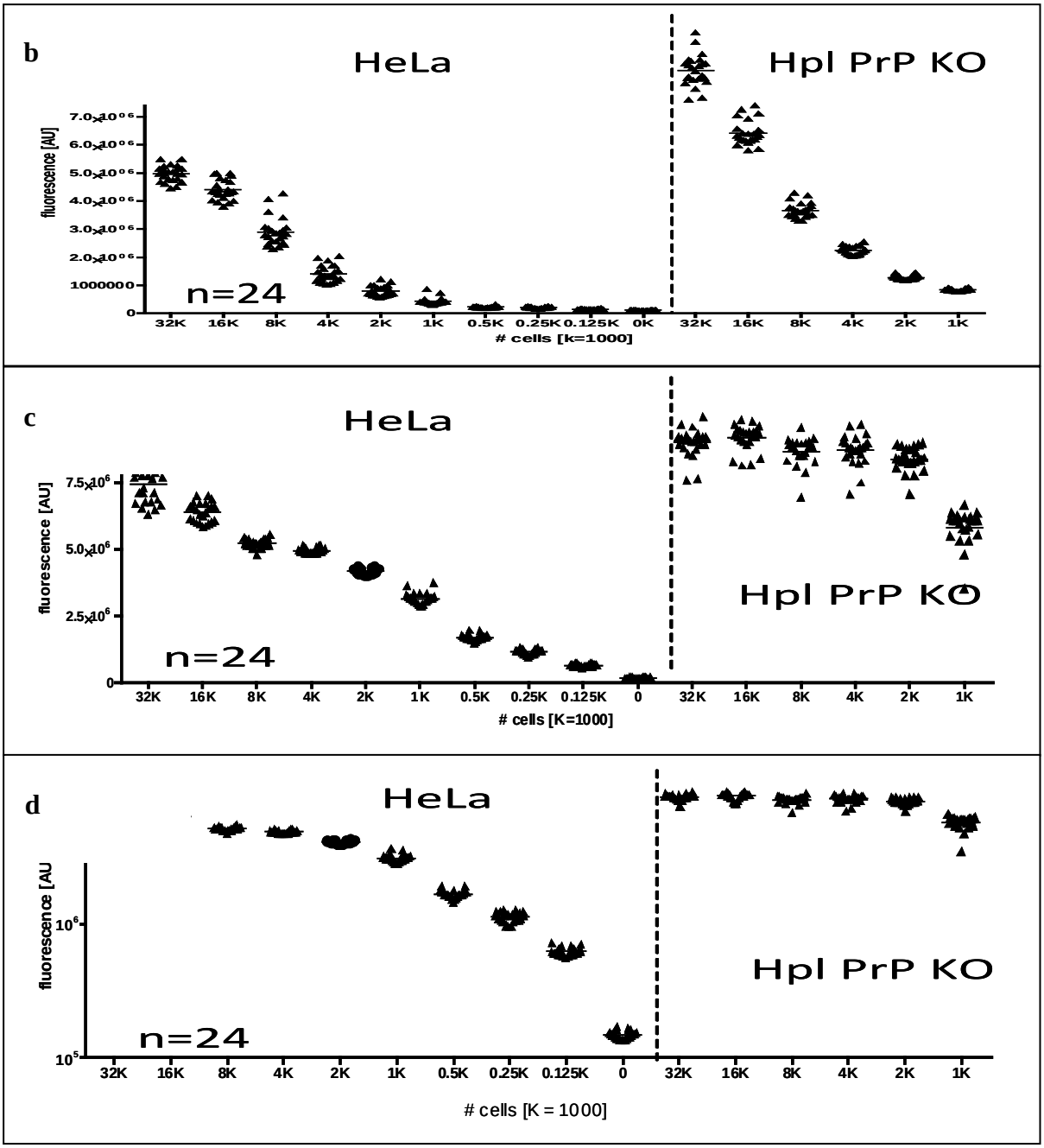
b
HeLa
Hpl PrP KO
fluorescence [AU]
7.0x10^6
6.0x10^6
5.0x10^6
4.0x10^6
3.0x10^6
2.0x10^6
1000000
0
n=24
32K 16K 8K 4K 2K 1K 0.5K 0.25K 0.125K 0K 32K 16K 8K 4K 2K 1K
cells [k=1000]
c
HeLa
Hpl PrP KO
fluorescence [AU]
7.5x10^6
5.0x10^6
2.5x10^6
0
n=24
32K 16K 8K 4K 2K 1K 0.5K 0.25K 0.125K 0 32K 16K 8K 4K 2K 1K
cells [K=1000]
d
HeLa
Hpl PrP KO
fluorescence [AU
10^6
10^5
n=24
32K 16K 8K 4K 2K 1K 0.5K 0.25K 0.125K 0 32K 16K 8K 4K 2K 1K
cells [K = 1000]

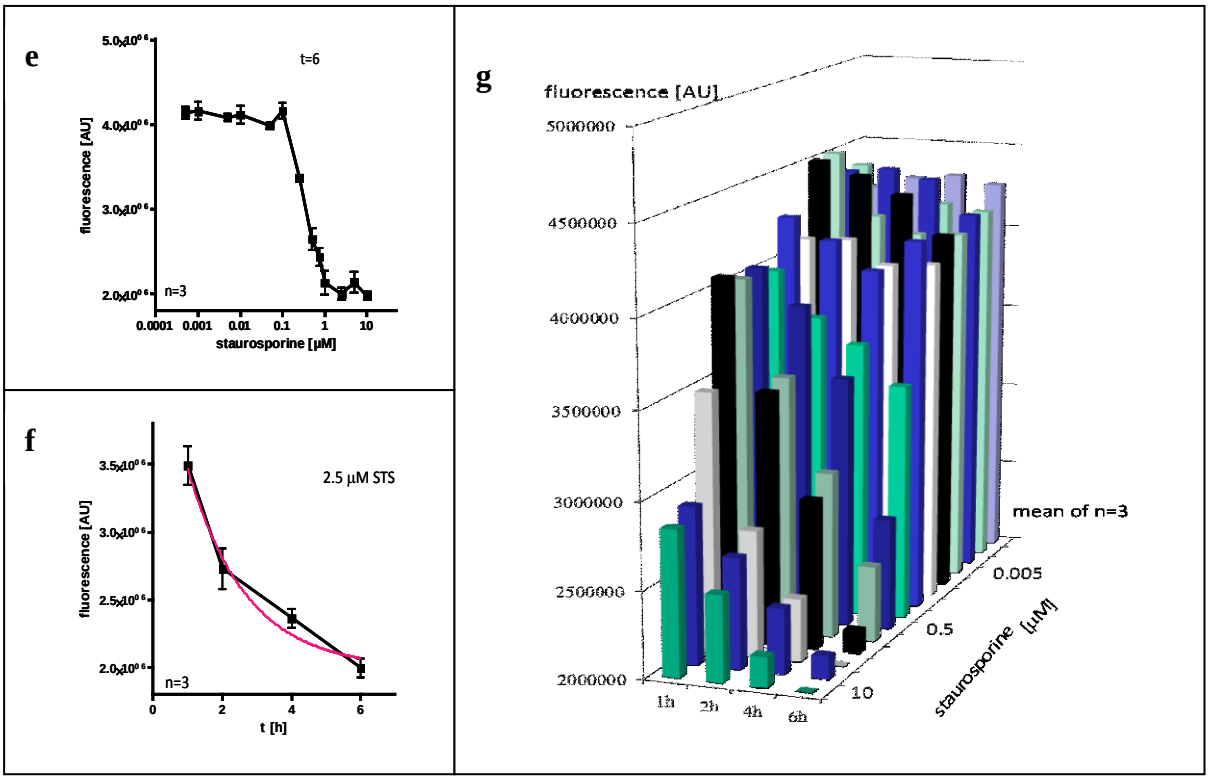

Figure 42. AlamarBlue viability assay (opposite page)

Viability of HeLa and Hpl PrP KO cells was monitored over three days, **(a)** day one **(b)** day two **(c)** day three. Induction of cell death by Staurosporine treatment for six hours **(d)** and at a concentration of 2.5 µM over six hours. In **(e)** is shown the summary of STS treatment. AU: Arbitrary Units.

PrP^C Cell Surface Detection of Intact Human Cells with TR-FRET

I tried to detect PrP^C on the surface of two different human cell lines, namely HeLa and A549 (lung epithelial cells) cells. Best results from FRET antibody titration experiments revealed, that POM antibodies with binding epitopes in or near the N-terminal region of PrP^C could be used either as donor or acceptor FRET antibody in both cell lines **(Fig. 43)**. Routinely, I utilized POM2Eu as donor FRET antibody, because POM2's four binding epitopes at the N-terminal region of PrP^C generated higher FRET signals compared to other members of the POM antibody family, especially in low PrP^C expressing cells.

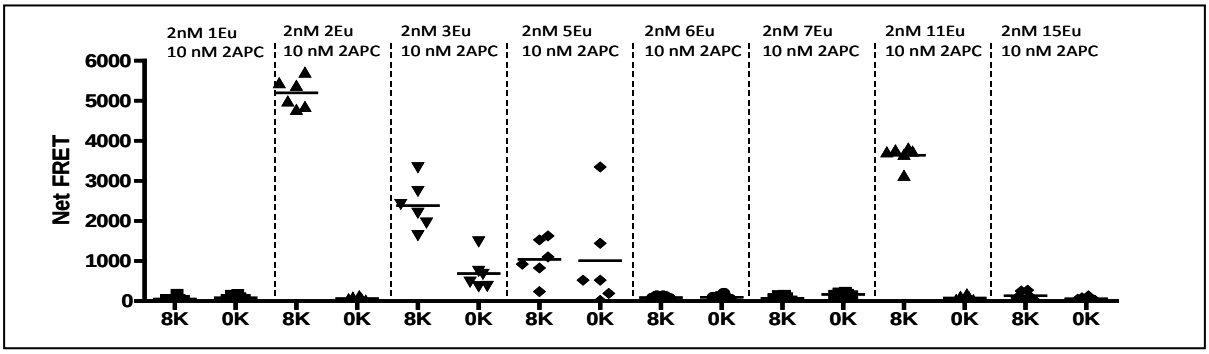

Figure 43. Best POM antibody pair analysis for PrP^C cell surface detection by solid phase FRET (opposite page)

Various FRET antibody combinations were tested for detection of PrP^C on the cell surface of living A549 cells. APC-coupled POM2 antibody (2APC) was used as FRET acceptor molecule for all experiments. Various POM antibodies (POM1, 2, 3, 5, 6, 7, 11, 15) were coupled to Eu and tested. Shown are results from hexaplicates ± SD in the HTRF mode (100 µs time delay; 400 µs time window).

Additionally, PrP^C expression levels of HeLa and A549 cells were confirmed by ELISA experiments **(Figure 44)**. The highest OD signals of PrP^C were achieved when using the POM2/POM2 antibody combination **(Fig. 44a)**, followed by the POM2/POM11 **(Fig. 44b)** and POM11/POM2 **(Fig. 44c)** antibody pair. The POM11/POM11 ELISA experiment had the lowest OD values, presumably because only two POM11 binding epitops are available **(Fig. 44d)**. A549 cells contain about 1.5 ng/ml PrP^C in 100 µg/ml crude cell lysate and have similar PrP^C levels as murine N2a cells. These results were confirmed by all four different ELISA experiments. HeLa cells express PrP^C less than nine times compared to A549 cells and N2a cells.

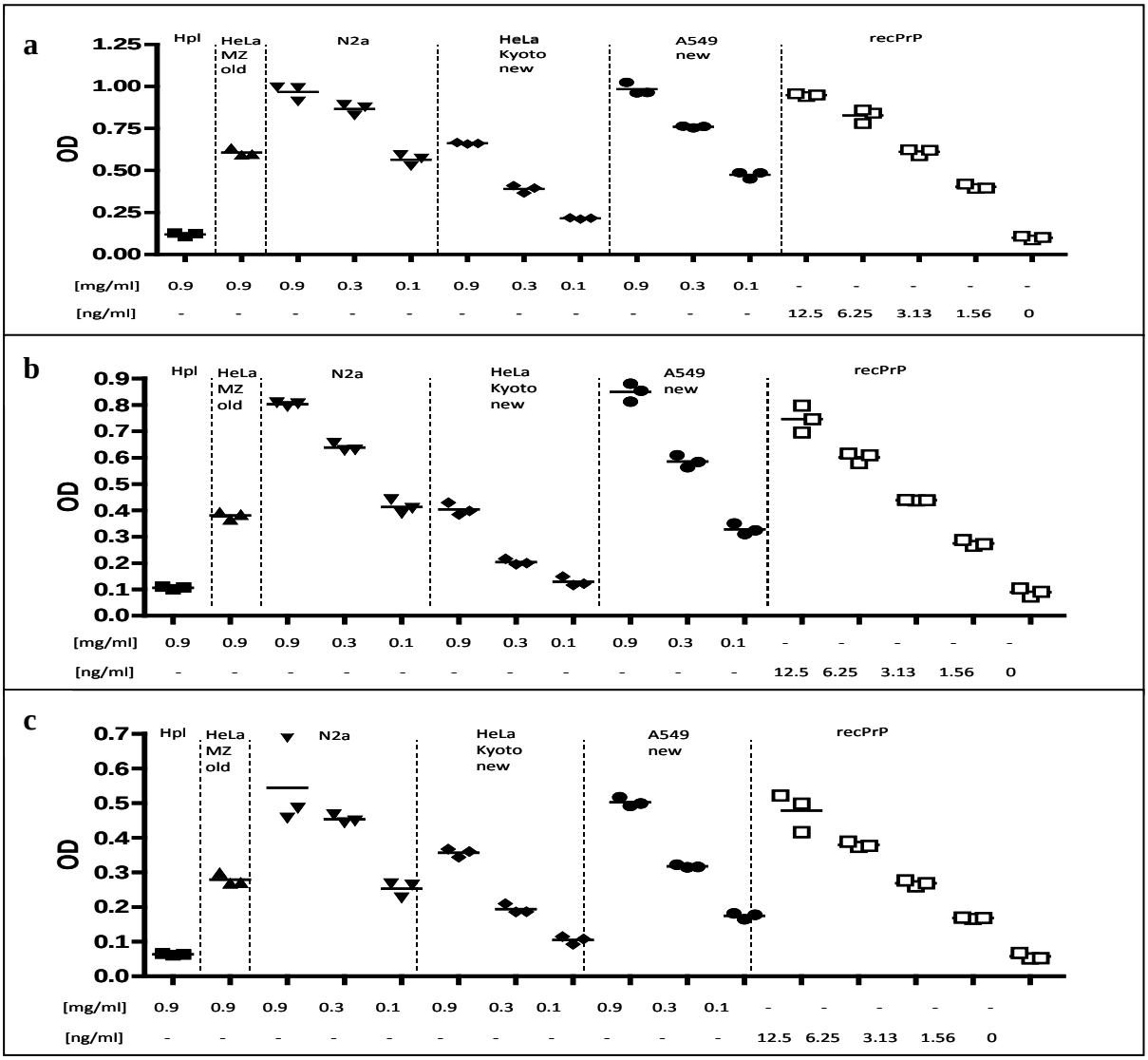

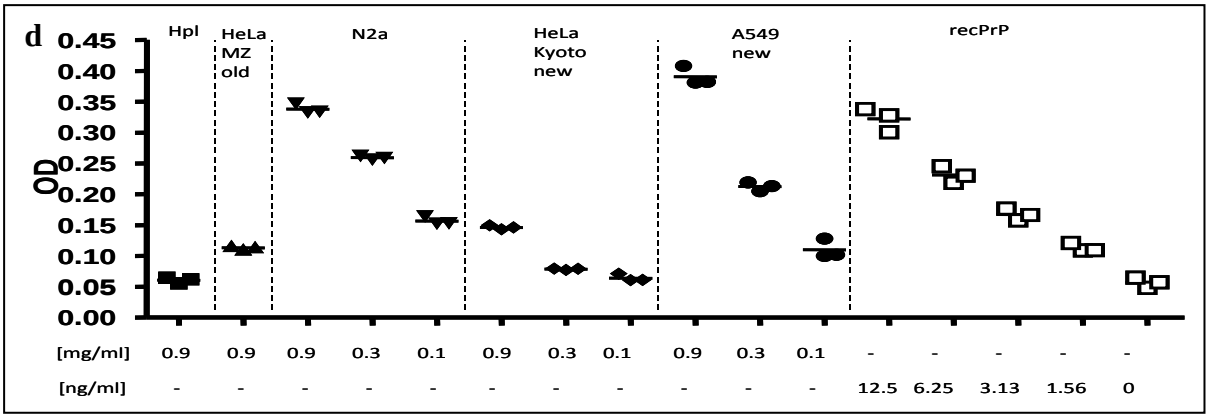

Figure 44. Detection of PrP^C in HeLa and A549 cell lysates by sandwich ELISA

PrP^C expression levels were determined by four different ELISAs. Plates were coated either with POM2 or POM11 antibody and detected with either biotinylated (bio) POM2 or POM11 antibody. In **(a)** POM2/POM2bio, **(b)** POM2/POM11bio, **(c)** POM11/POM2bio **(d)** POM11/POM11. Shown are results from triplicates.

I further characterized the POM2/POM2 antibody combination in ELISA and FRET experiments. In ELISA experiments, either full length recPrP **(Fig. 45a)** or brain homogenates of NGPI mice (Δ141-225) **(Fig. 45b)** was used to validate the POM2/POM2 specificity. In both ELISA experiments the POM2/POM2 ELISA antibody pair enabled the detection of PrP. In FRET experiments, the N1-fragment of recPrP (residues 23-111) was used **(Fig. 45c)**. As positive controls, the POM2Eu/POM2APC and as a negative control the POM1Eu/POM2APC FRET antibody pair was utilized. The N1-fragment was detectable with the POM2Eu/POM2APC antibody pair but not with the POM1Eu/POM2APC pair, because the POM1 epitope is not present within the N1-fragment of PrP.

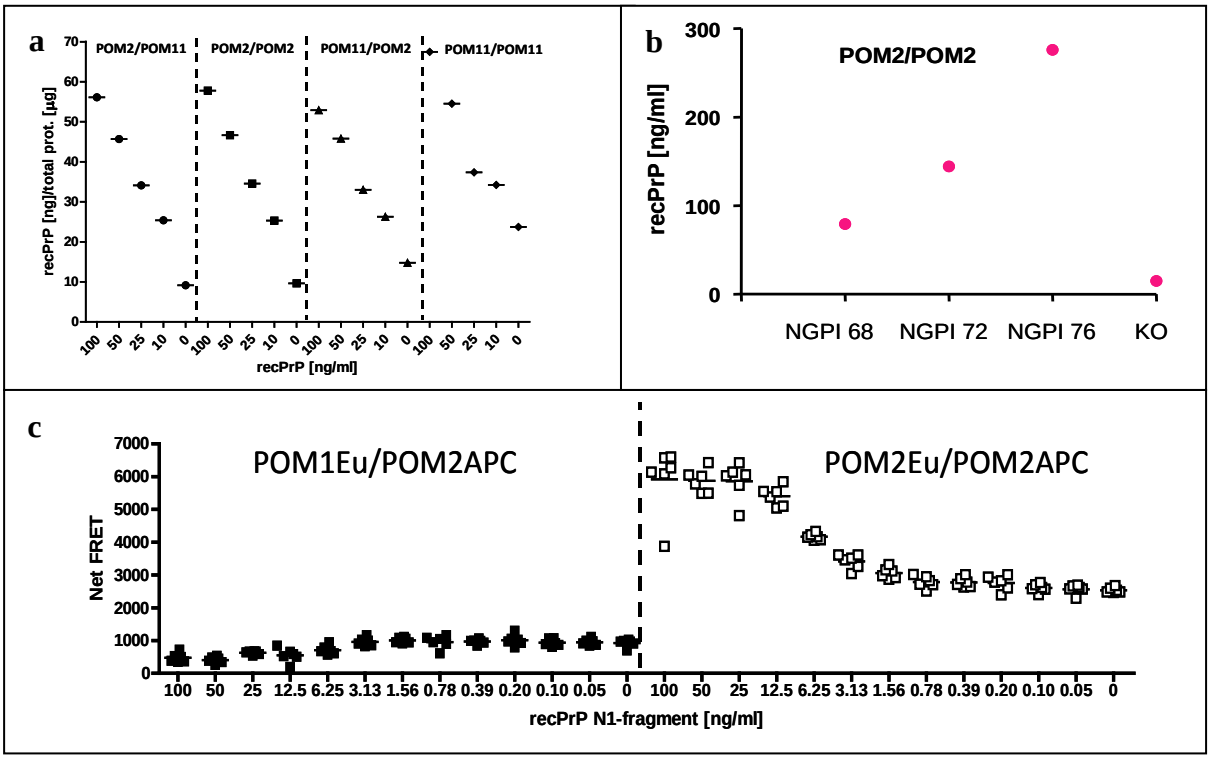

Figure 45. POM2/POM2 ELISA and homogeneous FRET experiments (opposite page)

The specificity of PrP detection by the POM2/POM2 antibody pair is shown by ELISA experiments, in **(a)** recPrP spiked in Hpl PrP KO cell lysate and in **(b)** brain homogenates from different ages (day68 to day76) of N-GPI mice. Shown is the mean of triplicates. **(c)** The corresponding FRET experiment was done with recombinant PrP N1-fragment. As negative control, the POM1Eu/POM2APC pair was used. Shown are hexaplicates.

Based on these results, I focused in more detail on the POM2Eu and POM2APC FRET antibody pair (2Eu/APC). To verify 2Eu/APC, cell titration experiments were performed. Different amounts of Hela cells were plated one day before in 384-well plates **(Fig. 46)**. Hpl PrP KO cells were used as negative control. A cell number dependent FRET signal was detected. A linear correlation of the dynamic range was found in the HTRF mode from 0 to 8000 cells (R2 = 0.92) and a slightly better one in the TR-FRET mode (R2 = 0.98). The 2Eu/APC FRET pair enables PrP^{C} cell surface detection for 500 HeLa cells in both measurement modes. The higher FRET signals measured in the HTRF mode may be due to a saturated state of the FRET antibodies which disappears after a washing step in the TR-FRET mode. The assay performances are summarized below. The coefficients of variation (%CV) as well as the signal-to-noise (S/N) ratio and the Z' factor are better in the HTRF mode compared to the TR-FRET mode. This is most likely due to the washing step in the TR-FRET mode.

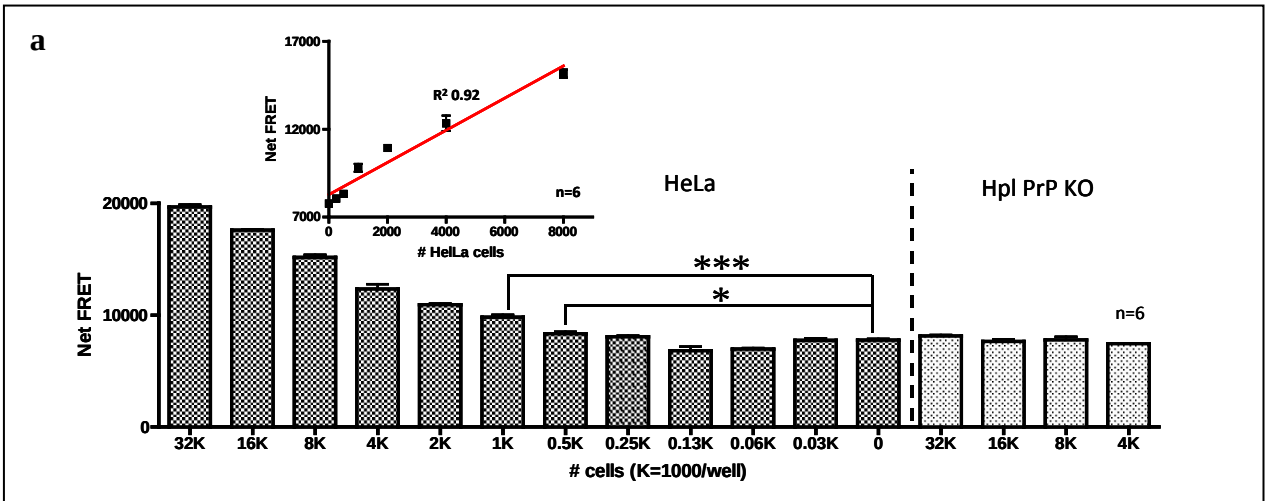

# HeLa	32000	16000	8000	4000	2000	1000	500	250	125	62.5	31.25	0
%CV	2.65	1.22	3.72	8.71	2.24	5.65	5.66	3.02	13.65	3.40	6.26	3.68
S/N	20.06	27.53	11.71	4.11	8.41	3.28	1.01	0.80				
Z'	0.80	0.85	0.66	0.11	0.50							

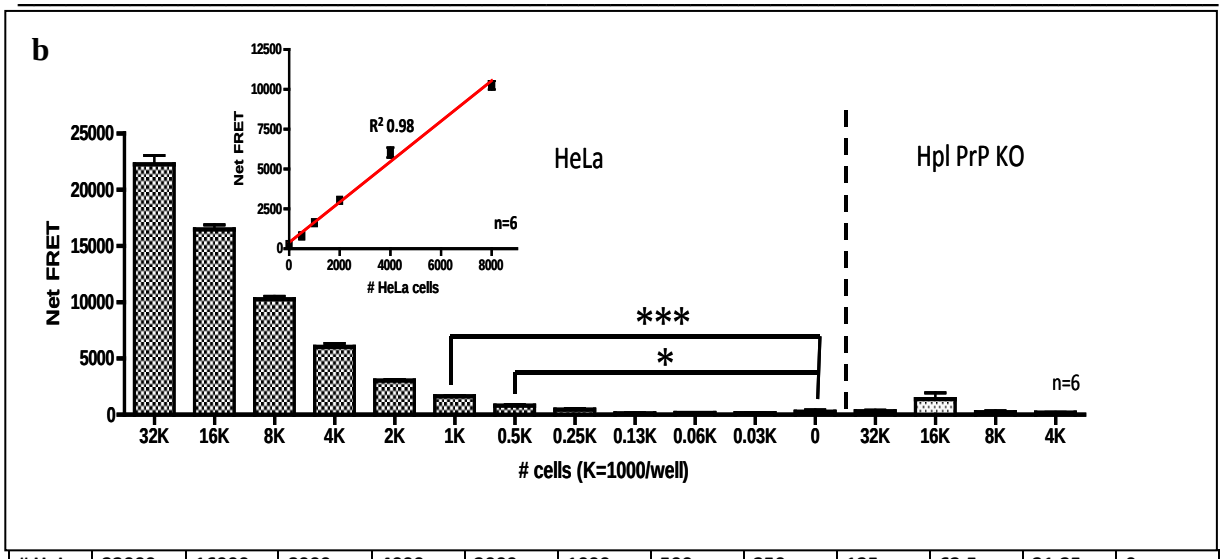

# HeLa	32000	16000	8000	4000	2000	1000	500	250	125	62.5	31.25	0
%CV	8.81	6.02	6.33	12.63	7.93	8.96	24.07	57.39	55.15	74.25	45.27	15.9.4
S/N	10.97	15.10	12.98	6.66	5.79	3.12	1.20	0.4				
Z'	0.68	0.74	0.68	0.39	0.29							

Figure 46. PrP^C cell surface detection on HeLa cells by solid-phase FRET

The specificity of human PrP^C detection in living HeLa cells by 2Eu/2APC FRET antibody pair is shown in a cell number titration experiment. **(a)** HTRF mode and **(b)** TR-FRET mode. *: $p < 0.05$; **: $p < 0.01$; ***: $p < 0.001$.

Similar results were found for the A549 cell titration experiments using the POM2Eu/POM2APC FRET antibody combination **(Fig. 47)**.

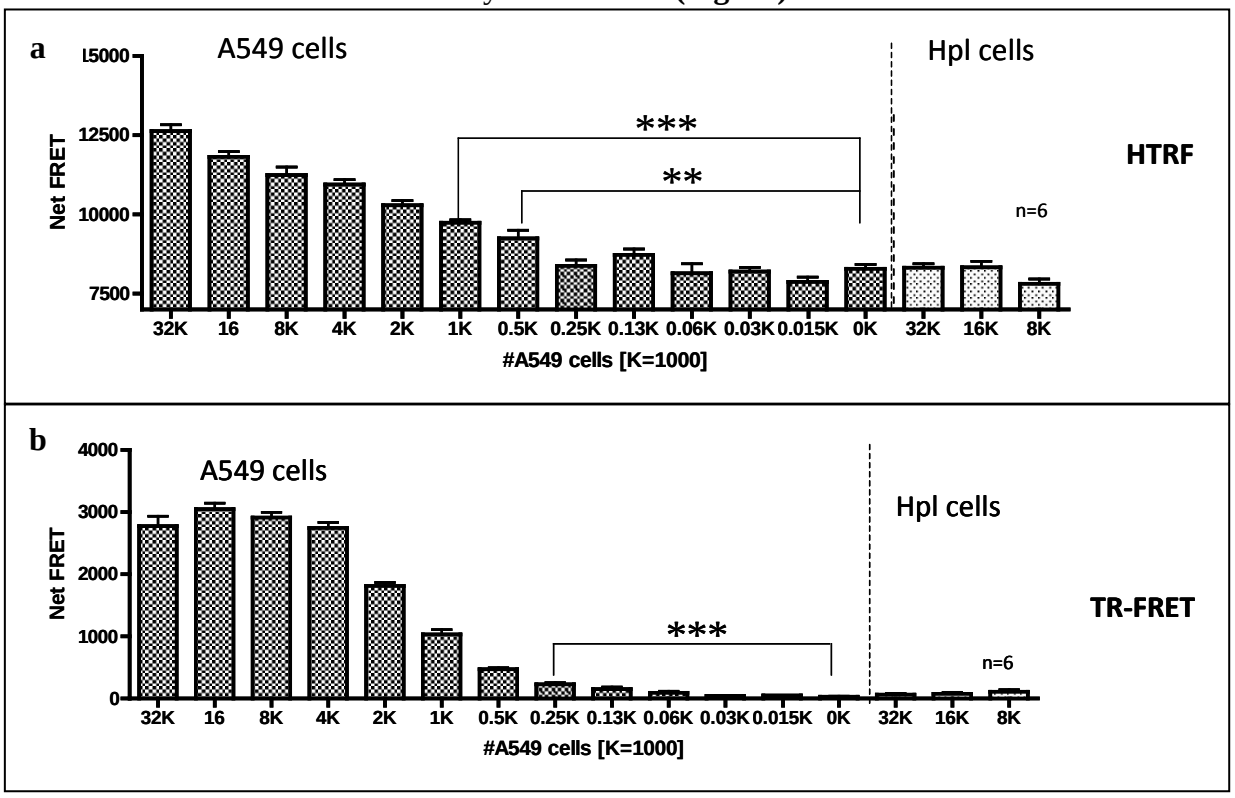

Figure 47. PrP^C cell surface detection on A549 cells by solid-phase FRET (opposite page)

The specificity of human PrP^C detection in living A549 cells by 2Eu/2APC FRET antibody pair is shown in a cell number titration experiment. **(a)** HTRF mode and **(b)** TR-FRET mode. *: $p < 0.05$; **: $p < 0.01$; ***: $p < 0.001$.

In the next experiments, PrP^C cell surface detection with 2Eu/APC was further validated. First, a blocking experiment was performed. A constant amount of intact HeLa cells was pre-incubated with different concentrations of unlabeled holo POM2 antibody for 30 min at 4°C. After removal of unbound antibodies by a washing step, the cells were labelled with 2Eu/APC for 30 min at 4°C. Results in the HTRF and TR-FRET mode showed an increase of FRET intensity with decreasing POM2 concentrations **(Fig. 48a** and **b)**. In **Fig. 48c** and **d**, HeLa cells were first labelled with 2Eu/APC and then exposed to trypsin digestion for 30 min at 37°C. Shown are results before digest and thereafter in the HTRF and TR-FRET mode. In the presence of trypsin, no FRET signal was detectable. Next, GPI-anchored PrP^C was removed by different concentrations of PI-PLC. A549 cells were first labelled with 2Eu/2APC **(Fig. 48f)** and then digested with PI-PLC for 30 min at 4°C. The supernatant was transferred into a new plate and incubated with the POM2Eu/POM2APC for 30 min at 4°C. PI-PLC digestion leads to a dose-dependent reduction of PrP^C on the surface of A549 cells and to an increase in the medium **(Fig. 48g** and **h)**. PI-PLC treatment had no effect on viability of A549 cells **(Fig. 48i)**.

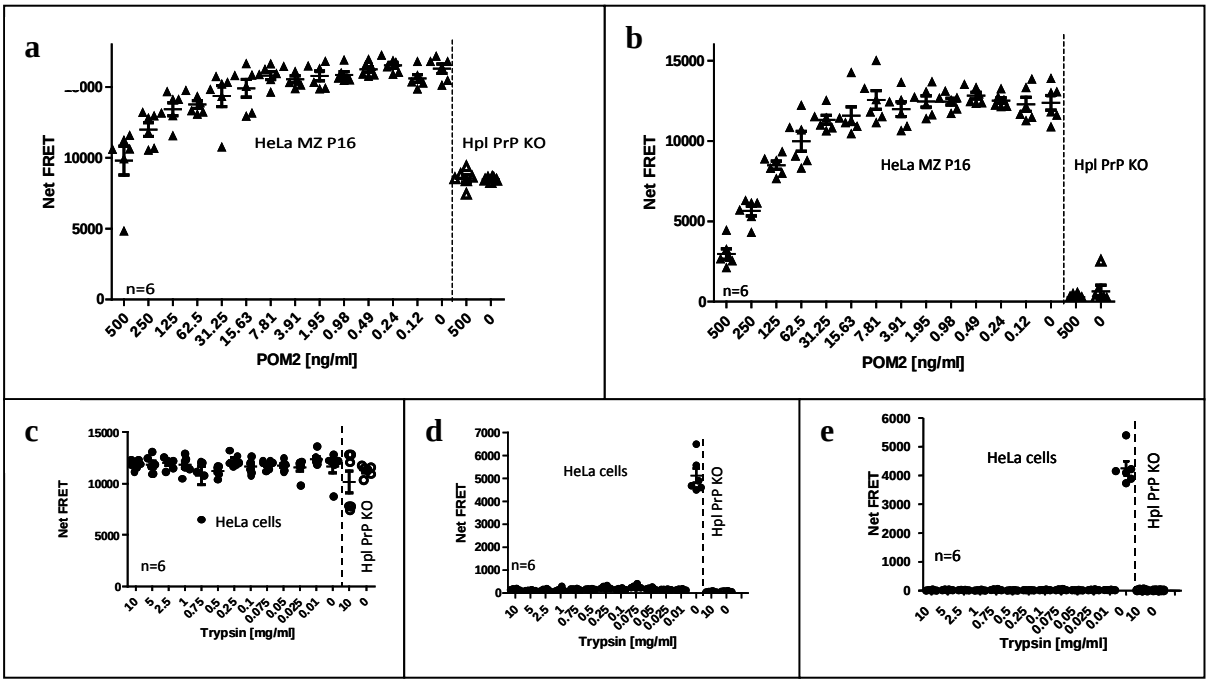

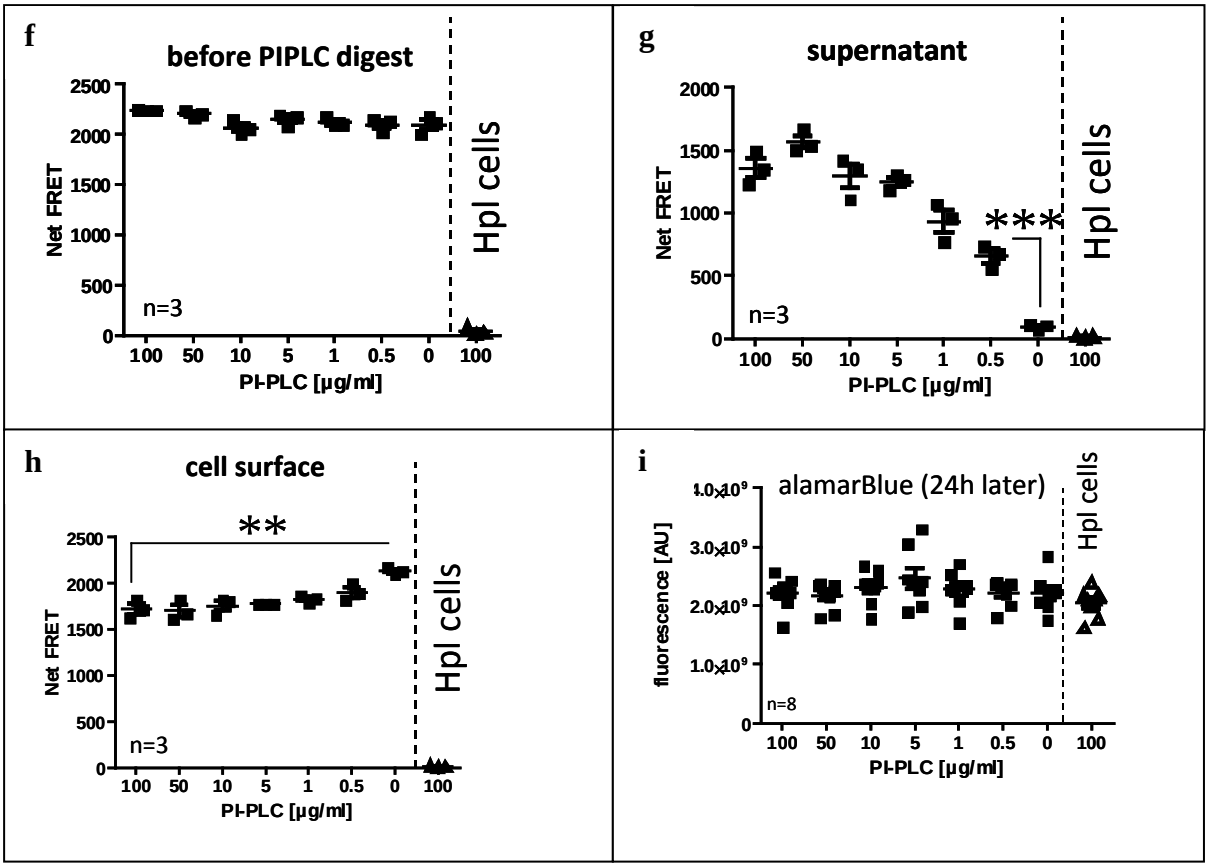

Figure 48. POM2/POM2 ELISA and FRET experiments

The specificity of PrP^C detection by 2Eu/APC is shown by a blocking experiment with unlabelled POM2 in **(a)** in the HTRF and **(b)** in TR-FRET mode. Trypsin digestion is shown in **(c-e)**. PI-PLC digestion of A549 cells is shown in **(f-h).** In **(f)** FRET signals before PI-PLC digestion. In **(g)** accumulation of cleaved PrP^C in the supernatant and in **(h)** the PrP^C level on the cell surface after PI-PLC treatment. **(i)** Viability was monitored by the alamarBlue assay. AU: Arbitrary Units.

Pharmacological manipulation of the PrP^C expression level at the surface of living HeLa or A549 cells was done with BFA treatment **(Fig. 49a** and **Fig. 49b)**. Potential toxic effects of BFA were monitored by the alamarBlue assay. A BFA concentration of 1 µg/ml had no effect on the viability of A549 cells and decreased the expression of PrP^C at the cell surface **(Fig. 49c)**.

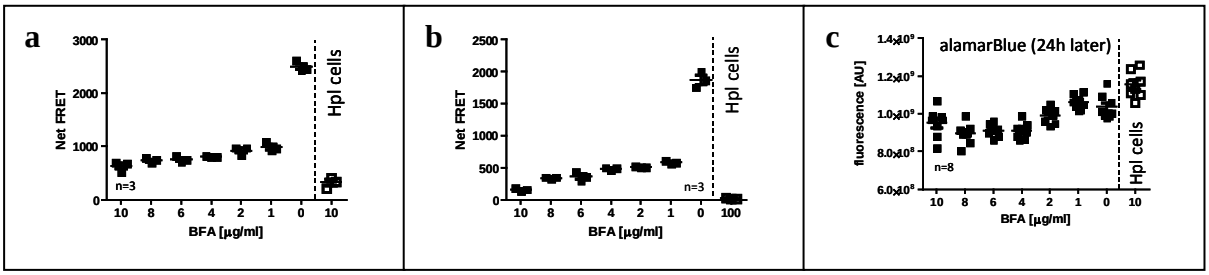

Figure 49. Manipulation of PrP^C cell surface expression by BFA treatment

One day before the experiment, 4000 HeLa cells were seeded into a 384-well plate. Cells were treated with different concentrations of BFA for 18 hours at 37°C. BFA was removed and one part of the plate was used for

the 2Eu/APC cell surface FRET experiments. The other part of the plate was used for the alamarBlue assay, measured 24h after BFA treatment. **(a)** HTRF mode, **(b)** TR-FRET mode and **(c)** alamarBlue viability assay. BFA was dissolved in DMSO and the concentration was kept constant at 0.75%. AU: Arbitrary Units.

Genetic manipulation of the PrP^C expression level at the surface of living A549 cells was done with PRNP siRNA treatment **(Fig. 50a)**. Scrambled as well as GAPDH siRNAs were used as negative controls additionally to Hpl PrP KO cells. A decrease of PrP^C expression level on the surface of living A549 cells was found, depending on PRNP siRNA concentration. No toxic effects of siRNA were monitored by the alamarBlue assay. To induce cell death chlorpromazine (CPZ) was used as control **(Fig. 50b)**.

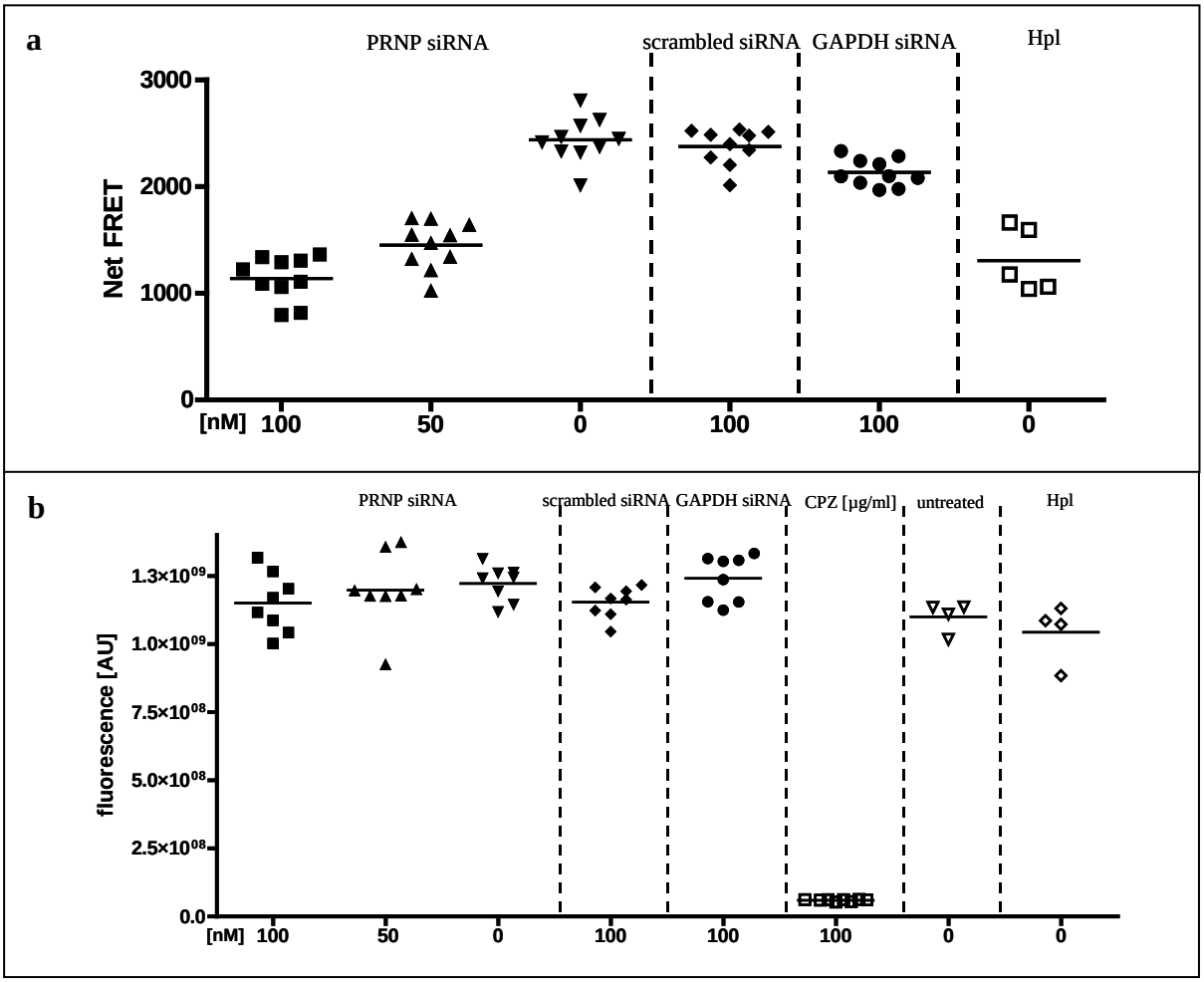

Figure 50. Manipulation of PrP^C cell surface expression by siRNA treatment

Four days before, 500 A549 cells were seeded into a 384-well plate. Cells were treated with different concentrations of PRNP siRNA and control siRNAs for 3 days at 37°C. Cells were labelled with POM2Eu/3F4APC. **(a)** PrP^C cell surface expression in HTRF mode, **(b)** alamarBlue viability assay of siRNA treated A549 cells. CPZ: chlorpromazine.

PrP^C Endocytosis Assay in Human Cells with solid-phase TR-FRET

During establishing the cell surface detection of PrP^C by FRET technology, the question arose whether this assay could also be used to measure the internalisation of human PrP^C. The rationale behind the endocytosis assay is to first label the cells with the donor FRET antibody (POM2Eu). After removing of unbound antibodies, exposure to 37°C induces the uptake of the antibody-labelled PrP^C present at the cell surface. By labelling the cells with the acceptor FRET antibody (POM2APC) at various time intervals, endocytosis can be monitored over time **(Fig. 51a)**. To calculate the endocytosis of PrP^C, baseline experiments are performed, where both FRET antibodies are simultaneously given to the cells **(Fig. 51b)**. To measure the temporal uptake of PrP^C, only POM2Eu antibodies are incubated with the cells at 37°C. At different time points, POM2APC antibodies are added **(Fig. 51c)**. The temporal decrease in FRET intensity is due to endocytosed Eu-labelled PrP^C. The endocytosis rate of PrP^C (FRET τ_0 and τ_1) is normalized against the basal uptake of PrP^C (FRET τ_0) and calculated according to the formula in **Fig. 51d**.

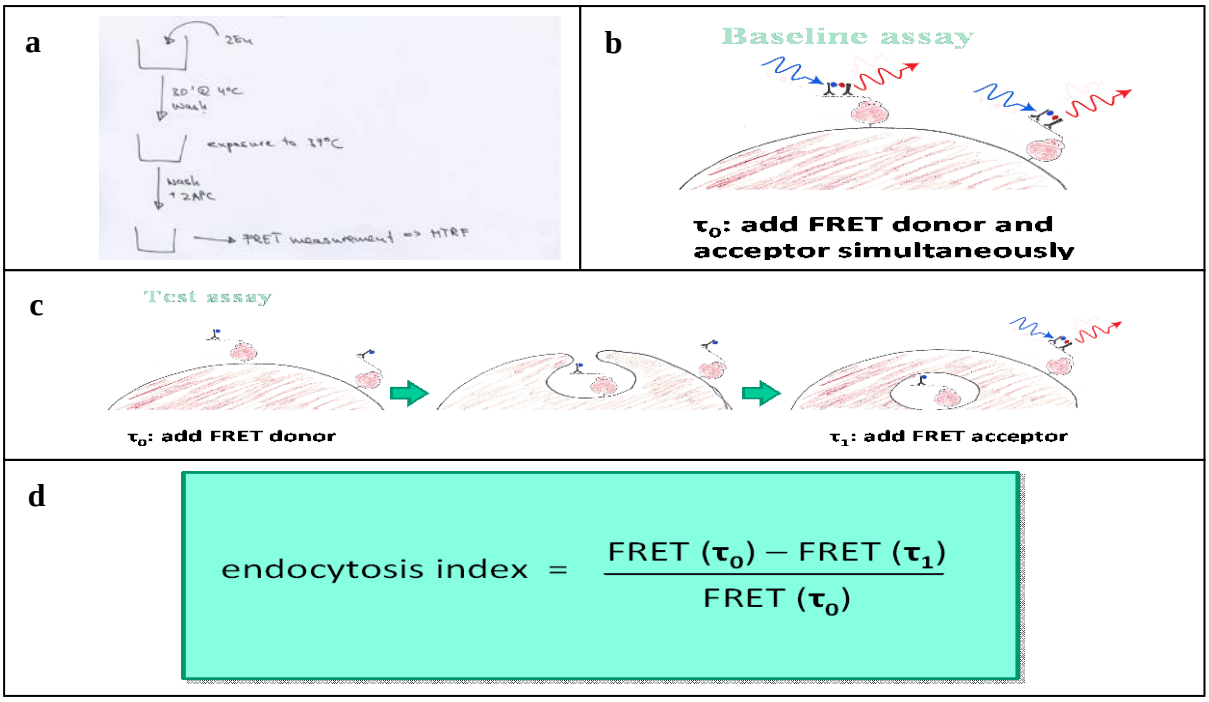

Figure 51. Experimental protocol and calculation of the endocytosis index of PrP^C

(a) The experimental protocol of the PrP^C endocytosis assay takes the advantage that the FRET phenomenon occurs in a distance-dependent manner. By the addition of the FRET antibodies separately and at different time points, the distance increases in the course of endocytosis which can be monitored by decreasing FRET signal intensities. **(b)** Endocytosis base line experiment. At time point t=0, both donor and acceptor antibodies are given simultaneously. **(c)** Endocytosis experiment. At time point t=0, only the donor FRET antibody is given. Over time, PrP^C is internalised by the cells. This is detected by decreased FRET signals after addition of the acceptor antibody at different time points. **(d)** Endocytosis index formula. **(b-d)**. By courtesy of A. Aguzzi 2013.

In a first set of experiments, different antibody combinations for the FRET endocytosis experiments were tested. Good results were found for the FRET antibody combinations 2Eu/3F4APC and 2Eu/2APC. It is irrelevant whether first the Eu- or APC-labelled antibody is added, although slightly higher FRET signals were obtained when the donor antibody was added first.

To calculate the endocytosis index of PrP^C, A549 cells were labelled first with 2Eu (endocytosis assay) **(Fig. 52a** and **b)** or 2Eu/2APC (baseline experiments) **(Fig. 52c** and **d)**. After washing the labelled cells, endocytosis was induced at 37°C in DMEM medium without FBS, antibiotics and phenol red to prevent any cross reaction wth the FRET signal. At different time points (t=0 to 70 min) 2APC was added. FRET signals were measured directly after addition of the last 2APC **(Fig. 52a)** and a second time after 30 min incubation at 4°C **(Fig. 52b)**.

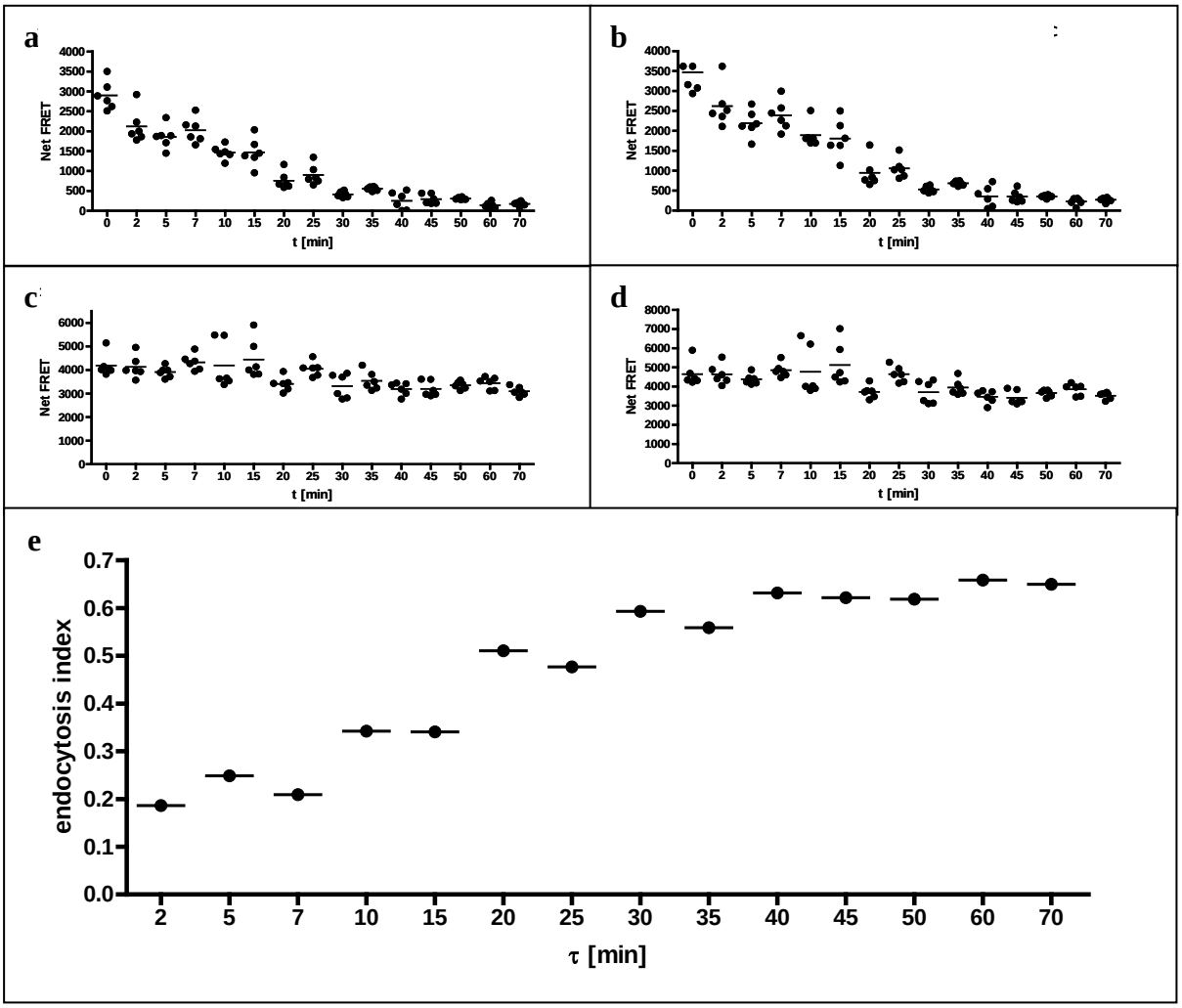

Figure 52. Kinetics of PrP^C internalisation in A549 cells

(a) and **(b)** shows the FRET signals in the endocytosis assay without or after 30 min of incubation at 4°C, respectively. **(c/d)** and summarizes the baseline experiments measured the same way as in (a) and (b). **(e)** Kinetics of PrP^C endocytosis. Calculated according to formula in **Fig. 52d**.

In the endocytosis assay, the FRET signal is decreasing over time, indicating the uptake of PrP^C. In baseline experiments, the FRET signal stays constant over the whole time period. An explanation could be cross-linking between PrP^C molecules at the cell surface by the simultaneously binding of 2Eu/APC and therefore preventing internalisation. A half life time of about 30 min for cell membrane PrP^C was determined which is in line with a previous report [Shyng, 1993]. A steady state was reached at about 40 min at 37°C **(Fig. 52c)**.

To exclude that PrP^C is not released from the cell surface by shedding processes, which will also result in a decrease of FRET signal intensity over time, I performed a further control experiment. A549 cells were labelled with 2Eu for 30 min at 4°C. After washing, cells were incubated with DMEM medium without FBS, antibiotics and phenol red for 30 min at 37°C to induce endocytosis. Cells were washed an incubated with 100 µg/ml PI-PLC for 30 min at 4°C. Supernatant with cell surface cleaved PrP^C was transferred into a new plate and 3F4APC was added to the treated cells as well as into the supernatant for 30 min at 4°C. Results in **Fig. 53a** show the cell surface PrP^C expression after PI-PLC treatment. A clear decrease in FRET signal intensity could be detected in the presence of PI-PLC. No labelled 2Eu-PrP^C is released into the medium without PI-PLC treatment **(Fig. 53b)**, indicating that no detectable PrP^C is released by shedding processes from the cell surface.

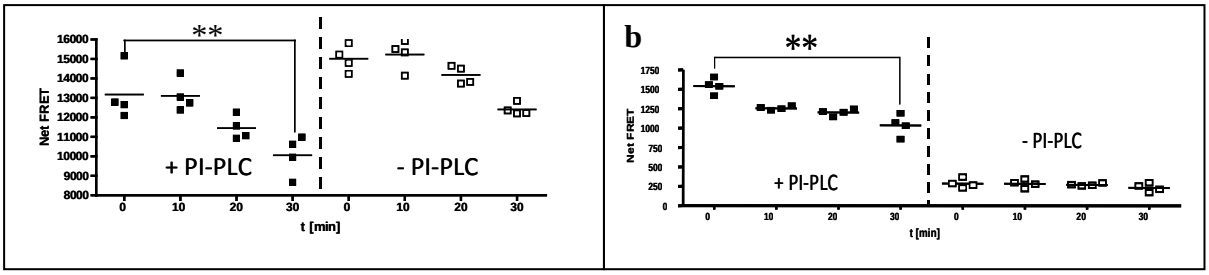

Figure 53. No detectable PrP^C is released from the cell surface by shedding processes

PI-PLC was used to detect released instead of internalised cell surface expressed PrP^C. **(a)** shows PrP^C levels on the cell surface of A549 cells in the presence or absence of PI-PLC. **(b)** summarizes the PI-PLC cleaved PrP^C levels in the supernatant. No PrP^C was detected in the supernatant without PI-PLC digest. **: $p < 0.01$.

Pharmacological Inhibition of PrP^C Endocytosis

To further validate the endocytosis assay, I wanted to inhibit the endocytosis of PrP^C. Clathrin- as well as lipid-raft-mediated internalisation processes are involved in PrP^C uptake. In a first set of experiments, sucrose was used as an inhibitor of clathrin-mediated endocytosis processes. HeLa cells, labelled with 2Eu, were exposed for 30 min at 37°C in the presence of different hypertonic sucrose solutions ranging from 0 to 0.5 M. FRET was measured in HTRF and TR-FRET mode after 2APC labelling. Toxic effects of sucrose were monitored by the

alamarBlue assay. Sucrose shows a weak effect on inhibition of PrP^C uptake in HeLa cells. A slightly higher FRET signal was found for a 0.4 M sucrose solution which is in line with the literature and is due to the inhibition of clathrin-mediated endocytosis [Sunyach et al. 2003]. However, sucrose also influences the viability of HeLa cells in a dose dependent manner **(Fig. 54)**.

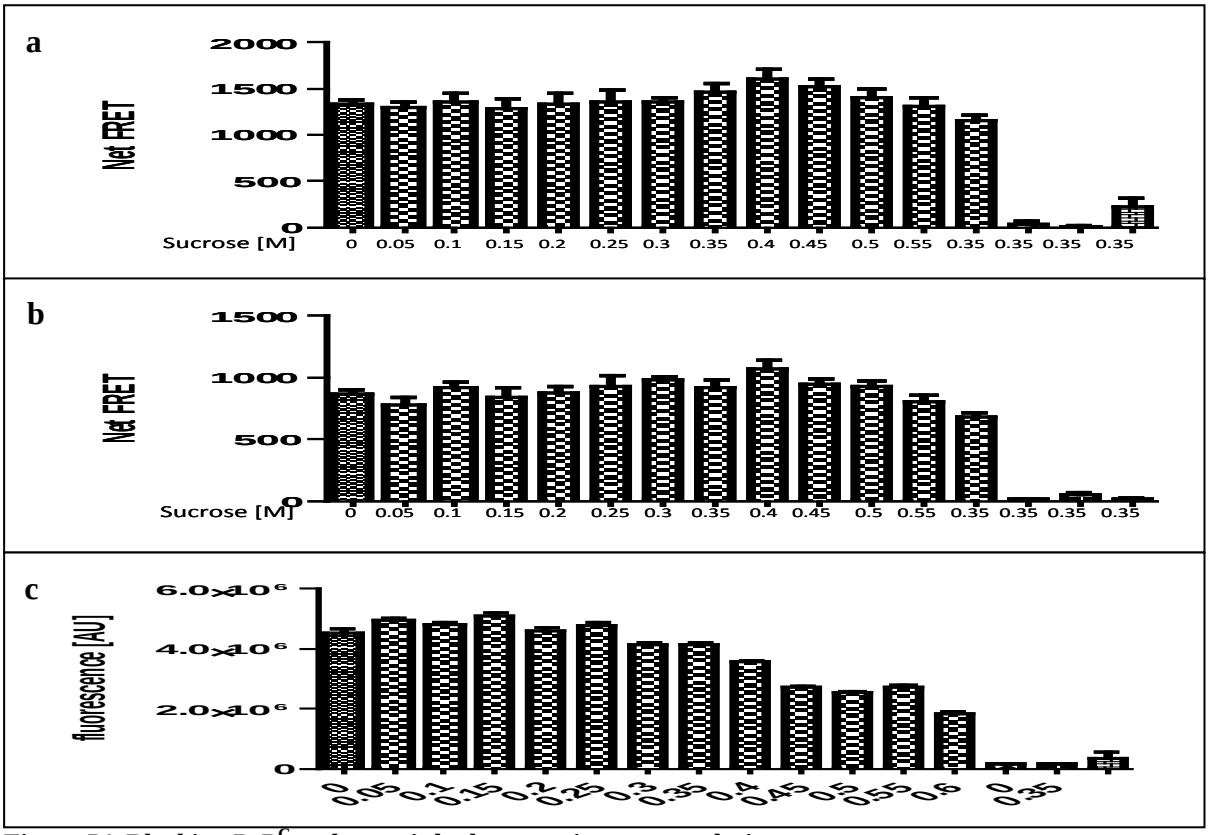

Figure 54. Blocking PrP^C endocytosis by hypertonic sucrose solutions

One day before the start of the experiment, 4000 HeLa cells were seeded per well in a 384-well plate. Next day, cells were labelled with 2Eu for 30 min at 4°C. Cells were washed once and incubated for 30 min in the presence of increasing sucrose concentrations ranging from 0 to 0.5 M. Results are shown in **(a)** for the HTRF and in **(b)** for TR-FRET mode. Viability of the cells is shown by the alamarBlue assay in **(c).** Hpl cells were used in control experiments.

As an inhibitor for lipid-raft-mediated endocytosis processes, methyl-β-cyclodextrine (MβCD) was used. POM2Eu labelled cells were incubated in the presence of decrasing MβCD-concentrations ranging from 10 to 0 mM for 30 min at 37°C. FRET was measured in HTRF and TR-FRET mode. An inhibitory effect for MβCD was found in a concentration range of 1 to 0.1 mM. Toxic effects of MβCD were monitored by the alamarBlue assay **(Fig. 55)**.

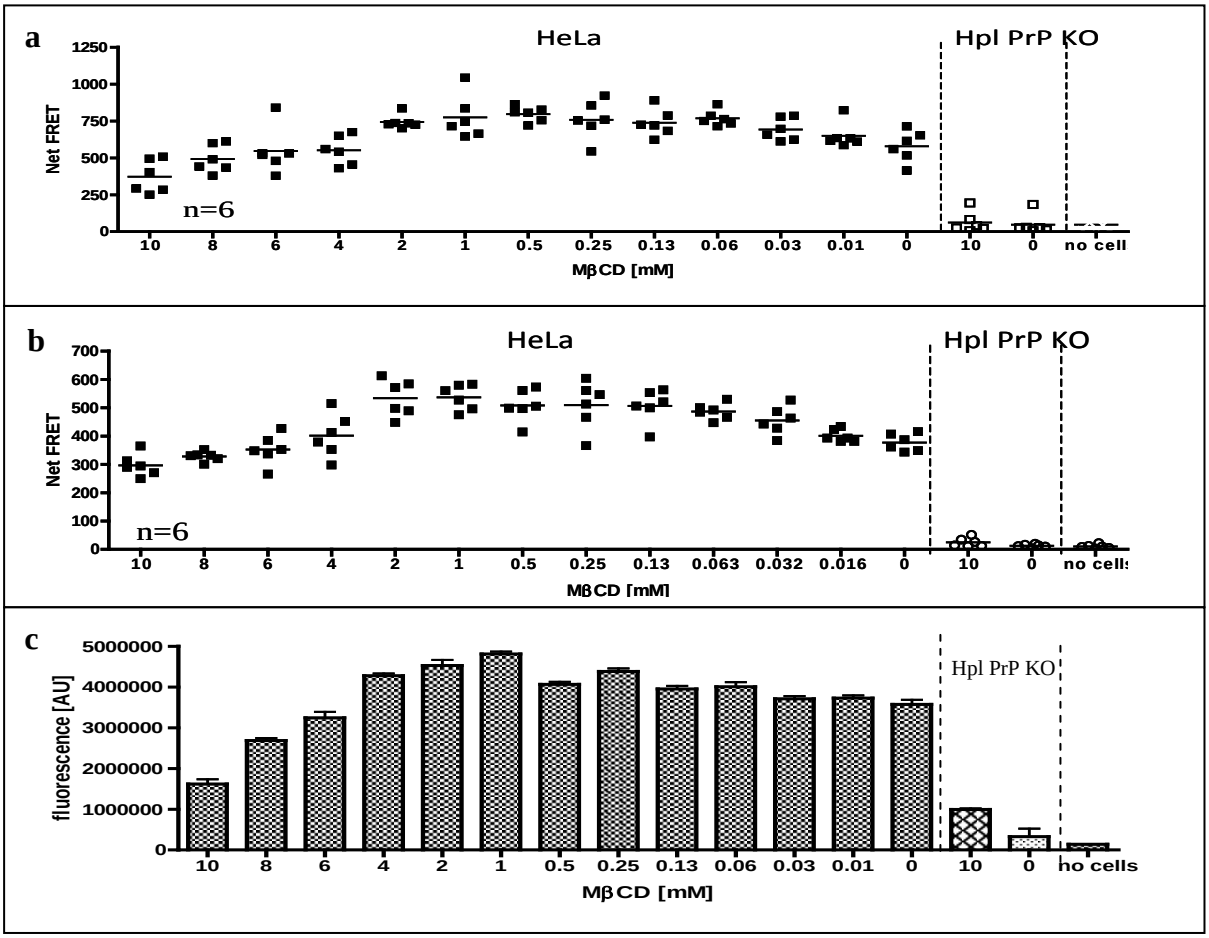

Figure 55. Blocking PrP^C endocytosis by MβCD

One day before the start of the experiment, 400 HeLa cells were seeded per well in a 384-well plate. Next day, cells were labelled with 2Eu for 30 min at 4°C. Cells were washed once and incubated for 30 min in the presence of MβCD ranging from 0 to 10 mM. Results are shown in **(a)** for the HTRF and in **(b)** for TR-FRET mode. Viability of the cells is shown in **(c).** Hpl cells were used in control experiments.

To achieve a maximal inhibitory effect of PrP^C's uptake, MβCD and hypertonic sucrose solutions were administered at the same time. Cell viability was again measured via the alamarBlue assay. Sucrose alone had no effect on PrP^C's endocytosis, but on viability. Slightly better was the treatment with MβCD. Best results were found for a mixture of MβCD and sucrose which did not influence cell viability **(Fig. 56)**.

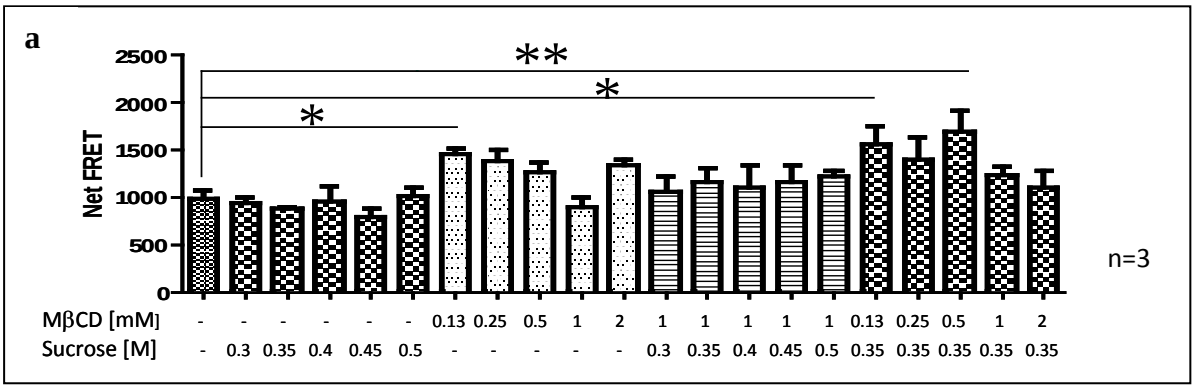

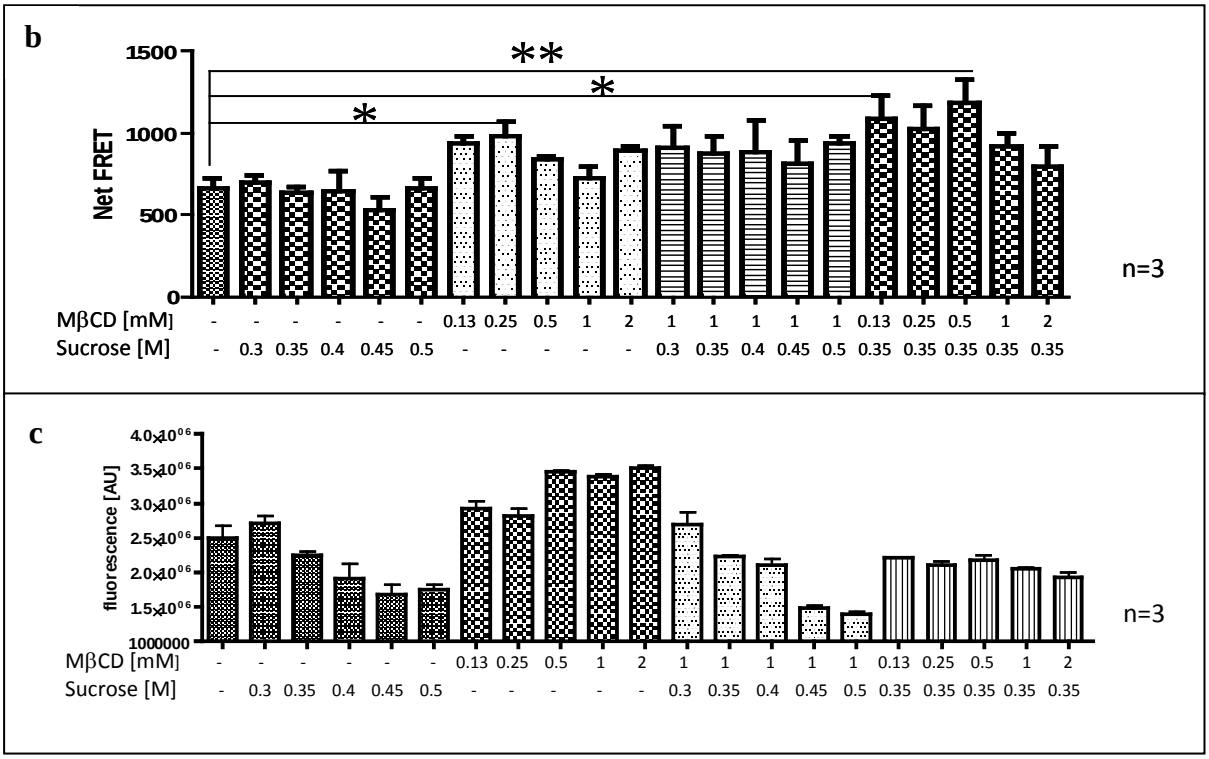

Figure 56. Blocking PrP^C endocytosis by hypertonic sucrose solution and MβCD

One day before the start of the experiment, 400 HeLa cells were seeded per well in a 384-well plate. Next day, cells were labelled with 2Eu for 30 min at 4°C. Cells were washed once and incubated for 30 min in the presence of sucrose or MβCD or both together. Results are shown in **(a)** for the HTRF and in **(b)** for TR-FRET mode. Viability of the cells is shown in **(c).** Hpl cells were used in control experiment. *: $p < 0.05$; **: $p < 0.01$.

Additional experiments were performed in A549 cells. To block clathrin-dependent endocytosis processes, chlorpromazine was used **(Fig. 57a)**. A concentration of 1 µg/ml of chlorpromazine was sufficient to block endocytosis of PrP^C without effecting viability of A549 cells **(Fig. 57b)**. Higher concentrations were toxic for the cells. To inhibit raft mediated internalisation pathways MβCD was used **(Fig. 57c)**. A concentration of 5 mM MβCD blocked endocytosis of PrP^C without any toxic effect on cell viability as monitored by the alamarBlue assay **(Fig. 57d)**.

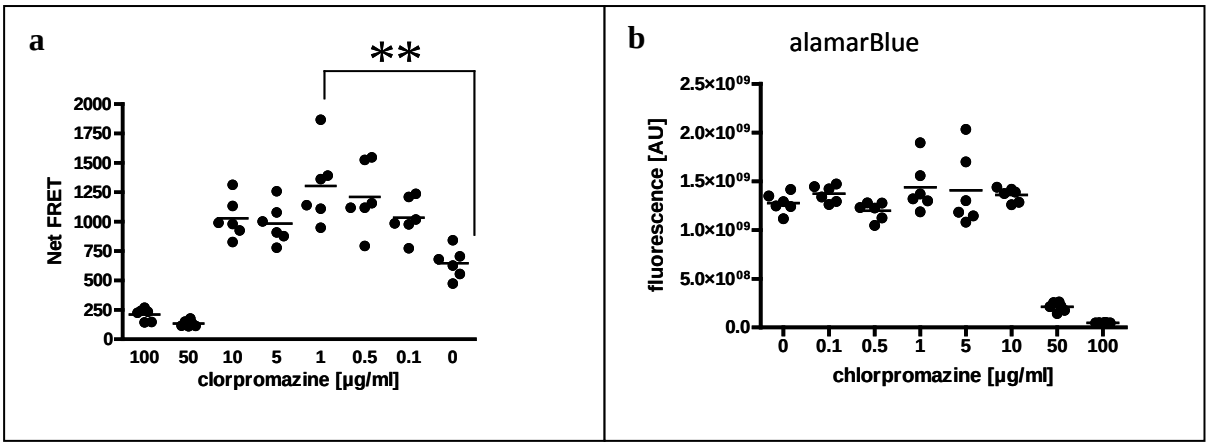

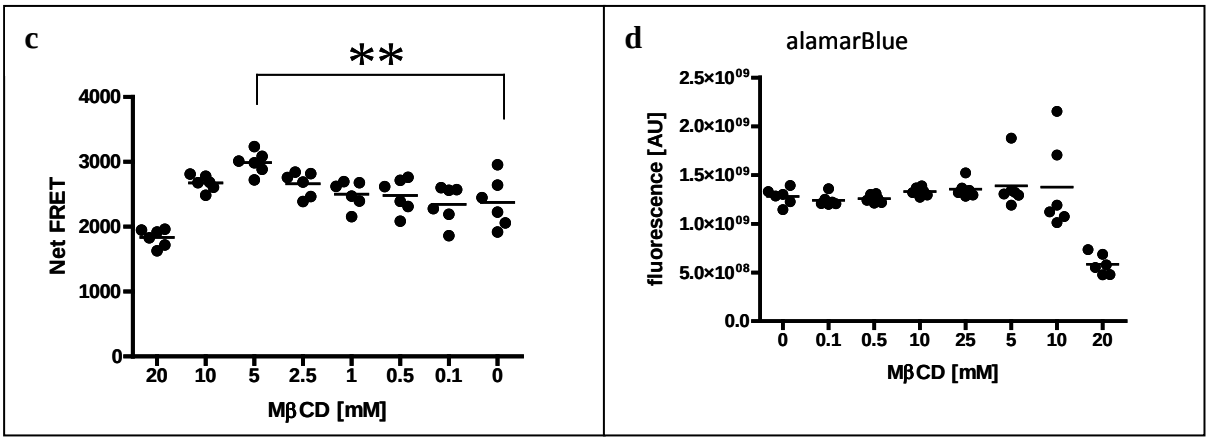

Figure 57. Blocking PrP^C endocytosis by hypertonic sucrose solution and MβCD

One day before, 400 HeLa cells were seeded per well in a 384-well plate. Next day, cells were labelled with 2Eu for 30 min at 4°C. Cells were washed once and incubated for 30 min in the presence of sucrose or MβCD or both together. Results are shown in **(a)** for the HTRF and in **(b)** for TR-FRET mode. Viability of the cells is shown in **(c).** Hpl cells were used in control experiment.

Inhibition of PrP^C Endocytosis by Gene Silencing

Next, I wanted to block the endocytosis of PrP^C by siRNA treatment. For that, seven different siRNAs were selected which have an impact on endocytosis processes **(Tab. 6)**.

AP2M1	Encodes the adaptor protein 2 (AP-2) which is involved in clathrin-dependent endocytosis (Boucrot et al., 2010)
EHD1	Encodes the EH domain-containing protein 1, plays a role in endocytosis (Rainey et al., 2010)
GIT2	Encodes the ARF GTPase-activating protein GIT2 (Premont et al., 2004)
M6PR	Encodes the mannose 6-phosphate receptor, interacts with the AP1 clathrin adaptor complex (Le Borgne et al., 1997)
Rab5a	G-protein, required for the fusion of plasma membranes and early endosomes (Gulappa et al., 2011)
VPS28	Encodes the vacuolar protein sorting-associated protein 28 homolog, involved in endosomal sorting of cell surface receptors (Bishop et al., 2001)
VPS35	Encodes the vacuolar sorting-associated protein 35, involved in retrograde transport of proteins from endosomes to the trans-Golgi network (Bonifacino & Hurley, 2008)

Tab. 6. Used siRNAs for gene knockdown

All siRNAs were functional and lowered the mRNA expression of the target gene as shown by quantitative PCR **(Fig. 58a-g)**.

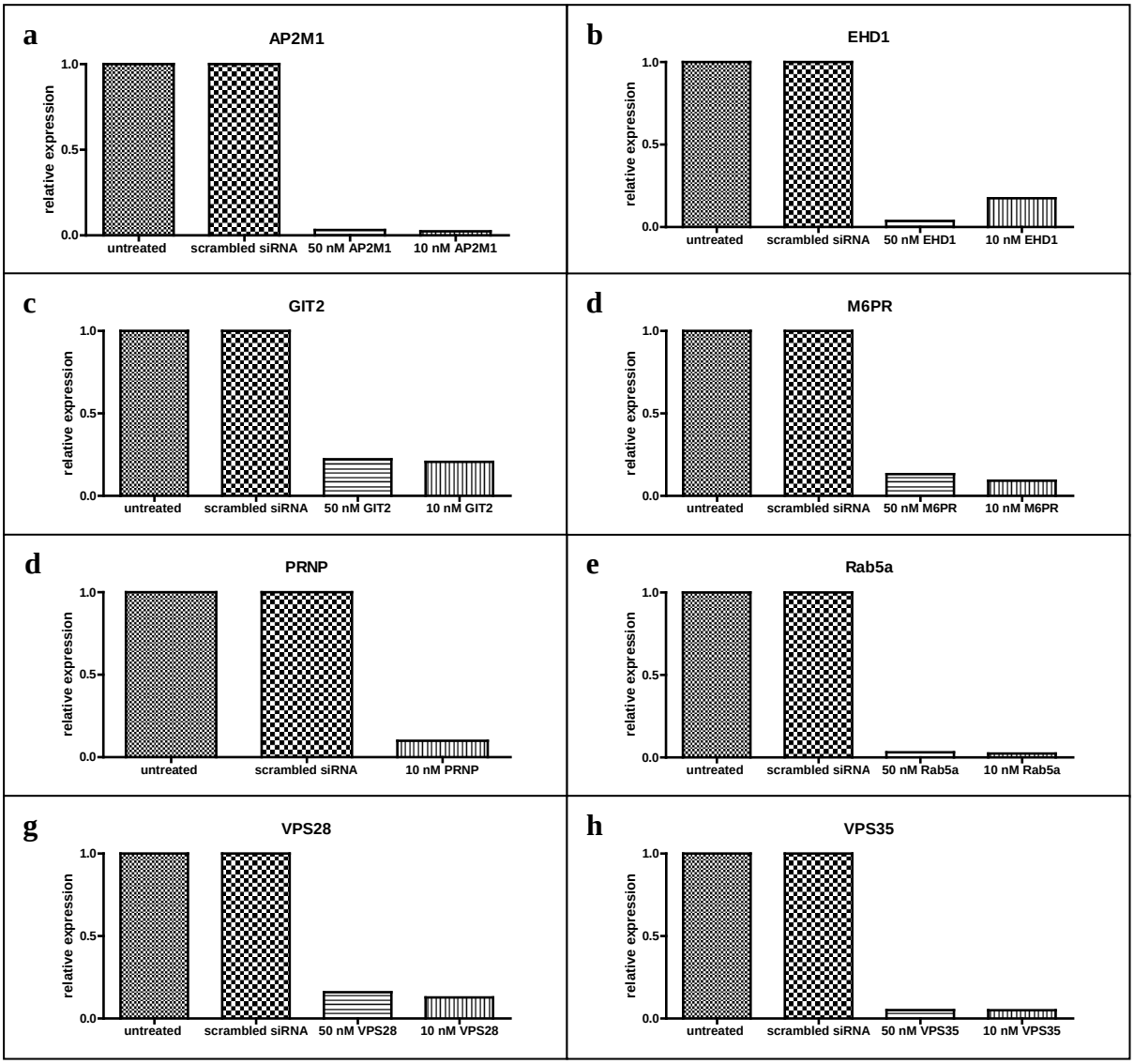

Figure 58. Gene knockdown in A549 cells

Quantitation of gene silencing in A549 cells treated 3 days with siRNA by real-time PCR for **(a)** AP2M1, **(b)** EHD1, **(c)** GIT2, **(d)** M6PR, **(e)** PRNP, **(f)** RAB5a, **(g)** VPS28 and **(h)** VPS35. mRNA levels were normalized by using GAPDH mRNA. Shown are technical triplicates.

The siRNA treatment had no influence on cell viability **(Fig. 59a** and **b)**.

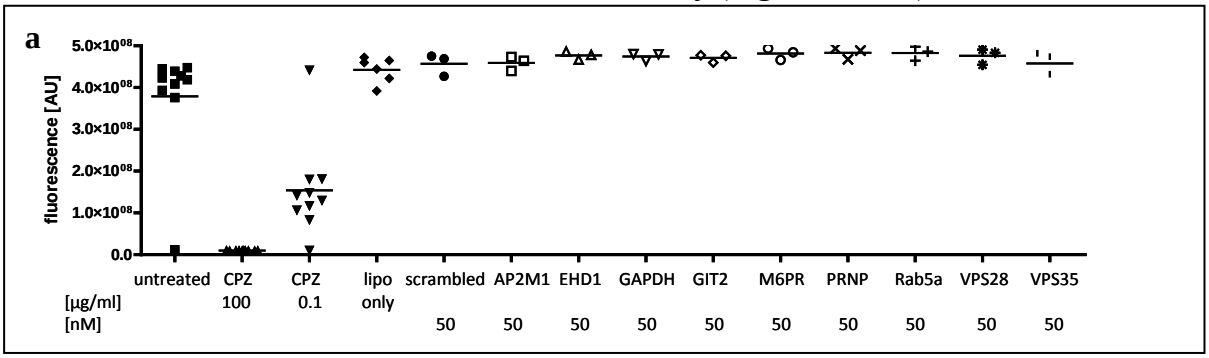

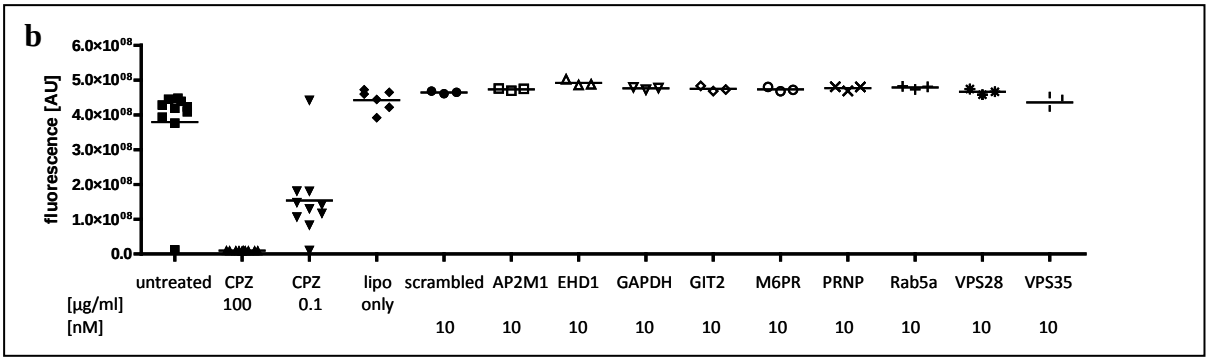

Figure 59. Viability of siRNA treated A549 cells

A549 cells were treated for three days either with 50 nM **(a)** or with 10 nM siRNA **(b)**. Cell viability was assessed by the alamarBlue assay. Chlorpromazine (CPZ) was used as a positive control for cell death. Shown are biological triplicates of siRNA treated cells.

The final experiment was to elucidate genes involved in the endocytosis of PrP^C. Two genes, AP2M1 and RAB5a strongly blocked the endocytosis of PrP^C. Other genes such as M6PR and VPS35 had also influence on the internalisationof PrP^C, but EHD1 and VPS28 showed no effect. Interestingly, GIT2 even enhanced the endocytosis of PrP^C. In a control experiment, siRNA against the prion protein gene were used.

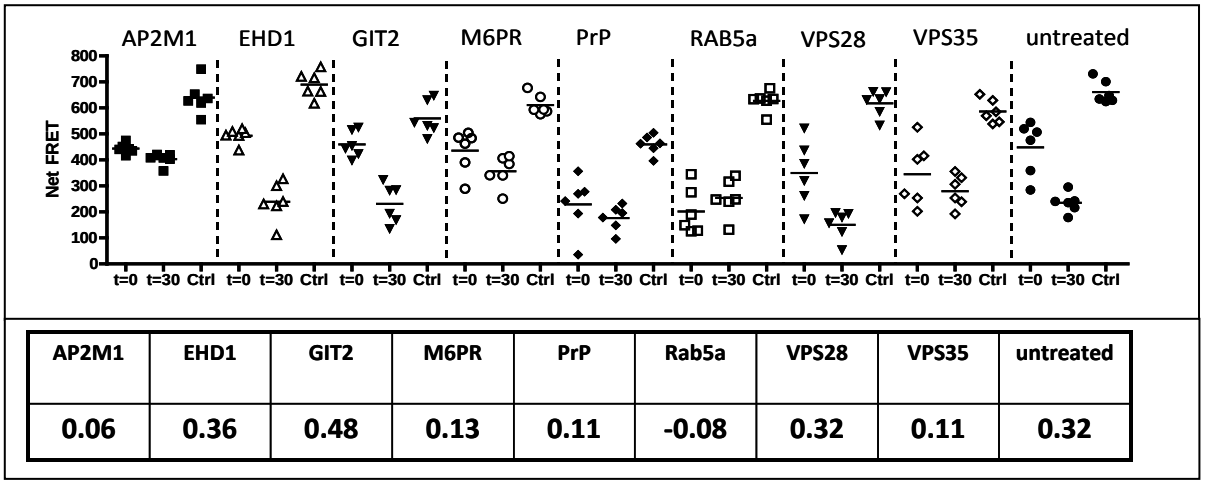

AP2M1	EHD1	GIT2	M6PR	PrP	Rab5a	VPS28	VPS35	untreated
0.06	0.36	0.48	0.13	0.11	-0.08	0.32	0.11	0.32

Figure 60. Blocking PrP^C endocytosis by siRNA treatment and determing the endocytosis index

A549 cells were treated for three days with 50 nM siRNA and then, the endocytosis assay was performed. Shown are hexaplicates. The endocytosis index was calculated for each gene.

Induction of PrP^C Endocytosis

Instead of blocking endocytosis, I also wanted to induce the uptake of PrP^C at the surface of human cells. Copper sulphate ($CuSO_4$) is a known activator of endocytosis of PrP^C [Taylor 2005 and Taylor and Hooper 2007].

In a first set of experiments, HeLa cells were labelled with 2Eu, washed and exposed for 30 min at 37°C in the presence of $CuSO_4$ solutions with concentrations ranging from 0 to 400 µM diluted in DMEM cell culture media. In control experiments, $CuSO_4$ was pre-incubated with glycine, a known copper chelator, to inhibit the $CuSO_4$–mediated endocytosis of PrP^C. In both measurement modes (**Fig. 61a** HTRF and **Fig. 61c** TR-FRET), a reduction of PrP^C at the cell surface was measured in the presence of $CuSO_4$. Moreover, addition of the copper chelator glycine slowed down the reduction of PrP^C at the cell surface. Surprisingly, the highest concentration of $CuSO_4$ had no effect on the cell viability **(Fig. 61 b** and **d)**, but glycine stimulated cell metabolism. However, to determine the effect of $CuSO_4$, I performed additional control experiments. Copper is assumed to bind at the same region as POM2 antibodies do. For that reason, I did a solid phase recPrP FRET assay which prevents a washing step. Here, recPrP was coated onto a 384-well plate over night and incubated with different concentrations of $CuSO_4$. Results showed that $CuSO_4$ interferes with Europium, as mentioned by the manufacturer [www.perkinelmer.com/LANCE] as well compete with the POM2 antibody for binding sites **(Fig. 61e)**. The Eu/APC FRET endocytosis assay is not suitable to measure $CuSO_4$-induced PrP internalisation.

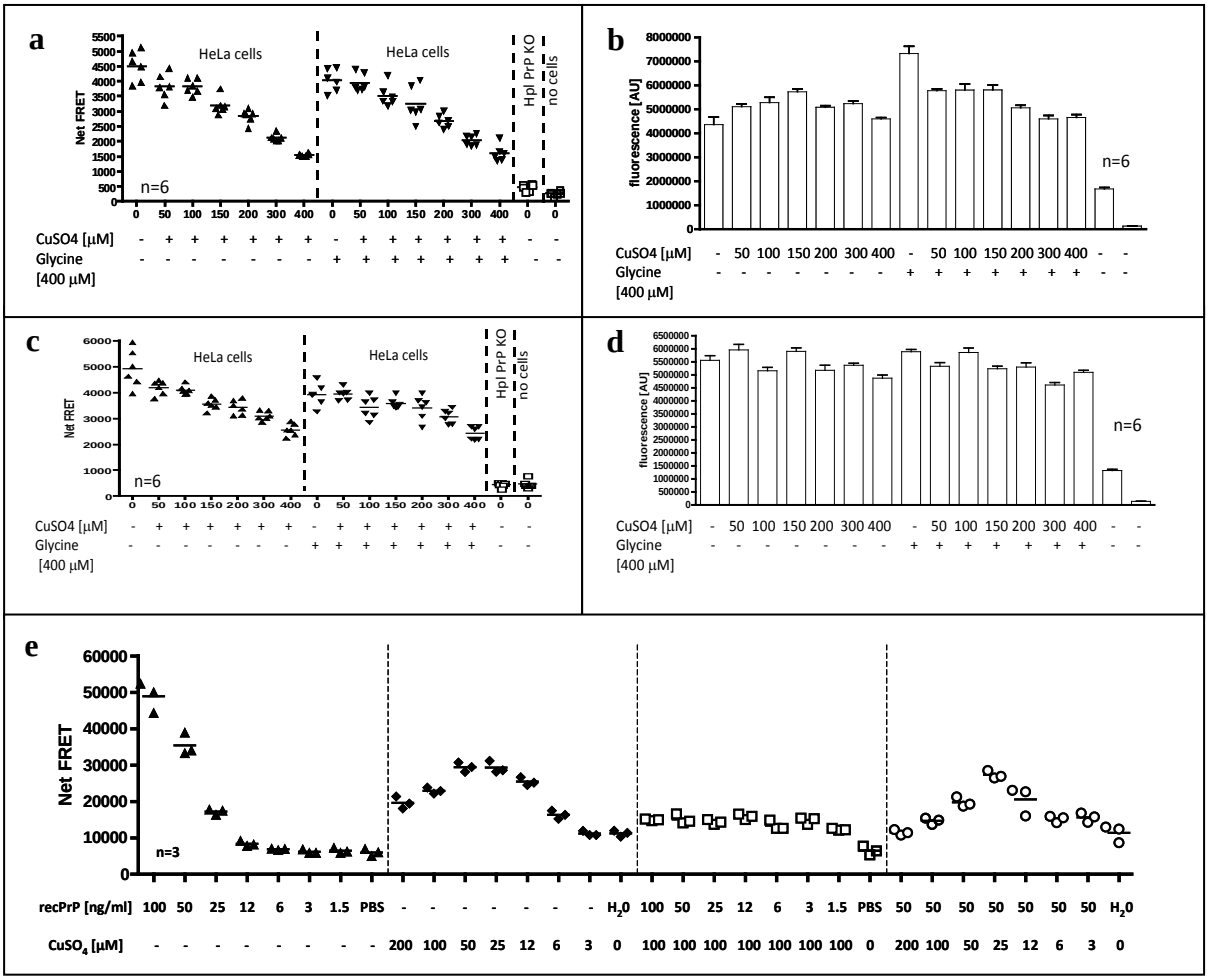

Figure 61. Induction of PrP^C endocytosis (opposite page)

$CuSO_4$-induced internalisation of PrP^C is shown in the HTRF mode **(a)** and in TR-FRET mode **(c)**. In control experiments, $CuSO_4$ was complexed with glycine. In **(c)** and **(d)** the effect of $CuSO_4$ on cell viability is shown. **(e)** Influence of $CuSO_4$ on FRET signal intensity.

DISCUSSION

Prion Protein Time-Resolved FRET Assay

To develop a PrP TR-FRET assay, I labelled our in-house anti-prion protein POM antibodies with Europium or APC as donor and acceptor fluorophores, respectively. I obtained good labelling degrees in the range of 3 to 6 (IgG/Eu) and 1-2 for IgG/APC. The Wallac EnVision reader showed an excellent dynamic range (10^{-6} to 10^{4} pM) and a limit of detection (0.05 pM) for Eu^{3+}. These results are in line with the performance being indicated by the manufacturer of the Wallac Envision reader [www.perkinelmer.com/LANCE].

Recombinant PrP Time-Resolved FRET assay

In this part I tested, whether the POM antibodies enabled the detection of recPrP by time-resolved FRET in a homogeneous phase. By titration experiments, I identified POM1Eu and POM2APC as the best FRET antibody pair to dectect recPrP in Tris/Krebs buffer. This non-competitive assay displayed excellent Z' factors, high signal to noise ratios and a very low variability. A limit of detection for full length recPrP lower than 0.125 ng/ml was detected in spiking experiments with Hpl PrP KO cell lysate which is more sensitive compared to my results obtained from ELISA experiments.

In summary, the established recPrP FRET assay is characterized by high sensitivity (LOD < 125 pg/ml) and specificity (spiking experiments), high-throughput potential (96-/384-well format, Z' factor), fast (within 30 min), the possibility to manipulate the system (enzymatic digestion, blocking/binding experiments) and the use of different recPrP variants and FRET-labelled POM antibody combinations.

PrP^{C} Time-Resolved FRET Assay

In the next step, I tried to detect PrP^{C} either from murine cell lysates or brain homogenates. A LOD of 16 µg/ml N2a cell lysate was obtained. These results differ when comparing with human PrP^{C} from cell lysates due to a lower expression level of PrP^{C}. A linear range was found for 0 to 1 mg/ml crude N2a cell lysate. In a next set of experiments, cell lysates were enzymatically digested with PK or trypsin. In both cases, less PrP^{C} could be detected by increasing enzyme concentration. A nice control experiment was shown in the tryptic digestion experiment by using FRET antibodies with resistant enzymatic epitopes.

In summary, the established PrP^C FRET assay in cells and BH has a similar sensitivity as a Western blot assay (LOD 16 µg/ml). According to signal-to-noise ratios, high-throughput may be possible at the current state, but rather in a 96- than in a 384-well plate format. The possibility to manipulate the system (enzymatic digestion, blocking/binding experiments) offers some perspectives. However, further optimisation of various parameters (e.g. detergent concentration and lysis conditions) is needed to improve the performance of the PrP^C FRET assay.

PrP^{Sc} Time-Resolved FRET Assay

The discrimination of PrP^C and PrP^{Sc} was successfully by using PK digestion which completely removes PrP^C, but not after tryptic proteolysis. After PK digestion, a LOD for PrP^{Sc} of 0.01% was detected in prion-infected brain homogenate with the C-terminus targeted POM1Eu/POM19APC FRET antibody combination. This result was improved by denaturation of PrP^{Sc} with NaOH to a 10^{-5} diluted brain homogenate. Here, the SSCA is much more sensitive and is able to detect PK-resistant PrP^{Sc} in dilutions of 10^{-9} [Klohn et al., 2003].
The detection of PK-resistant PrP^{Sc} depends on multiple variables. Although PK is the standard method to distinguish between normal and pathological PrP isoforms, prion infectivity can be detected in the absence of PK-resistant PrP^{Sc} [Lasmezas et al., 1997].
To improve the performance of the PrP^{Sc} FRET assay other proteolytic enzymes could be tested to improve the LOD, such as subtilisin [Pilon et al., 2009], chymotrypsin [Pan et al., 2004], or pepsin [Jackson et al., 2005]. Another important issue is the choice of lysis buffer and detergent concentration [Breyer et al., 2012]. It is conceivable that by testing other POM antibody pairs, better results can be achevied.

PrP^C Cell Surface Time-Resolved FRET Assay

In a first set of experiments, I tried to detect PrP^C at the surface of living N2a cells in a homogeneous way (HTRF mode), without removing unbound antibodies. Using different Europium- and APC-coupled POM antibodies, I was able to detect PrP^C on intact N2a cells in a 96- as well as a 384-well-plate format. Best results were found for the POM2Eu/POM1APC FRET tandem pair. In N2a cell number titration experiments, a statistical significant result was found for 500 N2a cells plated in a 384-well plate one day before. A similar result was found for the FRET antibody pair POM1Eu/POM2APC, whereas when using POM2Eu and POM2APC a weaker FRET signal was found.

In a further set of experiments, the TR-FRET signal was measured after washing out the unbound antibodies, as previously shown by others [Maurel et al., 2004]. The TR-FRET signal was observed only when using the POM2Eu and POM1APC antibody combination. Compared to the TR-FRET assay, the signal intensity measured under HTRF conditions is higher, likely because some cells and unbound antibodies are lost during the washing process. Surprisingly, the results are statistically stronger in the TR-FRET mode than in the HTRF mode. No FRET signal was detected in the TR-FRET mode for PrP-deficient Hpl cells or medium only, which clearly demonstrates the specificity of this FRET assay for extracellular PrP^C epitopes. The FRET signal in the HTRF and TR-FRET mode measured by POM2Eu and POM1APC for PrP^C was found to be directly proportional to the amount of PrP^C proteins at the cell surface of N2a cells. A linear correlation was found in the range of 500 to 8000 in the HTRF mode and 250 to 8000 in the TR-FRET mode.

PrP^C Endocytosis Time-Resolved FRET Assay

I have studied the endocytosis of endogenously expressed murine and human PrP^C on cells *in vitro*. By the addition of the FRET antibodies separately and at different time points, the distance between the antibodies increases in the course of endocytosis which can be monitored by decreasing FRET signal intensities. A cell surface half life time of about 30 min of PrP^C could be determined which is in agreement with previous results [Shyng, 1993]. No detectable PrP^C was found during labelling or endocytosis process in the culture medium, confirming that PrP^C is mainly endocytosed and not released from the cell surface. In control experiments, MβCD and chlorpromazine inhibited endocytosis of PrP^C without affecting cell viability as reported in earlier publications [Marella et al., 2002; Sarnataro et al., 2009].

Next, I wanted to know which genes are involved in the endocytosis of PrP^C. For that reason I tested several siRNAs which have an influence on the various endocytosis pathways. All utilized siRNAs were able to reduce the expression of the target gene on the mRNA level and had no implications on cell viability. Among the tested siRNAs, AP2M1 and Rab5a showed a stong inhibition of PrP^C's internalisation. AP2M1 codes for the AP-2 adaptor protein which is involved in clathrin-dependent endocytosis pathways [Boucrot et al., 2010]. It was shown by earlier studies that AP-2 is co-localized in the inner surface of the membrane with PrP^C [Sunyach et al., 2003]. Rab5a showed even a small increase of the PrP^C cell surface expression after 30 min and completely blocked the endocytosis of PrP^C. Similar results were found by Magalhaes et al., who has shown that green fluorescent protein (GFP)-tagged PrP^C is endocytosed via Rab5-containing early endosomes, implying a coated pit-dependent uptake

of the hybrid protein but not of GPI-GFP [Magalhaes et al., 2002]. Knock-down of the VPS35 and M6PR also block endocytosis of PrP^C but less prominent. Mannose-6-phosphate receptors regulate the formation of clathrin-coated vesicles [Le Borgne et al., 1997]. The VPS35 gene (vacuolar protein sorting 35 homolog) belongs to a multimeric complex, termed the retromer complex which is involved in retrograde transport of proteins from endosomes to the trans-Golgi network [Bonifacino & Hurley, 2008].

In summary, the FRET-based PrP endocytosis assay can be used as a read-out for the efficiency of compounds or small molecules that genetically or pharmacologically block or induce PrP endocytosis. It is able to measure the internalisation rate, to characterize the different endocytosis pathways as well as to discover genes involved in the uptake of PrP. The assay can be performed in 384-well plates and allows high-throughput applications and automatisation.

OUTLOOK

The time-resolved FRET assay can be applied as novel technical tool to address several questions in prion biology and for HTS screening applications. In the following paragraphs are some examples described: One question in prion biology concerns genes involved in cell-to-cell transmission of prions [Aguzzi & Rajendran, 2009]. Answers to this question would be helpful in understanding other neurodegenerative diseases such as Alzheimer or Parkinson disease which show a similar prion-like spread [Ashe & Aguzzi, 2013; Dunning et al., 2013]. To answer this questions the PrP^{Sc} FRET assay could be very helpful to study the transmission of prions as well as factors determining prion infectivity.

In a recent publication from our laboratory it could be shown, that antibodies targeting the globular domain of PrP induce rapid neurotoxicity in mice and cerebellar organotypic slice cultures. Interestingly, deletion in the octapeptide repeats of PrP prevented neurotoxicity of globular domain ligands, assuming that the flexible N-terminal part of PrP may exert regulatory and executive functions [Sonati et al., 2013]. Here, the FRET-based recPrP assay is used in competition experiments to screen for ligands, which bind to the N-terminal part of recPrP. Positive hits will be tested *in vitro* as well as *in vivo* to prevent globular domain ligand-induced neurotoxicity.

PrP^{Sc} needs PrP^{C} to replicate. The PrP^{C} cell surface FRET assay can be used as a screening platform. A similar PrP-FRET assay has recently been used for the search of compounds which downregulate the expression of PrP^{C} at the cell surface and therefore influence the propagation of PrP^{Sc} [Karapetyan YE et al., 2013]. Moreover, many interaction partners for PrP have been proposed. Here, the PrP^{C} cell surface FRET assay can be used to study interactions with other proteins.

The physiological role of PrP^{C} is unknown. However, PrP^{C} is rapidly internalized from the cell membrane and is believed to be involved in a number of cellular processes. How PrP^{C} endocytosis influences them *in vivo* is unknown. The PrP^{C} FRET-based endocytosis assay could be used to screen for kinases [Sorkin & Zastrow, 2009] which are involved in the internalization of PrP^{C}. This could be helpful to elucidate the physiological function of PrP^{C} and to understand the mechanisms involved in prion-induced neurodegeneration [Aguzzi, Baumann & Bremer, 2008].

MATERIAL AND METHODS

Mice

All organotypic cerebellar slice cultures were performed by Ilan Margalith according to Swiss federal regulations. The pups used for most experiments were F1 offspring of wt, tga20 or KO males on a 129SV/BL background.

Cell Culture

PK1 N2a (a subclone of neuroblastoma N2a cells), CAD and Hpl PrP KO cells were cultured in 75-cm tissue culture flasks in OptiMeM medium supplemented with 10% (vol/vol) fetal bovine serum (FBS) and 1% Pen/Strep. Cells were removed with 2mM EDTA/PBS and split 1:3 every third day. Human HeLa and A549 cells were cultured in DMEM medium supplemented with 10% (vol/vol) fetal bovine serum and 1% Pen/Strep. In FRET experiments, all cell lines were cultured in medium without FBS, antibiotics and phenol red. To determine cell numbers and viability, resuspended cells were diluted in trypan blue solution and counted in a Neubauer counting chamber.

Preparation of CD1 and RML6 Crude Brain Homogenate

20% wt/vol RML6 or CD1 brain homogenates in 0.32M sucrose in PBS were prepared by three runs in a PreCellys tissue homogenizer with cooling on ice between each run. Protein concentrations of RML6 or CD1 brain homogenates were determined using the bicinchoninic acid assay (Pierce) and normalized to 1 mg/ml total protein with 0.32M sucrose in PBS.

Scrapie Cell End-Point Assay of COCSBH

COCSBH normalized to 1 mg/ml total protein was diluted 1 to 100 fold in cell culture medium to obtain a final dilution of 10^{-4} from full brain. These samples were then serially diluted in cell culture medium containing a 10^{-4} dilution of CD1 BH. Prion-susceptible neuroblastoma cells (N2aPK1) were exposed to different COCSBH concentrations ranging from 10^{-4} to 10^{-9} in a 96-well plate for 3 days. Cells were splitted 3 times 1:3 every second day and 3 times 1:10 every third day. Experimental runs comprised 4 plates including a COCSBH from six weeks old prion-infected, untreated tissue as a standard plate. The infection of N2a-PK1 cells and subsequent processing of the SCEPA were performed as previously described (Klohn et al., 2003). Before reaching cell confluence, cells from each 96-well were filtered onto the membrane of an ELISPOT plate, treated with PK, denatured

and PK-resistant PrP^{Sc} was detected by immunocytochemistry using alkaline-phosphatase-conjugated POM1 mouse anti-PrP antibody and alkaline phosphatase conjugate substrate kit (BioRad). Samples were quantified by total luminescence per well or in end-point format by counting positive wells according to established methods.

Proteolysis of COCSBH and Western Blot Analysis

PrP^{Sc} was detected by limited proteolysis with proteinase K (PK) (Roche) and analysed by Western blotting according to Ilan Margalith's protocol. 20 μg protein aliquots were digested with 25 μg/ml PK in lysis buffer containing 0.5% wt/vol sodium deoxycholate, 0.5% vol/vol Nonidet P-40 and 10% vol/vol PBS for 60 min at 37°C and rotating at 700 rpm on a thermoshaker in a total volume of 20 μl. This condition allowed specific detection of PrP^{Sc}. PK digestion was terminated by adding 6.7 μl of 4x LDS loading buffer (NuPAGE, Invitrogen) and boiling the samples at 95 °C for 5 min. 20 μl of the samples were separated on a 12% Bis-Tris SDS polyacrylamide gel (NuPAGE, Invitrogen) and blotted onto a nitrocellulose membrane. Membranes were blocked with 5% wt/vol Topblock (Fluka) in Tris-buffered saline supplemented with Tween (150 mM NaCl, 10 mM Tris HCl, 0.05% Tween 20 (vol/vol)) and incubated with POM1 mouse IgG1 antibody to PrP^{C} (anti-PrP^{C}) (200 ng/ml) as primary antibody. Horse radish peroxidase (HRP)-conjugated rabbit anti–mouse IgG1 (1:10,000, Zymed) was used as a secondary antibody. The blots were developed using SuperSignal West Pico chemiluminescent substrate (Pierce) and detected in a LAS3000 system (FUJI).

ELISA

For ELISA, COCSBH were diluted ten-fold in TBSTT [50 mM Tris-HCl (pH 7.5)/137 mM NaCl/1% Tween20/1% Triton X-100] to obtain a final concentration of 0.1 mg/ml total protein. Digestion with proteinase K (PK) was performed in a 96-well plate for 60 min at 37 °C, rotating at 700 rpm on a thermoshaker in a total volume of 50 μl containing 50 μg ml^{-1} PK. Digestion was halted by adding 2 mM phenylmethanesulfonylfluoride (PMSF, Calbiochem) and Complete Mini protease inhibitor cocktail (Roche). Digested samples were denatured with an equal volume of 3 M GdnSCN for 30 min at 37 °C and diluted with four volumes of 0.1 M $NaHCO_3$ pH 8.9. The samples were then detected by sandwich ELISA. Briefly, ELISA plates were coated with POM1-antibodies (400 ng/well) in coating buffer overnight. After washing with PBST, plates were blocked with blocking buffer (5% TopBlock in PBST) for 2 hrs at room temperature. Next, samples were incubated for 2 hours on ELISA

plates (Nunc, MaxiSorb). Captured samples were detected with POM19 antibody (1 mg/ml, 1 hour, diluted in sample buffer) and horse radish peroxidase (HRP)-avidin conjugate (1 mg/ml, 1 hour, diluted in sample buffer) (BD Pharmingen). Samples were analysed by ELISA in technical triplicates and washed five times with PBS 0.05% Tween20 between each antibody and conjugate incubations. Finally, TMB substrate (Invitrogen) was added to the wells and incubated for 15 min at room temperature and stopped by adding 0.5 M H_2SO_4. The absorbance was read at 450 nm in a VERSAmax microplate reader and validated with the SOFTmax PRO software.

FRET Antibody Labelling

The monoclonal full length and single chain POM antibodies or recombinant PrP were labelled in house for FRET applications. The donor fluorophore was Europium chelate (Eu-W1024 ITC chelate, AD0096, PerkinElmer). Coupling of proteins/peptides to Eu chelate occurs at alkaline pH via reaction of lysine residues and free N termini with the aromatic isothiocyanate group of the Europium chelate. To remove compounds interfering with labelling, protein and peptides were dialyzed over night. POM antibodies and recPrP were diluted in 1 or 0.5 ml 100 mM sodium carbonate (Na_2CO_3), pH 9-9.3, respectively. Dialysis cassettes (Slide-A-Lyzer®, Thermo scientific) were preincubated in ddH_2O for 2 min and proteins or peptides were loaded with a 24G syringe. In both cases, a dialysis cassette with a cut-off of 7 kDa was used, however, for POM antibodies cut-offs of 10-20 kDa are also suitable. Dialysis was done under stirring in a volume of 2 l of 100 mM Na_2CO_3 at 4°C over night. Dialysis buffer was changed after 4-6 h of incubation at 4°C. Proteins and peptides were concentrated by Centricon concentrators (Millipore). Protein concentration was adjusted by the Bradford or BCA assay to a concentration of about 5 mg/ml. Lyophilized Eu-W1024 ITC chelate (0.1 mg) was stored at –20°C and immediately before use reconstituted in 100 µl distilled water which gives a concentration of 1.4 mM. A molar excess of 24x of Europium chelate over IgG was added into the protein (peptide) solution on ice and incubated in 100 mM Na_2CO_3 over night at 4°C. Separation of the labelled protein from non-reacted chelate was performed by size exclusion chromatography (Superdex 200 column, GE Healthcare). Elution from column was done with 50 mM Tris-HCl pH 7.8 + 0.9% sodium chloride. Sample fractions of 500 µl were collected. Superdex column was decontaminated with 10 mM phthalate buffer pH 4.1 containing 0.01% DTPA. Fractions were pooled and concentrated with Micron centrifugal filters (Amicon). Labelling ratio and concentration of labelled proteins were assessed by a Eu standard solution (Perkin Elmer) and Nano drop measurement,

respectively. Aliquots of antibodies were stored at 4°C in the dark. Allophycocyanin (APC, AnaTag^{TM} Labeling Kit 72111, Anaspec) was used as acceptor fluorophore for conjugation to POM antibodies. Maleimide groups of APC react with sulfhydryl groups on the target antibody to form a covalent bond during conjugation. POM antibodies were concentrated to 2-10 mg/ml in a volume of 100 µl with Centricon concentrators (Millipore). Antibodies were reduced with 20 µl dithiothreithol (DTT) per ml of IgG solution for 30 min without agitation at room temperature. Depending on reaction volume, reduced antibodies were desalted either by spin or gravity columns. Protein concentration was assessed by Nanodrop measurement. For the conjugation reaction, 1.5 mg of activated APC per mg reduced IgG was added to the reduced antibodies solution and incubated for 1 h at room temperature with agitation. By adding DMSO and NEM for 30 min at room temperature, free thiol groups were blocked. To remove free APC molecules from antibody solution, reaction mixture was purified via a protein G sepharose column (Sigma). The column was washed with water and 10 volumes of 20 mM phosphate buffer pH 7 to equilibrate. Samples were added and washed with five volumes 20 mM phosphate buffer pH 7. Flow through was collected. The column was eluated with 0.1 M glycine pH 2.3 and diluted with 1 M TrisHCl pH 8. APC-labelled POM antibodies were characterized with Nanodrop (A280 and A650). Aliquots of antibodies were stored at 4°C in the dark.

FRET Experiments

PrP^{C} cell surface FRET labelling: Cells were plated one day before into 96- or 384-well microtiter plates (Perkin Elmer) in cell culture medium without phenol red at the desired density. Cells were washed once and FRET antibody labelling was performed at 4°C in a total volume of 50 µl containing 1 nM Eu-labeled and 5 nM APC-labelled antibodies in Tris/KREBS buffer (20 mM Tris pH 7.4, 118 mM NaCl, 5.6 mM glucose, 1.2 mM KH_2PO_4, 1.2 mM $MgSO_4$, 4.7 mM KCl, 1.8 mM $CaCl_2$, 1% BSA). FRET signals were measured with the Wallac EnVision reader (homogeneous FRET assay). Thereafter, plates were washed with Tris/KREBS buffer and the FRET signal was measured again (TR-FRET assay).

Pharmacological treatment of cells was done with brefeldine A (), diluted in DMSO (), for 18 h incubation at 37°C. DMSO concentration was kept constant at 0.75%. Cells were washed once with ice-cold Tris/KREBS buffer and labelled with FRET antibodies as mentioned above. Enymatic treatment of cells was done with PI-PLC. PI-PLC was dialyzed in PBS over night and protein concentration was assessed by the Bradford assay (BioRad). Digestion was carried out either at 4°C or at 37°C for 1 h during shaking (450 rpm). Supernatant was

transferred into a new plate and medium and cells were labelled with FRET antibodies. The neuronal Hpl PrP KO cell line [Sakudo A et al., 2007] was used as negative control for assay development and optimisation.

Preparation of Recombinant Mouse mPrP (23-231)

Recombinant mouse PrP comprising residues 23-231 and the N1 fragment were expressed and purified by Simone Hornemann (Zahn et al., 2000; Lysek and Wüthrich, 2004; Hornemann et al., 2009). Murine PrP(23-231) fibers were produced by incubating the protein at 37 ºC for 48 hours in 50 µM Tris-HCl, 1 M GdnHCl, 150 mM sodium chloride, pH 7.5 and shaking at 600 rpm (Apetri et al., 2005).

siRNA Treatment

Lyophilyzed human siRNA (Ambion®) was diluted in 500 µl RNase-free water at a stock solution of 10 µM and placed on a shaker for 90 min at 37°C. Aliquots were stored at –20°C. To transfect siRNA into mammalian cells, Lipofectamine™ 2000 (Invitrogen™) was utilized. Briefly, one day before transfection, 2500 cells in 80 µl DMEM cell culture medium without antibiotics were seeded into a 96-well plate per well. SiRNA:Lipofectamine™ 2000 complexes were prepared as follows: 5 µl siRNA (1 µM) was diluted in 5 µl prewarmed DMEM cell culture medium without serum and antibiotics and mixed gently. 0.1 µl Lipofectamine™ 2000 was diluted in 9.9 µl prewarmed DMEM cell culture medium without serum and antibiotics. After an incubation of 5 min at room temperature, the diluted Lipofectamine™ 2000 was combined with the diluted siRNA. To allow formation of siRNA:Lipofectamine™ 2000 complexes, the combined solutions were mixed and incubated for 20 min at room temperature. 20 µl of siRNA:Lipofectamine™ 2000 complexes were added to each well of the 96-well plate and cells were cultured at 37°C in a CO_2 incubator for 72 h.

Quantitative PCR

Cell cultures were prepared and incubated as stated above. Cells were washed once with PBS and total RNA was extracted using the RNeasy® mini kit (Qiagen) according to the manufacturer's protocol. RNA concentration and purity was determined by Nanodrop measurements. cDNA was synthesized from 0.5 µg total RNA with QuantiTect reverse transcription kit (Qiagen) using random hexamers according to the manufacturer's protocol. Before cDNA synthesis, genomic DNA was eliminated. Successful cDNA synthesis and contamination of total RNA with genomic DNA was tested by PCR with primer specific for

GAPDH. Quantitative real-time PCR was performed using the SYBR Green master mix (Applied Biosystems) on a ABI Prism VIIA7 sequence detector (PerkinElmer). Fold regulation was calculated relative to untreated cells after normalization to the GAPDH signal. The following primer pairs were used: VPS28 sense (NM_016208): 5'–TTG TTC CCA GGG GCT CCT AT-3', antisense: 5'–ATC TTC CCG ACC GCG AG-3'. RAB5A sense (NM_004162): 5'-TTA GAA AAG CAG CCC CAA TG-3', antisense 5'-GTA CTT CTG GGA GAG TCC GC-3'. AP2M1 sense (NM_004068): 5'-AAT CAT GGC GGC AGA TCA GT-3', sense 5'-ATC TTG GGA TCC GGA GAG TG-3'. GIT2 sense (NM_014776): 5'-AGA CAA ATC CAG GCT GCT GT-3', antisense 5'-GCG CCT CGT GGA AAT ACA GT-3'. EHD1 sense (NM_006795): 5'-AAG AGC AGG ATG ATG CGG T-3', antisense 5'-CCT GTC TGG AGA GAA GCA GC-3'. M6PR sense (NM_002355): 5'-ATT CTC TCA CTG CCA CAG CC-3', antisense 5'-TGG CTA CTC CAG TTT CCC AC-3'. VPS35 sense (NM_018206): 5'-CAC TGA TAG TCT GGT GGG CA-3', antisense 5'-CAG CTT ACC AGC TGG CTT TT-3'. PRNP sense (NM_000311): 5'-AGT GTT CCA TCC TCC AGG C-3', antisense 5'-GAG CTT CTC CTC TCC TCA CG-3'. GAPH sense (NM_002046): 5'-CAT GAG AAG TAT GAC AAC AGC CT, antisense 5'-AGT CCT TCC ACG ATA CCA AA GT-3'.

Cell Viability Assay

The alamarBlue® assay (Invitrogen) was utilized to assess cell viability according to the manufacturer's protocol. All experiments were performed in cell culture medium without antibiotics and phenol red. Cells were incubated with the alamarBlue dye at 37°C and viability was measured after 4-12 hrs.

REFERENCES

Aguzzi A (2006). Prion diseases of humans and farm animals: epidemiology, genetics, and pathogenesis. J Neurochem 97:1726-1739.

Aguzzi A, Heikenwalder M, Polymenidou M (2007). Insights into prion strains and neurotoxicity. Nat Rev Mol Cell Biol 8:552-61.

Aguzzi A, Calella AM (2009). Prions: protein aggregation and infectious diseases. Physiol Rev 89:1105-52.

Aguzzi A, Rajendran L (2009). The transcellular spread of cytosolic amyloids, prions, and prionoids. Neuro 64:783-90.

Aguzzi A and Glatzel M (2005). Prion infectious, blood and transfusions. Nature clinical practice neurology 2:321-329.

Aguzzi A, Polymenidou M (2004). Mammalian prion biology. One century of evolving concepts. Cell 116:313-327.

Aguzzi A, Weissmann C (1997). Prion research: the next frontiers. Nature 389:795-798.

Alper T, Haig DA, Clarke MC (1966). The exceptionally small size of the scrapie agent. Biochem Biophys Res Commun. 22:278-84.

Alper T, Cramp WA, Haig DA, Clarke MC (1967). Does the agent of scrapie replicate without nucleic acid? Nature 214:764-766.

Alpers M (1979). Delivery of health care in Papua New Guinea. PNG Med J 3:159-162.

Anoopkumar-Dukie S, Carey JB, Conere T, O'Sullivan E, Van Pelt FN, Allshire A (2005). Resazurin assay of radiation response in cultured cells. Brit J Radiol 78:945-7.

Apetri AC, Vanik DL, Surewicz WK (2005). Polymorphism at residue 129 modulates the conformational conversion of the D178N variant of human prion protein 90-231. Biochemistry 44:15880-15888.

Appleby BS, Lyketsos CG (2011). Rapidly progressive dementias and the treatment of human prion diseases. Expert Opin Pharmacother 12:1-12.

Ashe KH, Aguzzi A (2013). Prions, prionoids and pathogenic proteins in Alzheimer disease. Prion 7:55-9.

Beekes M, Baldauf E, Diringer H (1996). Sequential appearance and accumulation of pathognomonic markers in the central nervous system of hamsters orally infected with scrapie. J Gen Virol 77:1925-34.

Berry BB, Lu D, Geva Michal, Watts JC, Bhardwaj S, Oehler A, Renslo AR, DeArmond SJ, Prusiner SB, Giles K (2013). Drug resistance confounding prion therapeutics. Proc Natl Acad Sci USA 110:4160-9.

Basler K, Oesch B, Scott M, Westaway D, Walchli M, Groth DF, McKinley MP, Prusiner SB, and Weissmann C (1986). Scrapie and cellular PrP isoforms are encoded by the same gene. Cell 46:417-428.

Bishop N, Woodman P (2001). TSG101/mammalian VPS23 and mammalian VPS28 interact directly and are recruited to VPS4-induced endosomes. J Biol Chem 276-11735-42.

Blättler T, Brandner S, Raeber AJ, Klein MA, Voigtländer T et al., (1997). PrP-expressing tissue is required for transfer of scrapie infectivity from spleen to brain. Nature 389:69-73.

Bolton DC, McKinley MP, Prusiner SB (1982). Identification of a protein that purifies with the scrapie prion. Science 218:1309-1311.

Bolton DC, Seligman SJ, Bablanian G, Windsor D, Scala LJ, Kim KS, et al., (1991). Molecular location of a species-specific epitope on the hamster scrapie agent protein. J Virol 65:3667-75.

Bonifacino JS, Hurley JH (2008). Retromer. Curr Opin Cell Biol 20:427-36.

Borchelt DR, Scott M, Taraboulos A, Stahl N, Prusiner SB (1990) Scrapie and cellular prion proteins differ in their kinetics of synthesis and topology in cultured cells. J Cell Biol 110:743-752.

Bosque PJ, Ryou C, Telling G, Peretz D, Legname G, DeArmond SJ and Prusiner SB (2002). Prions in skeletal muscle. Proc Natl Acad Sci USA 99:3812-7.

Boucrot E, Saffarian S, Zhang R, Kirchhausen T (2010). Roles of AP-2 in clathrin-mediated endocytosis. PLOS One 5.

Bremer J, Baumann F, Tiberi C, Wessig C, Fischer H, Schwarz P, Steele AD, Toyka KV, Nave KA, Weis J, Aguzzi A (2010). Axonal prion protein is required for peripheral myelin maintenance. Nat Neurosci 13:310-318.

Brown P, Cathala F, Castaigne P, Gajdusek DC (1986). Creutzfeldt-Jakob disease: clinical analysis of a consecutive series of 230 neuropathologically verified cases. Ann Neurol 20:597-602.

Brown P and Bradley R (1998) 1755 and all that: a historical primer of transmissible spongiform encephalopathy. BMJ 317, 1688-92.

Brown DR (2001). Copper and Prion disease. Brain Res Bull 55:165-173.

Bruce ME, Dickinson AG (1987). Biological evidence that scrapie agent has an independent genome. J Gen Virol 68:79-89.

Bruce ME, Will RG, Ironside JW, McConnell I, Drummond D, Suttie A, McCardle L, Chree A, Hope J, Birkett C, et al. (1997). Transmissions to mice indicate thet “new variant” CJD is caused by the BSE agent. Nature 389:498-501.

Büeler HR, Fischer M, Lang Y, Bluethmann H, Lipp HP, DeArmond SJ, Prusiner SB, Aguet M, Weissmann C (1992). Normal development and behaviour of mice lacking the neuronal cell-surface PrP Protein. Nature 356:577-82.

Büeler HR, Aguzzi A, Sailer A, Greiner RA, Autenried P, Aguet M, Weissmann C (1993). Mice devoid of PrP are resistant to scrapie. Cell 73:1339-1347.

Bueno C, Villegas ML, Bertolotti SG, Previtali CM, Neumann MG, Encinas MV (2002). The excited-state interaction of resazurin and resorufin with amines in aqueous solutions. Photophysics and photochemical reactions. Photochem Photobiol 76:385-90.

Carlson GA, Westaway D, DeArmond SJ, Peterson-Torchia M, Prusiner SB (1989). Primary structure of prion protein may modify scrapie isolate properties. Proc Natl Acad Sci USA 86:7475-9.

Carlson GA, Ebeling C, Yang SL, Telling G, Torchia M, Groth D, Westaway D, DeArmond SJ, Prusiner SB (1994). Prion isolate specific allotypic interactions between the cellular and scrapie prion proteins in congenic and transgenic mice. Proc Natl Acad Sci USA 91:5690-4.

Casalone C, Zanusso G, Acutis P, Ferrari S, Capucci L, Tagliavini F, Monaco S, Caramelli M (2004). Identification of a second bovine amyloidotic spongiform encephalopathy: molecular similarities with sporadic Creutzfeldt-Jakob disease. Proc Natl Acad Sci USA 101:3065-70.

Caspi S, Halimi M, Yanai A, Sasson SB, Taraboulos A, Gabizon R (1998). The anti-prion activity of Congo red. Putative mechanism. J Biol Chem 273:3484-3489.

Castilla J, Saa P, Hetz C, Soto C (2005). In vitro generation of infectious scrapie prions. Cell 121:195-206.

Caughey BW, Dong A, Bhat KS, Ernst D, Hayes SF, Caughey WS (1991). Secondary structure analysis of the scrapie-associated protein PrP 27-30 in water by infrared spectroscopy. Biochem 30:7672-7680.

Caughey B, Raymond GJ, Beesen RA (1998). Strain-dependent differences in beta-sheet conformations of abnormal prion protein. J Biol Chem 273:32230-5.

Caughey B and Race RE (1992). Potent inhibition of scrapie-associated PrP accumulation by congo red. J Neurochem 59:768-771.

Caughey B and Raymond GJ (1993). Sulfated polyanion inhibition of scrapie-associated PrP accumulation in cultured cells. J Virol 67:643-650.

Chae HJ, Kang JS, Byun JO, Han KS, Kim DU, Oh SM, Kim HW, Chae SW, Kim HR (2000). Molecular mechanism of staurosporine-induced apoptosis in osteoblasts. Pharm Res 42:373-381.

Chandler RL (1961). Encephalopathy in mice produced by inoculation with scrapie brain material. Lancet 1:1378-9.

Chandler RL, Fisher J (1963). Experimental Transmission of Scrapie to Rats. Lancet 2:1165.

Chatelain J, Cathala F, Brown P, Raharison S, Court L, Gajdusek DC (1981). Epidemiologic comparison between Creutzfeldt-Jakob disease and scrapie in France during the 12-year period 1968-1979. J Neurol Sci 3:329-37.

Chazot G, Broussolle E, Lapras CI, Blättler T, Aguzzi A, Kopp N (1996). New variant of Creutzfeldt-Jakob disease in a 26-year-old French man. Lancet 347:1181.

Chesebro B, Trifilo M, Race R, Meade-White K, Teng C, LaCasse R, Raymond L, Favara C, Baron G, Priola S, Caughey B, Masliah E, Oldstone M (2005). Anchorless prion protein results in infectious amyloid disease without clinical scrapie. Science 308:1435-1439.

Chiarini LB, Freitas AR, Zanata SM, Brentani RR, Martins VR, Linden R (2002). Cellular prion protein transduces neuroprotective signals. EMBO J 21:3317-26.

Cohen FE, Pan KM, Huang Z, Baldwin M, Fletterick RJ, Prusiner SB (1994). Structural clues to prion replication. Science 264:530-1.

Cohen FE and Prusiner SB (1998). Pathologic conformations of prion proteins. Annu Rev Biochem 67:793-819.

Collinge J, Palmer MS, Dryden AJ (1991). Genetic predisposition to iatrogenic Creutzfeldt-Jakob disease. Lancet 337:1441-2.

Collinge J, Whittington MA, Sidle KC, Smith CJ, Palmer MS, Clarke AR, Jefferys JG (1994). Prion protein is necessary for normal synaptic function. Nature 370:295-297.

Collinge J, Sidle KC, Meads J, Ironside J, Hill AF (1996). Molecular analysis of prion strain variation and the aetiology of "new variant" CJD. Nature 383:685-690.

Creutzfeldt HG (1920). Über eine eigenartige herdförmige Erkrankung des Zentralnervensystems. Z ges Neurol Psychiatr 57:1-19.

Crowther JR (2001). The ELISA guidebook. Humana Press.

Cuille J and Chelle PL (1939). Experimental transmission of trembling to the goat. C R Seances Acad Sci 208:1058-1160.

Deleault NR, Harris BT, Rees JR, Supattapone S (2007). Formation of native prions from minimal components in vitro. Proc Natl Acad Sci USA 104:9741-9746.

Dickinson AG (1976). Scrapie in sheep and goats. Front Biol 44:209-241.

Doh-Ura K, Iwaki T, Caughey B (2000). Lysosomotropic agents and cysteine protease inhibitors inhibit scrapie-associated prion protein accumulation. J Virol 74:4894-7.

Ducrot C, Arnold M, de Koeijer A, Heim D, Calavas D (2008). Review on the epidemiology and dynamics of BSE epidemics. Vet Res 39:15.

Duff P, Wolf J, Collins G, DeVoe AG, Streeten B, Cowen D (1974). Letter: possible person-to-person transmission of Creutzfeldt-Jakob disease. N Engl J 290:692-3.

Dunning CJ, George S, Brundin P (2013). What's to like about the prion-like hypothesis for spreading of aggregated α-synclein in Parkinson disease? Prion 7:92-7.

Falsig J, Julius C, Margalith I, Schwarz P, Heppner FL, and Aguzzi A (2008). A versatile prion replication assay in organotypic brain slices. Nat Neurosci. 11(1):109-117.

Forloni G, Iussich S, Awan T, Colombo L, Angeretti N, Girola L, Bertani I, Poli G, Caramelli M, Grazia Bruzzone M, Farina L, Limido L, Rossi G, Giaccone G, Ironside JW, Bugiani O, Salmona M, Tagliavini F (2002). Tetracyclines affect prion infectivity. Proc Natl Acad Sci USA 99:10849-54.

Gabizon R, McKinley MP, Groth D, Prusiner SB (1988). Immunoaffinity purification and neutralization of scrapie prion infectivity. Proc Natl Acad Sci USA 85:6617-6621.

Gajdusek DC, Zigas V (1957). Degenerative disease of the central nervous system in New Guinea – the endemic occurence of „kuru“ in the native population. N Engl J Med 257:974-978.

Gajdusek DC, Gibbs CJ, Alpers M (1966). Experimental transmission of a Kuru-like syndrome to chimpanzees. Nature 209:794-796.

Gajdusek DC (1977) Unconventional viruses and the origin and disappearance of kuru. Science 197:943-960.

Gambetti P, Kong Q, Zou W, Parchi P, Chen SG (2003). Sporadic and familial CJD: classification and characterisation. Br Med Bul 66:213-239.

Gasset M, Baldwin MA, Fletterick RJ Prusiner SB (1993). Perturbation of the secondary structure of the scrapie prion protein under conditions that alter infectivity. Proc Natl Acad Sci USA 90:1-5.

Gauczynski S, Peyrin JM, Haik S, Leucht C, Hundt C, Rieger R, Krasemann S, Deslys JP, Dormont D, Lasmezas CI, Weiss S (2001). The 37-kDa/67-kDa laminin receptor acts as the cell-surface receptor for the cellular prion protein. EMBO J 20:5863-75.

Gibbs CJ, Jr, Gajdusek DC, Asher MP, Beck E, Daniel PM, Matthews WB (1968). Creutzfeldt-Jakob disease (spongiform encephalopathy): transmission to the chimpanzee. Science 161:388-389.

Gibbs CJ jr, Gajdusek DC, Latarjet R (1978). Unusual resistance to ionizing radiation of the viruses of kuru, Creutzfeldt-Jakob disease, and scrapie. Proc Natl Acad Sci USA 75:6268-70.

Glasse R (1967). Cannibalism in the Kuru region of New Guinea. Trans NY Acad Sci 29:748-54.

Glatzel M, Heppner FL, Albers KM, Aguzzi A (2001). Sympathetic innervation of lymphoreticular organs is rate limiting for prion neuroinvasion. Neuron 31:25-34.

Goldenthal KL, Pastan I, Willingham MC (1984). Initial steps in receptor-mediated endocytosis. The influence of temperature on the shape and distribution of plasma membrane clathrin-coated pits in cultured mammalian cells. Exp Cell Res 152:558-64.

Gordon WS (1946). Advances in veterinary research. Vet Res 58:516-20.

Graner E, Mercadante AF, Zanata SM, Forlenza OV, Cabral AL, Veiga SS, Juliano MA, Roesler R, Walz R, Minetti A, Izquierdo I, Martins VR, Breantani RR (2000). Cellular prion protein binds laminin and mediates neuritogenesis. Brain Res Mol Brain Res 76:85-92.

Grathwohl KU, Horiuchi M, Ishiguro N, Shinagawa M (1997). Sensitive enzyme-linked immunosorbent assay for detection of PrP^{Sc} in crude tissue extracts from scrapie-affected mice. J Virol Methoods 64:205-16.

Griffith JS (1967). Self-replication and scrapie. Nature 215:1043-1044.

Gulappa T, Clouser CL, Menon KM (2011). The role of Rab5a GTPase in endocytosis and post-endocytic trafficking of the hCG-human luteinizing hormone receptor complex. Cell Mol Life Sci 68:2785-95.

Hadlow WJ (1959). Scrapie and kuru. Lancet 2:289-290.

Haraguchi T, Fisher S, Olofsson S, Endo T, Groth D, Tarentino A, Borchelt DR, Teplow D, Hood L, Burlingame A, and et al., (1989). Asparagine-linked glycosylation of the scrapie and cellular prion proteins. Arch Biochem Biophys 274:1-13.

Harris DA (2003). Trafficking, turnover and membrane topology of PrP. Br Med Bull 66:71-85.

Harris DA (1999). Cellular Biology of Prion Diseases. Clin Microbiol Rev 12:429-444.

Hetz C, Maundrell K, Soto C (2003). Is loss of function of the prion protein the cause of prion disorders? Trends Mol Med 9:237-43.

Heppner FL, Christ AD, Klein MA, Prinz M, Fried M et al., (2001). Transepithelial prion transport by M cells. Nat Med 7:976-77.

Hill AF, Desbruslais M, Joiner S, Sidle KC, Gowland I, Collinge J, Doey LJ, Lantos P (1997). The same prion strain causes vCJD and BSE. Nature 389:448-450.

Hope J, Ritchie L, Farquhar C, Sommerville R, Hunter N (1989). Bovine spongiform encephalopathy: a scrapie-like disease of British cattle. Prog Clin Biol Res 317:659-667.

Hornemann S, Christen B, von Schroetter C, Perez DR, Wuthrich K (2009). Prion protein library of recombinant constructs for structural biology. Febs J 276:2359-2367.

Hossszu LL, Baxter NJ, Jackson GS, Power A, Clarke AR, Waltho JP, Craven CJ, Collinge J (1999). Structural mobility of the human prion protein probed by backbone hydrogen exchange. Nat Struct Biol 6:740-43.

Houston F, Foster JD, Chong A, Hunter N, Bostock CJ (2000). Transmission of BSE by blood transfusion in sheep. Lancet 356:999-1000.

Hsiao K, Baker HF, Crow TJ, Poulter M, Owen F, Terwilliger JD, Westaway D, Ott J, Prusiner SB (1989). Linkage of a prion protein missense variant to Gerstmann-Straussler syndrome. Nature 338:342-345.

Hsiao KK, Groth D, Scott M, Yang SL, Serban H, Rapp D, Foster D, Torchia M, Dearmond SJ, Prusiner SB (1994). Serial transmission in rodents of neurodegeneration from transgenic mice expressing mutant prion protein. Proc Natl Acad Sci U S A 91:9126-9130.

Ingrosso L, Ladogana A, Pocchiari M (1995). Congo red prolongs the incubation period in scrapie-infected hamsters. J Virol 69:506-508.

Inoue Y, Yamakawa Y, Sakudo A, Kinumi T, Nakamura Y, Matsumoto Y, Saeki K, Kamiyama T, Onodera T, Nishijima M (2005). Infection route-independent accumulation of splenic abnormal prion protein. Jpn J Infect Dis 58:78-82.

Jakob A (1921). Über eine eigenartige Erkrankung des Zentralnervensystems mit bemerkenswertem anatomischem Befunde. (Spasitische Pseudosklerose-Encephalomyelophatie mit disseminierten Degenerationsherden). Z ges Neurol Psychiatr 64:147-228.

James LT, Liu H, Ulyanov NB, Farr-Jones S, Zhang H, Donne DG, Kaneko K, Groth D, Mehlhorn I, Prusiner SB, Cohen FE (1997). Solution structure of a 142-residue recombinant prion protein corresponding to the infectious fragment of the scrapie isoform. Proc Natl Acad Sci USA 94:10086-91.

Jarrett JT and Lansbury PT jr (1993). Seeding “one-dimensional crystallization” of amyloid: a pathogenic mechanism in Alzheimer’s disease and scrapie? Cell 73:1055-58.

Jin T, Gu Y, Zanusso G, Sy M, Kumar A, Cohen M, Gambetti P, Singh N. The chaperone protein BiP binds to a mutant prion protein and mediates its degradation by the proteasome. J Biol Chem 275:38699-38704.

Kaeser PS, Klein MA, Schwarz P, Aguzzi A (2001). Efficient lymphoreticular prion propagation requires PrPC in stromal and hematopoietic cells. J Virol 75:7097-106.

Kaneko K, Zulianello L, Scott M, Cooper CM, Wallace AC, James TL, Cohen FE, Prusiner SB (1997). Evidence for protein X binding to a discontinous epitope on the cellular prion protein during scrapie prion propagation. Proc Natl Acad Sci USA 94:10069-74.

Kang YS, Zhao X, Lovaas J, Eisenberg E, Greene LE (2009). Clathrin-independent internalization of normal cellular prion protein in neuroblastoma cells is associated with the Arf6 pathway. J Cell Sci 122:4062-9.

Karapetyan YE, Sferrazza GF, Zhou M, Ottenberg G, Spicer T, Chase P, Fallahi M, Hodder P, Weissmann C, Lasmézas CI (2013). Unique drug screening approach for prion diseases identifies tacrolimus and astemizole as antiprion agents. Proc Natl Acad Sci USA 110:7044-9.

Kimberlin RH, Cole S, Walker CA (1987). Temporary and permanent modifications to a single strain of mouse scrapie on transmission to rats and hamsters. J Gen Virol 68:1875-81.

Klatzon I, Gajdusek DC, Zigas V (1959) . Pathology of Kuru. Lab Invest 8:799-847.

Klein MA, Frigg R, Flechsig E, Raeber AJ, Kalinke U, Bluethmann H, Bootz F, Suter M, Zinkernagel RM, Aguzzi A (1997). A crucial role for B cells in neuroinvasive scrapie. Nature 390:687-690.

Klein MA, Kaeser PS, Schwarz P, Weyd H, Xenarios I, Zinkernagel RM, Carroll MC, Verbeek JS, Botto M, Walport MJ, et al. (2001). Complement facilitates early prion pathogenesis. Nat Med 7:488-492.

Klohn PC, Stoltze L, Flechsig E, Enari M, Weissmann C (2003). A quantitative, highly sensitive cell-based infectivity assay for mouse scrapie prions. Proc Natl Acad Sci USA 100:11666-11671.

Koch TK, Berg BO, DeArmond SJ, Gravina RF (1985). Creutzfeldt-Jakob disease in a young adult with idiopathic hypopituitarism. Possible relation to the administration of cadaveric human growth hormone. N Engl J Med 313:731-3.

Kocisko DA, Come JH, Priola SA, Chesebro B, Raymond GJ, Lansbury PT, Caughey B (1994). Cell-free formation of protease resistant prion protein. Nature 370:471-474.

Korth C, May BC, Cohen FE, Prusiner SB (2001). Acridine and phenothiazine derivatives as pharmacotherapeutics for prion disease. Proc Natl Acad Sci USA 98:9836-9841.

Kretzschmar HA, Ironside JW, DeArmond SJ, Tateishi J (1996). Diagnostic criteria for sporadic Creutzfeldt-Jakob disease. Arch Neurol 53:913-20.

Kronick MN (1986). The use of phycobiliproteins as fluorescent labels in immunoassay. J Immunol Methods 92:1-13.

Laurén J, Gimbel DA, Nygaard HB, Gilbert JW, Strittmatter SM (2009). Cellular prion protein mediates impairment of synaptic plasticity by amyloid-beta oligomers. Nature 457:1128-32.

Le Borgne R, Hoflack B (1997). Mannose 6-phosphate receptors regulate the formation of clathrin-coated vesicles in the TGN. J Cell Biol 137:335-45.

Lee KS, Magalhaes AC, Zanata SM, Brentani RR, Martins VR, Prado Ma (2001). Internalization of mammalian fluorescent cellular prion protein and N-terminal deletion mutants in living cells. J Neurochem. 79:79-87.

Legname G, Baskakov IV, Nguyen HO, Riesner D, Cohen FE, DeArmond SJ, Prusiner SB (2004). Synthethic mammalian prions. Science 305:673-6.

Liberski PP (2012). Historical overview of prion diseases: a view from afar. Folia Neuropathol 50:1-12.

Li J, Browning S, Mahal SP, Oelschlegel AM, Weissmann C (2010) Darwinian evolution of prions in cell culture. Science 327:869-872.

Llewelyn CA, Hewitt PE, Knight RS, Amar K, Cousens S, Mackenzie J, Will RG (2004). Possible transmission of variant Creutzfeldt-Jakob disease by blood transfusion. Lancet 363:417-21.

Low MG (1987). Biochemistry of the glycosyl-phosphatidylinositol membrane protein anchors. Biochem J 244:1-13.

Lu X, Wintrode P, Surewicz WK (2007). Beta-sheet core of human prion protein amyloid fibrils as determined by hydrogen/deuterium exchange. Proc Natl Acad Sci USA 104:1510-1515.

Luk KC, Kehm V, Carroll JC, Zhang B, O'Brien P, Trojanowski JQ, Lee VMY (2012). Pathological α-synclein transmission initiates Parkinson-like neurodegeneration in nontransgenic mice. Science 338:949-953.

Lysek DA, Wüthrich K (2004). Prion protein interaction with the C-terminal SH3 domain of Grb2 studied using NMR and optical spectroscopy. Biochemistry 43:10393-10399.

Leopoldt JG (1759). Nützliches und auf die Erfahrung gegründete Einleitung zur Landwirtschaft, Berlin Friedrich Günther.

Mabbott NA, Bruce ME (2001). The immunobiology of TSE diseases. J Gen Virol 82:2307-18.

Mabbott NA, Young J, McConnell I, Bruce ME (2003). Follicular dendritic cell dedifferentiation by treatment with an inhibitor of the lymphotoxin pathway dramatically reduces scrapie susceptibility. J Virol 77:6845-54.

Madec JY, Vanier A, Dorier A, Bernillon J, Belli P, Baron T (1997). Biochemical properties of protease resistant prion protein PrP^{Sc} in natural sheep scrapie. Arch Virol 142:1603-12.

Magalhaes AC, Silva JA, Lee KS, Martins VR, Prado VF, Ferguson SS, Gomez MV, Brentani RR, Prado Ma (2002). Endocytic intermediates involved with the intracellular trafficking of a fluorescent cellular prion protein. J Biol Chem 277:33311-8.

Mahal SP, Baker CA, Demczyk CA, Smith EW, Julius C, Weissmann C (2007). Prion strain discrimination in cell culture: the cell panel assay. Proc Natl Acad Sci USA 104: 20908-13.

Mallucci GR, Ratte S, Asante EA, Linehan J, Gowland I, Jefferys JG, Collinge J (2002) Post-natal knockout of prion protein alters hippocampal CA1 properties, but does not result in neurodegeneration. Embo J 21:202-210.

Mallucci GR, White MD, Farmer M, Dickinson A, Khatun H, Powell AD, Brandner S, Jefferys JG, Collinge J (2007). Targeting cellular prion protein reverses early deficits and neurophysiological dysfunction in prion-infected mice. Neuron 53:325-35.

Marella M, Lehmann S, Grassi J, Chabry J (2002). Filipin prevents pathological prion protein accumulation by reducing endocytosis and inducing cellular PrP release. J Biol Chem 277:25457-64.

Margalith I, Suter C, Ballmer B, Schwarz P, Tiberci C, Sonati T, Falsig J, Nyström S, Hammarström P, Aslund A, Nilsson KP, Yam A, Whitters E, Hornemann S, Aguzzi A (2012). Polythiophenes inhibit prion propagation by stabilizing prion protein (PrP) aggregates. J Biol Chem 287:18872-87.

Marsh RF, Dees C, Castle BE, Wade WF, German TL (1984). Purification of the scrapie agent by density gradient centrifugation. J Gen Virol 65:415-21.

Marsh RF, Hadlow WJ (1992). Transmissible mink encephalopathy. Rev Sci Tech 11:539-550.

Martins VR, Brentani RR (2002). The biology of the cellular prion protein. Neurochem Int. 41:353-5.

Masters CL, Richardson EP Jr (1978). Subacute spongiform encephalopathy (Creutzfeldt-Jakob disease). The nature and progression of spongiform change. Brain 101:333-44.

May BC, Fafarman AT, Hong SB, Rogers M, Deady LW, Prusiner SB, Cohen FE (2003). Potent inhibition of scrapie prion replication in cultured cells by bis-acridines. Proc Natl Acad Sci USA 100:3416-21.

McGowan JP (1922). Scrapie in sheep. Scottish J Agric 5:365-375

McKinley MP, Bolton DC, Prusiner SB (1983). A protease-resistant protein is a structural component of the scrapie prion. Cell 35:57-62.

McMahon HT and Boucrot E (2011). Molecular mechanism and physiological functions of clathrin-mediated endocytosis. Nat Rev Mol Cell Biol 12:517-33.

Medori R, Tritschler HJ, LeBlanc A, Villare F, Manetto V, Chen HY, Xue R, Leal S, Montagna P, Cortelli P, et al (1992). Fatal familial insomnia, a prion disease with a mutation at codon 178 of the prion protein gene. New England Journal of Medicine 326:444-449.

Meier P, Genoud M, Prinz M, Maissen M, Rüllicke T, Zurbriggen A, Raeber AJ, Aguzzi A (2003). Soluble dimeric prion protein binds PrP(Sc) in vivo and antagonizes prion disease. Cell 113:49-60.

Merz PA, Wisniewski HM, Somerville RA, Bobin SA, Masters CL, Iqbal K (1983). Ultrastructural morphology of amyloid fibrils from neuritic and amyloid plaques. Acta Neuropathol 60:113-24.

Montrasio F, Frigg R, Glatzel M, Klein MA, Mackay F, Aguzzi A, Weissmann C (2000). Impaired prion replication in spleens of mice lacking functional follicular dendritic cells. Science 288:1257-9.

Moore RC, Hope J, McBride PA, McConnell I, Selfridge J, Melton DW, Manson JC (1998). Mice with gene targetted prion protein alterations show that Prnp, Sinc and Prni are congruent. Nat Genet 18:118-25.

Moore RC, Lee IY, Silverman GL, Harrison PM, Strome R, Heinrich C, Karunaratne A, Pasternak SH, Chishti MA, Liang Y et al. (1999). Ataxia in prion protein (PrP)-deficient mice is associated with upregulation of the novel PrP-like protein doppel. J Mol Biol 292:797-817.

Mouillet-Richard S, Ermonval M, Chebassier C, Laplanche JL, Lehmann S, Launay JM, Kellermann (2000). Signal transduction through prion protein. Science 289:1925-8.

Nebenführ A, Ritzenthaler C, Robinson DG (2002). Brefeldin A: deciphering an enigmatic inhibitor of secretion. Plant Physiol. 130:1102-8.

Nilsson KP, Herland A, Hammarström P, Inganäs O (2005). Conjugated polyelectrolytes: conformation-sensitive optical probes for detection of amyloid fibril formation. Biochemistry 44:3718-24.

Oesch B, Westaway D, Wälchli M, McKinley MP, Kent SB, Aebersold R, Barry RA, Tempst P, Teplow DB, Hood LE (1985). A cellular gene encodes scrapie PrP27-30 protein. Cell 40:735-46.

Oesch B, Jensen M, Nilsson P, Fogh J (1994). Properties of the scrapie prion protein: quantitative analysis of protease resistance. Biochemistry 33:5926-31.

Oidtmann B, Simon D, Holtkamp N, Hoffmann R, Baier M (2003). Identification of cDNA from japanese pufferfish (Fugu rubripes) and Atlantic salomon (Salmo salar) coding homologues to tetrapod prion proteins. FEBS Lett. 538:96-100.

Pan KM, Baldwin M, Nguyen J, Gasser M, Serban A, Groth D, Mehlhorn I, Huang Z, Fletterick RJ, Cohen FE et al. (1993). Conversion of alpha-helices into beta-sheets features in the formation of the scrapie prion proteins. Proc Natl Acad Sci USA 90:10962-6.

Pattison IH (1965). Resistance of the scrapie agent to formalin. J Comp Pathol 75:159-64.

Pattison IH, Millson GC (1961). Experimental transmission of scrapie to goats and sheep by the oral route. J Comp Pathol 71:171-6.

Pauly PC, Harris DA (1998). Copper stimulates endocytosis of the prion protein. J Biol Chem 273:33107-33110.

Perera WS, Hooper NM (2001). Ablation of the metal ion-induced endocytosis of the prion protein by disease-associated mutation of the octarepeat region. Curr Biol. 11:519-23.

Peretz D, Williamson RA, Matsunaga Y, Serban H, Pinilla C, Bastidas RB, Rozenshteyn R, James TL, Houghton RA, Cohen FE, Prusiner SB, Burton DR (1997). A conformational transition at the N-terminus of the prion protein features in formation of the scrapie isoform. J Mol Biol. 273:614-22.

Peters PJ, Mironov A Jr, Peretz D, van Donselaar E, Leclerc E, Erpel S, DeArmond SJ, Burton DR, Williamson RA, Vey M, Prusiner SB (2003). Trafficking of prion proteins through a caveolae-mediated endosomal pathway. J Cell Biol 162:703-17.

Pocchiari M, Schmittinger S, Masullo C (1987). Amphotericin B delays the incubation period of scrapie in intracerebrally inoculated hamsters. J Gen Virol 68 (Pt 1):219-223.

Polymenidou M, Moos R, Scott M, Sigurdson C, Shi YZ, Yajima B, Hafner-Bratkovic I, Jerala R, Hornemann S, Wuthrich K, Bellon A, Vey M, Garen G, James MN, Kav N, Aguzzi A (2004). The POM monoclonals: a comprehensive set of antibodies to non-overlapping prion protein. PLoS One 3.

Polymenidou M, Stoeck K, Glatzel M, Vey M, Bellon A, Aguzzi A (2005). Coexistence of multiple PrP^{Sc} types in individuals with Creutzfeldt-Jakob disease. Lancet Neurol 4:805-14.

Prado MA, Alves-Silva J, Magalhaes AC, Prado VF, Linden R, Martis VR, Brentani RR (2004). PrP^{C} on the road: trafficking of the cellular prion protein. J Neurochem 88:869-81.

Premont RT, Perry SJ, Schmalzigaug R, Roseman JT, Xing Y, Claing A (2004). The GIT/PIX complex: an oligomeric assembly of GIT family ARF GTPase-activating proteins and PIX family Rac1/Cdc42 guanine nucleotide exchange factors. Cell Signal 16:1001-11.

Priola SA, Chesebro B (1995). A single hamster PrP amino acid blocks conversion to protease resistant PrP in scrapie-infected mouse neuroblastoma cells. J Virol 69:7754-8.

Priola SA, Chesebro B, Caughey B (2003). Biomedicine. A view from the top – prion diseases from 10'000 feet. Science 300:917-19.

Prusiner SB, Hadlow WJ, Garfin DE, Cochran SP, Baringer JR, Race RE, Eklund CM (1978). Biochemistry 17:4993-9.

Prusiner SB (1982). Novel proteinaceous infectious particles cause scrapie. Science 216 :136-144.

Prusiner SB, McKinley MP, Bowman KA, Bolton DC, Bendheim PE, Groth DF, Glenner GG (1983). Scrapie prions aggregate to form amyloid-like birefringent rods. Cell 35:349-358.

Prusiner SB (1989). Scrapie prions. Annu Rev Microbiol 43:345-74.

Prusiner SB (1990). Novel structure and genetics of prions causing neurodegeneration in humans and animals. Biologicals 18:247-62.

Prusiner SB (1996). Molecular biology and pathogenesis of prion diseases. Trends Biochem Sci 21:482-7.

Prusiner S (2012). Cell biology. A unifying role for prions in neurodegenerative diseases. Science 336:1511-3.

Rabinovici GD, Wang PN, Levin J et al., (2006). First symptom in sporadic Creutzfeldt-Jakob disease. Neurology 66:286-287.

Rainey MA, George M, Ying G, Akakura R, Burgess DJ, Siefker E, Bargar T, Doglio L, Crawford SE, Todd GL, Govindarajan V, Hess RA, Band V, Nakamura M, Band H (2010). The endocytic recycling regulator EHD1 is essential for spermatogenesis and male fertility in mice. BMC Dev Biol 10:37-45.

Rieger R, Edenhofer F, Lasmezas CI, Weiss S (1997). The human 37-kDa laminin receptor precursor interacts with the prion protein in eukaryotic cells. Nature Med 3:1383-1388.

Riek R, Hornemann S, Wider G, Billeter M, Glockshuber R, Wuthrich K (1996). NMR structure of the mouse prion protein domain Prp(121-231). Nature 382:180-182.

Rivera-Milla E, Stuermer CA, Malaga-Trillo E (2003). An evolutionary basis for scrapie disease: identification of a fish prion mRNA. Trends Genet 19:72-75.

Safar J, Wille H, Itri V, Groth D, Serban H, orchia M, Cohen FE, Prusiner SB (1998). Eight prion strains have PrP^{Sc} molecules with different conformations. Nature Med 4:1157-1165.

Safar JG, Geschwind MD, Deering C, Didorenko S, Sattavat M, Sanchez H, Serban A, Vey M, Baron H, Giles K, Miller BL, Dearmond SJ, Prusiner SB (2005). Diagnosis of human prion disease. Proc Natl Acad Sci USA 102:3501-6.

Sailer A, Büeler H, Fischer M, Aguzzi A, Weissmann C (1994). No propagation of prions in mice devoid of PrP. Cell 77:967-8.

Sakudo A, Onodera T, Ikuta K (2007). Prion protein gene-deficient cell lines: powerful tools fro prion biology. Microbiol Immunol 51:1-13.

Salamat MK, Dron M, Chappuis J, Langevin C, Laude H (2011). Prion propagation in cells expressing PrP glycosylation mutants. J Virol 85:3077-85.

Sarnataro D, Caputo A, Casanova P, Puri C, Paladino S, Tivodar SS, Campana V, Tacchetti C, Zurzolo C (2009). PloS One 4.

Shmerling D, Hegyi I, Fischer M, Blattler T, Brandner S, Gotz J, Rulicke T, Flechsig E, Cozzio A, von Mering C, Hengartner C, Aguzzi A, Weissmann C (1998). Expression of amino-terminally truncated PrP in the mouse leading to ataxia and specific cerebellar lesions. Cell 93:203-214.

Shyng SL, Huber MT, Harris DA (1993). A prion protein cycles between the cell surface and an endocytic compartment in cultured neuroblastoma cells. J Biol Chem 268:15922-8.

Shyng SL, Lehmann S, Moulder KL, Harris DA (1995). Sulfated glycans stimulate endocytosis of the cellular isoform of the prion protein, PrP^{C}, in cultured cells. J Biol Chem 270:30221-30229.

Sigurdson CJ, Nilsson KP, Hornemann S, Manco G, Polymenidou M, Schwarz P, Leclerc M, Hammarström P, Wüthrich K, Aguzzi A (2007). Prion strain discrimination using luminescent conjugated polymers. Nat Methods 4:1023-30.

Sigurdson CL and Aguzzi A (2007): Chronic wasting disease. Biochim Biophys Acta 1772:610-8.

Silveira JR, Raymond GJ, Hughson AG, Race RE, Sim VL, Hayes SF, Caughey B (2005). The most infectious prion particles. Nature 437:257-61.

Scott M, Groth D, Foster D, Torchia M, Yang SL, DeArmond SJ, Prusiner SB (1993). Propagation of prions with artificial properties in transgenic mice expressing chimeric PrP genes. Cell 73:979-88.

Solforosi L, Criado JR, McGavern DB, Wirz S, Sanchez-Alavez M, Sugama S, DeGiorgio LA, Volpe BT, Wiseman E, Abalos G, Masliah E, Gilden D, Oldstone MB, Conti B, Williamson RA (2004). Cross-linking cellular prion protein triggers neuronal apoptosis. Science 303:1514-6.

Sonati T, Reimann RR, Falsig J, Baral PK, O'Connor T, Hornemann S, Yaganoglu S, Li B, Herrmann US, Wieland B, Swayampakula M, Rahman MH, Das D, Kav N, Riek R, Liberski PP, James MN, Aguzzi A (2013). The toxicity of antiprion antibodies is mediated by the flexible tail of the prion protein. Nature 501:102-106.

Sorkin A, von Zastrow M (2009). Endocytosis and signaling: intertwining molecular networks. Nat Rev Mol Cell Biol. 10:609-22.

Stahl N, Borchelt DR, Hsiao K, Prusiner SB (1987). Scrapie prion protein contains a phosphatidylinositol glycolipid. Cell 51:229-240.

Stör J, Watts JC, Mensinger ZL, Oehler A, Grillo SK, DeArmond SJ, Prusiner SB, Giles K (2012). Purified and synthethic Alzheimer's amyloid beta (Aβ) prions. Proc Natl Acad Sci USA 109:11025-30.

Strumbo B, Ronchi S, Bolis LC, Simonic T (2001). Molecular cloning of the cDNA coding for Xenopus laevis prion protein. FEBS Letters 508:170-174.

Sunyach C, Jen A, Deng J, Fitzgerald KT, Frobert Y, Grassi J, McCaffrey MW, Morris R (2003). The mechanism of internalization of glycosylphosphatidylinositol-anchored prion protein. EMBO J 22: 3591-601.

Supattapone S, Piro JR, Rees JR (2009). Complex polyamines: unique prion disaggregating compounds. CNS Neurol Disord Drug Targets 8:323-328.

Tamgüney G, Glies K, Gliden DV, Lessard P, Wille H, et al. (2008). Genes contributing to prion pathogenesis. J Gen Virol 89:1777-88.

Taraboulos A, Jendroska K, Serban D, Yang SL, DeArmond SJ, Prusiner SB (1992). Regional mapping of prion proteins in b rain. Proc Natl Acad Sci USA 89:7620-7624.

Taylor DR, Watt NT, Perera WS, Hooper NM (2005). Assigning functions to distinct regions of the N-terminus of the prion protein that are involved in its copper-stimulated, clathrin-dependent endocytosis. J Cell Sci 118:5141-53.

Taylor DR and Hooper NM (2007). The low-density lipoprotein receptor-related protein 1 (LRP1) mediates the endocytosis of the cellular prion protein. Biochem J 402:17-23.

Telling GC, Scott M, Mastrianni J, Gabizon R, Torchia M, Cohen FE, DeArmond SJ, Prusiner SB (1995). Prion propagation in mice expressing human and chimeric PrP transgenes implicates the interaction of cellular PrP with another protein. Cell 83:79-90.

Thadani V, Penar PL, Partington J, Kalb R, Janssen R, Schonberger LB, Rabkin CS, Prichard JW (1988). J Neurosurg 69:766-9.

Vey M, Pilkuhn S, Wille H, Nixon R, DeArmond SJ, Smart EJ, Anderson RG, Taraboulos A, Prusiner SB (1996). Subcellular colocalization of the cellular and scrapie prion proteins in caveolae-like membraneous domains. Proc Natl Acad Sci USA 93:14945-9.

Watt NT and Hooper NM (2003). The prion protein and neuronal zinc homeostasis. Trends Biochem Sci 28:406-10.

Watts JC and Westaway D (2007). The prion protein family: diversity, rivalry, and dysfunction. Biochim Biophys Acta 1772-654-72.

Wegner C, Römer A, Schmalzbauer R, Lorenz H, Windl O, Kretzschmar HA (2002). Mutant prion protein aquires resistance to protease in mouse neuroblastoma cells. J Gen Virol 83:1237-1245.

Weissmann C (1991). A “unified theory” of prion propagation. Nature 352:679-683.

Westermark GT and Westermark P (2010). Prion-like aggregates: infectious agents in human disease. Trends Mol Med 16:501-507.

Wild D (2005). The Immunoassay handbook. Elsevier Ltd.

Wilesmith JW, Wells GAH, Cranwell MP, Ryan JBM (1988). Bovine spongiform encephalopathy: epidemiological studies. Vet Rec 123:638-44.

Wiliams, Young (1980). Chronic wasting disease of captive mule deer: a spongiform encephalopathy. J Wildl Dis 16:89-98.

Will RG, Ironside JW, Zeidler M, Cousens SN, Estibeiro K, Alperovitch A, Poser S, Pocchhiari M, Hoffman A, Smith PG (1996). A new variant of Creutzfeldt-Jakob disease in the UK. Lancet 347:921-5.

Wilson DR, Anderson RD, Smith W (1950). Studies in scrapie. J Comp Pathol 60:267-82.

Wopfner F, Weidenhöfer G, Schneider R, von Brunn A, Gilch S, Schwarz TF, Werner T, Schätzl HM (1999). Analysis of 27 mammalian and 9 avian PrPs reveals high conservation of flexible regions of the prion protein. J Mol Biol 25:1163-78.

Wuthrich K and Riek R (2001). Three-dimensional structures of prion proteins. Adv Protein Chem 57:55-82.

Yam AY, Gao CM, Wang X, Wu P, Peretz D (2010). The octarepeat region of the prion protein is conformationally altered in PrPSc. Plos One 5:1-13.

Ying YS, Anderson RG, Rothberg KG (1992). Each caveolae contains multiple glycosyl-phosphatidylinositol-anchored membrane proteins. Cold Spring Harb Symp Quant Biol 57:593-604.

Yull HM, Ritchie DL, Langeveld JP, van Zijderveld FG, Bruce ME, Ironside JW, Head MW (2006). Detection of type 1 prion protein in variant Creutzfeldt-Jakob disease. Am J Pathol 168:151-157.

Zahn R, Liu A, Luhrs T, Riek R, von Schroetter C, Lopez Garcia F, Billeter M, Calzolai L, Wider G, Wuthrich K (2000). NMR solution structure of the human prion protein. Proc Natl Acad Sci U S A 97:145-150.

Zanusso G, Farinazzo A, Prelli F, Fiorini M, Gelati M, Ferrari S, Righetti PG, Rizzuto N, Frangione B, Monaco S (2004). Identification of distinct N-terminal truncated forms of prion protein in different Creutzfeldt-Jakob disease subtypes. J Biol Chem 279:38936-42.

Zlotnik I, Stamp JT (1961). Scrapie disease of sheep. World Neurol 2:895-907.

ACKNOWLEDGEMENT

I would like to express my gratitude to Professor Adriano Aguzzi for his support, brilliant ideas and guidance throughout my PhD thesis.

Prof. Lucas Pelkmans for his support as a member of my PhD committee.

Furthermore, I would like to express my graditude to a number of people who have helped me throughout:

Dr. Simone Hornemann has been a big help throughout my thesis. I thank her for the care that she took in my PhD education.

A big thank goes out to Rita Moos for helping and supporting me throughout my PhD, espcially in the production, purification and labelling of POM antibodies.

I am thankful to Thilo Enderle and Doris Roth from Roche who introduced me to the FRET technology.

Ilan Margalith for a fruitful and enjoyable collaboration on LCP-related projects.

Prisca Liberali from ETH for spending time and her contribution in the FRET endocytosis assay.

I would also like to thank all my current and former collegues at the institute of neuropathology for their help and andvice and for a friendly and stimulating atmosphere.

I would also like to extend my gratitude to Zentrum für Neurowissenschaften Zurich (ZNZ).

Finally, I would like to express my outmost gratitude to my family.